ION IMPLANTATION IN EPITAXIAL Ge_xSi_{1-x} on Si(100)

Thesis by

Yu-Chun Donald Lie

In Partial Fulfillment of the Requirements

for the Degree of

Doctor of Philosophy

California Institute of Technology

Pasadena, California

1996

(Submitted September 18, 1995)

c 1996

Yu-Chun Donald Lie

All Rights Reserved

To the Lord and my family

ACKNOWLEDGMENTS

First of all, I would like to give my deepest thanks to my Lord, Jesus Christ, for his grace and Providence during the period of my Ph.D. study at Caltech. For of him, and through him, and to him, are all things: to whom be glory forever. "Was the eye contrived without skill in optics," asked Sir Isaac Newton, "or the ear without knowledge of sounds?"

I want to express my sincere gratitude and appreciation to Professor Marc-A. Nicolet, my thesis advisor and a prominent scientist, for his wisdom, guidance and thoroughness. I also would like to acknowledge the help I received from Dr. Fred Eisen, a world-renowned researcher and a real gentleman, for his fellowship and numerous enlightening discussion. Dr. N. David Theodore, my SRC-mentor at Motorola Inc. and a faithful brother of mine in Christ, has taught me so much about how and when to give to the needy when you ought to: for I was one of the needy once. His expertise on defects in semiconductors and his close involvement in our SRC-project was indeed indispensable to my study.

I was extremely fortunate to be able to witness some of the most gifted people in our times at Caltech, such as Professor Axel Scherer, who is so knowledgeable and yet so humble and down-to-earth that everybody can understand him and enjoy his presence. I also want to sincerely thank Professor Thad Vreeland, Jr., Professor Harry Atwater, Professor Y.C. Tai, and Professor K. Vahala. Their advise and fellowship have been very valuable to me. I am also deeply indebted to Professor Bob De Angelis from University of Nebraska for his encouragement and mentorship. He has the charisma to win every soldier's loyalty in a platoon; if I ever become a professor, I want to be just like Bob.

I have to thank the Rotary International Foundation for generously providing me with a scholarship for my graduate study at Caltech. I am extremely grateful to Dr. Tim

and Annie Siu, Mr. Don Keenan, and the Rotarians of the Alhambra Rotary Club for their warm family-like support. Special thanks are also to the Rotary District 348 for taking great care of me during my ambassadorship as a Rotary International Scholar. I also want to acknowledge the financial sponsor for my Ph.D. work, the Semiconductor Research Corporation (SRC).

I would like to thank members of Professor Nicolet's group, in particular Dr. E. Kolawa, Dr. T. Workman, Dr. A. Bächli, Dr. S. Im, and Dr. J.H. Song. They have not only worked with me and helped me, but have also laughed with me and comforted me when necessary. I also would like to thank Mr. Gang He, Ms. Lynn Lowry, Professor H. Kubota, Dr. J.S. Reid, Mr. R. Johnson, Dr. G. Bai, Dr. A. Vantomme, Dr. J.M. Pereda, Dr. J.S. Chen, Dr. J. Mesli, Dr. Y.D. Kim, Dr. W.S. Liu, Ms. X. Sun, and Miss B. Tai for their generous help and friendship. I am especially indebted to Mr. R. Gorris and M. Easterbrook for their excellent technical assistance, and Ms. F. Castillo for her outstanding secretarial work and friendship.

I also would like to acknowledge Professor K.L. Wang and his excellent research group at UCLA with all my heart. I had great support from Dr. T.K. Carns, Mr. M.O. Tanner, Mr. S. Thomas, Dr. L.M. Tsau, Dr. H.S. Li and Dr. V. Arbet-Engels. I also want to thank the very talented Professor E.A. Fitzgerald at M.I.T., Professor S.S. Lau at UCSD, Professor J.W. Mayer at ASU, Dr. Chang at AT&T Bell Labs, Dr. J. Candelaria of Motorola Inc., and Professor D.L. Kwong, Dr. H. Kinoshita and Dr. Tze-Hsin Huang at UT Austin for their help and discussion regarding my experiments. Special thanks are also due to Mr. Lee Chung at Rockwell International for providing all kinds of support for my employment after graduation.

Last, but the sweetest, I want to thank my newly-wedded wife Wendy. She has helped me tremendously during this thesis writing process. We had to cancel our honeymoon trip due to the unexpected workload, but she never complained about it. Her love, joy, peace, patience, kindness, goodness, faithfulness, gentleness and self-control are

the sweetest fruits of the Spirit that a man can ever experience. I also want to thank all the brothers and sisters in our church, Mountain View Baptist Church of Claremont, for helping us during this very difficult yet memorable period of time.

"But if from thence thou shalt seek the Lord thy God, thou shalt find him, if thou seek him with all thy heart and with all thy soul." -Deut. 4:29.

ABSTRACT

The question of whether one can effectively dope or process epitaxial Si(100)/GeSi heterostructures by ion implantation is experimentally investigated. Results that cover several different ion species (Si, P, and As), doses ($1.0x10^{13}/cm^2$ to $1.5x10^{15}/cm^2$), implantation temperatures (RT to 150°C), as well as annealing techniques (steady-state and rapid thermal annealing) are included in this thesis. Implantation-induced damage and strain and their annealing behavior for both strained and relaxed GeSi are measured and compared with those in Si and Ge. The damage and strain generated in pseudomorphic GeSi by room-temperature implantation are considerably higher than the values interpolated from those of Si and Ge. Implantation at slightly elevated substrate temperatures (e.g., 100°C) can very effectively suppress the implantation-induced damage and strain in GeSi. The fractions of electrically active dopants in both Si and GeSi are measured and compared for several doses and under various annealing conditions. Solid-phase epitaxial regrowth of GeSi amorphized by implantation has also been studied and compared with regrowth in Si and Ge. For the case of metastable epi-GeSi amorphized by implantation, the pseudomorphic strain in the regrown GeSi is always lost and the layer contains a high density of defects, which is very different from the clean regrowth of Si(100). Solid-phase epitaxy, however, facilitates the activation of dopants in both GeSi and Si, irrespective of the annealing techniques used. For metastable GeSi films that are not amorphized by implantation, rapid thermal annealing is shown to outperform steady-state annealing for the preservation of pseudomorphic strain and the activation of dopants. In general, defects generated by ion implantation can enhance the strain relaxation process of strained GeSi during post-implantation annealing. The processing window that is optimized for ion-implanted Si therefore has to be modified considerably for ion-implanted GeSi.

TABLE OF CONTENTS

LIST OF PUBLICATIONS

(A) Journal Publications

1. "Damage and strain in epitaxial Ge_xSi_{1-x} films irradiated with Si," **D.Y.C. Lie**, A. Vantomme, F. Eisen, T. Vreeland, Jr., M-A. Nicolet, T.K. Carns, V. Arbet-Engels, and K.L. Wang, J. Appl. Phys. 74, 6039 (1993).

2. "Damage and strain in pseudomorphic versus relaxed Ge_xSi_{1-x} layers on Si," **D.Y.C. Lie**, A. Vantomme, F. Eisen, M-A. Nicolet, T. Vreeland, Jr., T.K. Carns, V. Arbet-Engels, and K.L. Wang, J. Electron. Mater., 23, 369 (1994).

3. "Advantage of rapid thermal annealing over furnace annealing for P-implanted metastable $Si(100)/Ge_{0.12}Si_{0.88}$," **D.Y.C. Lie**, J.H. Song, M-A. Nicolet, and N.D. Theodore, Appl. Phys. Lett. 66, 592 (1995).

4. "Dependence of damage and strain on the temperature of Si irradiation in epitaxial $Ge_{0.10}Si_{0.90}$ films on Si(100)," **D.Y.C. Lie**, J.H. Song, N.D. Theodore, A. Vantomme, M-A. Nicolet, T.K. Carns, and K.L. Wang, J. Appl. Phys. 77, 2329 (1995).

5. "Solid phase epitaxial regrowth and dopant activation of P-implanted metastable pseudomorphic $Ge_{0.12}Si_{0.88}$ on Si(100)," **D.Y.C. Lie**, N.D. Theodore, J.H. Song, and M-A. Nicolet, J. Appl. Phys. 77, 5160 (1995).

6. "Strain evolution and dopant activation in P-implanted metastable pseudomorphic $Si(100)/Ge_{0.12}Si_{0.88}$," **D.Y.C. Lie**, J.H. Song, M-A. Nicolet, and N.D. Theodore, J. Electron. Mater. (in press).

7. "Dopant activation and strain relaxation in metastable pseudomorphic $Si(100)/Ge_{0.12}Si_{0.88}$ implanted with P ions," **D.Y.C. Lie**, J.H. Song, and N.D. Theodore, Appl. Surf. Sci. (in press).

8. "Irradiation-induced damage and strain in epitaxial $Ge_{0.10}Si_{0.90}$ grown on Si(100)," **D.Y.C. Lie**, J.H. Song, and N.D. Theodore, J. of Mater. Chem. Phys. (in press).

9. "Hole mobility measurements in heavily boron doped Ge_xSi_{1-x} strained layers," T.K. Carns, S.K. Chun, M.O. Tanner, K.L. Wang, T.I. Kamins, J.E. Turner, **D.Y.C. Lie**, M-A. Nicolet, and R.G. Wilson, Trans. IEEE Electron Devices, 41, 1273 (1994).

10. "Ge epilayer of high quality on a Si substrate by solid-phase epitaxy," W.S. Liu, J.S. Chen, **D.Y.C. Lie**, and M-A. Nicolet, Appl. Phys. Lett. 63, 1405 (1993).

11. "Intersubband transitions in pseudomorphic InGaAs/GaAs/AlGaAs multiple step quantum wells," H.S. Li, Y.W. Chen, K.L. Wang, and **D.Y.C. Lie**, J. Vac. Sci. Tech. (B) 11, 1840 (1993).

12. "Solid-phase epitaxial regrowth of high-dose arsenic-implanted metastable pseudomorphic Si(100)/Ge_xSi_{1-x}," **D.Y.C. Lie**, J.H. Song, M-A. Nicolet, N.D. Theodore, M.O. Tanner, S. Thomas, and K.L. Wang, to be submitted to J. Appl. Phys. (in preparation).

(B) Conference Proceedings

1. "Generation of defects and strain by Si ion implantation in Ge(100) single crystals, and in pseudomorphic Ge_xSi_{1-x} films grown on Si(100)," **D.Y.C. Lie**, A. Vantomme, F. Eisen, M-A. Nicolet, V. Arbet-Engels, and K.L. Wang, Mat. Res. Soc. Symp. Proc. 262, 1079 (1992).

2. "Electrical and material properties of heavily doped pseudomorphic $Ge_{0.12}Si_{0.88}$ films by ^{31}P ion implantation," **D.Y.C. Lie**, A. Vantomme, F. Eisen, M-A. Nicolet, T.K. Carns, and K.L. Wang, Proc. SRC-Techcon, 552 (1993).

3. "The influence of impurities on the properties of the chromium/gold and chromium nitride/gold structures," **D.Y.C. Lie**, E. Kolawa, R. De Angelis, L. Lowry, and J. Scott-Monck, Mat. Res. Soc. Symp. Proc. ULSI-IX, 583 (1994).

4. "Dopant activation and epitaxial regrowth in P-implanted pseudomorphic $Ge_{0.12}Si_{0.88}$ layers on Si(100)," **D.Y.C. Lie**, F. Eisen, M-A. Nicolet, N.D. Theodore, T.K. Carns, and K.L. Wang, Mat. Res. Soc. Symp. Proc. 321, 485 (1994).

5. "Steady-state versus rapid-thermal annealing of phosphorus implanted pseudomorphic Si(100)/$Ge_{0.12}Si_{0.88}$," **D.Y.C. Lie**, J.H. Song, N.D. Theodore, F. Eisen, M-A. Nicolet, T.K. Carns, and K.L. Wang, Mat. Res. Soc. Symp. Proc. 342, 51 (1994).

6. "Solid phase epitaxial regrowth and dopant activation of arsenic-implanted metastable pseudomorphic $Ge_{0.08}Si_{0.92}$ and $Ge_{0.16}Si_{0.84}$ on Si(100)," **D.Y.C. Lie**, J.H. Song, M-A. Nicolet, N.D. Theodore, J. Candelaria, S.G. Thomas, M.O. Tanner, and K.L. Wang, Mat. Res. Soc. Symp. Proc. (in press).

7. "Epitaxial Ge_xSi_{1-x} films on Si : (1) oxidation and nitridation of Ge_xSi_{1-x} , (2) Ion implantation of Ge_xSi_{1-x}," M-A. Nicolet, **D.Y.C. Lie**, W.S. Liu, and A. Vantomme, Proc. 14th Solid State Phys. Symp. Semicon. Surf. Metal-Semicon. Interface, 1 (1992).

8. "Damage and strain in epitaxial $Ge_{0.10}Si_{0.90}$ after Si implantation from 40 to 150 °C," A. Vantomme, J. H. Song, **D.Y.C. Lie**, F. Eisen, M-A. Nicolet, T.K. Carns, and K.L. Wang, Mat. Res. Soc. Symp. Proc. 326, 121 (1994).

9. "Microstructure of oxidized $Ge_{0.8}Si_{0.2}$ annealed in a reducing ambient," N.D. Theodore, W.S. Liu, **D.Y.C. Lie**, M-A. Nicolet, T.K. Carns and K.L. Wang, Mat. Res. Soc. Symp. Proc. (in press).

CHAPTER 1: INTRODUCTION

The world-wide integrated circuits (ICs) market reached more than a hundred billion dollars in the year of 1994 alone, where the majority of the IC chips sold were fabricated using silicon as the substrate material [1]. The technology of silicon ICs, however, is approaching fundamental limits set by the atomic nature of matter. One cannot count on doubling the chip capacity by shrinking the sizes of Si devices forever. In the meantime, the rapidly growing telecommunications industries are driving the development of reliable and economical high-frequency devices with lower power dissipation. Si/Ge_xSi_{1-x} heterostructures are therefore under extensive study because they can provide adjustable bandgaps and improved carrier mobilities over those of Si homostructures [2]. Heterojunction bipolar transistors (HBTs) that utilize Si/GeSi heterolayers promise a very impressive extension of the high-frequency limit of Si-based bipolar technology to above 100 GHz, a frequency range that so far has been the domain of GaAs-based devices [3,4]. Modulation-doped field effect transistors (MODFETs) that employ GeSi as the channel layer have also shown considerable improvement in both speed and gain over their Si counterparts [5,6]. High-sensitivity photodetectors made with Si/GeSi have also been fabricated [7]. Several quantum size effects in strained GeSi layers and their potential in device applications are reviewed by Karunasiri and Wang [8]. In the near future, Si/GeSi heterojunction and superlattice-based devices may even play an important role in the integration of complex electronic circuitry with optoelectronic functionality on a single IC chip. For example, growing GaAs on high quality GeSi buffer layers on Si may combine laser diodes made of III-V materials with Si ICs [9]. Tensilely-strained Si can also be grown on these GeSi buffer layers and improved surface-channel devices have been demonstrated [10]. Si/GeSi heterostructures have therefore opened up a new, exciting avenue of research opportunities.

Fabrication processes for Si/GeSi devices are quite compatible with those routinely used for Si ICs. This is a major advantage for Si/GeSi over III-V compounds. This compatibility

ensures the continued use of the existing hundred-million-dollar Si IC Fabs for the manufacturing of Si/GeSi devices. This makes GeSi more cost effective than GaAs for technological evolution. However, GeSi has its problems too. One of the most important problems in fabricating Si/GeSi devices is associated with doping of the heterostructures using ion implantation, which is the focus of this thesis study [9]. To make millions of Si/GeSi transistors on a planar IC chip, one has to be able to effectively dope the heterostructure with great precision. Ion implantation is the dominant technology for the introduction of precise amounts of dopants in the current IC industry [11]. Implantation creates damage and additional strain in intrinsically strained GeSi, and post-implantation annealing is required to remove them [12]. The intrinsic strain in a Si/GeSi heterostructure is both a blessing and a curse. The presence of intrinsic pseudomorphic strain changes the band structure of Si/GeSi and can enhance the mobility of carriers. However, if strain relaxation takes place during post-implantation annealing, unwanted defects are introduced and the performance of Si/GeSi devices will be degraded considerably [13,14]. In general, defects generated by implantation can act as nucleation sites for dislocation formation, which is shown to enhance the undesired strain relaxation of GeSi [15]. High temperature thermal treatment of Si/GeSi can also introduce significant interdiffusion of Ge and Si [16]. Due to the problems of interdiffusion and strain relaxation, it is evident that post-implantation annealing for Si/GeSi devices requires a substantial decrease in the thermal budget over devices made of Si [17].

It is also reported that implantation-induced damage levels in GeSi are considerably higher than expected values interpolated from data for Si and Ge [18-20]. The amorphization dose for a $Ge_{0.10}Si_{0.90}$ film implanted with Si ions at room temperature is less than a third of that needed to amorphize a Si wafer implanted under the same conditions [18]. Implantation-induced amorphization and solid-phase epitaxy may also result in relaxed GeSi of poor crystalline quality, even with low temperature annealing at ~500-600°C [21-25]. It is thus important to perform a systematic study on ion-implanted GeSi to understand how to successfully apply ion implantation technology to fabricate reliable Si/GeSi devices.

In this thesis, the experimental results of implantation-induced damage and strain in Si/GeSi are reported, together with percentages of activated dopants, and values of electron Hall mobility after annealing treatments. Table I listed the ion species, doses, implantation temperatures, and annealing techniques for the experimental results presented in this thesis. Pseudomorphically strained, partially relaxed, as well as fully relaxed GeSi films were used in this work, with the Ge content in the alloy ranging from 8% to 35%. Si control samples as well as Ge samples were also implanted and annealed for reference. For the sake of brevity, unless otherwise specified, I will use expressions such as "x=0.10" to replace "pseudomorphic $Si/Ge_{0.10}Si_{0.90}$"; and "fully relaxed x=0.10" to refer to fully relaxed $Si/Ge_{0.10}Si_{0.90}$ films.

Five of my most representative journal papers have been selected and included in the appendix of this thesis for easy referencing. Paper A1 in the appendix discusses the damage and strain introduced in Si-implanted Si, Ge_xSi_{1-x} and Ge samples at room temperature for various dose and x-values. Paper A2 describes the behavior of implantation-induced damage and strain versus the implantation temperature for GeSi samples. Paper A3 describes the solid-phase epitaxial regrowth of high-dose P-implanted GeSi after furnace annealing and its resulting crystallinity, strain state, and percentage of dopant activation. Paper A4 provides a general discussion on P-implanted pseudomorphic GeSi after furnace annealing under both low-dose (non-amorphized) and high-dose (amorphized) conditions. Paper A5 demonstrates the advantage of rapid-thermal annealing over steady-state furnace annealing for processing low-dose P-implanted pseudomorphic GeSi samples. Results that are presented in these five papers in the appendix will be frequently referred to throughout this thesis. Expressions like "Fig. 1 of A3" refer to Fig. 1 of paper A3 in the appendix.

In Chapter 2 of this thesis, I provide a brief introduction to the experimental tools that are frequently used for this study. I summarize in Chapter 3 all important results available in the field of ion implantation of GeSi, and discuss the general features of these data. Whenever possible, comparison will be made between my data and those available in the literature. Chapter 3, Section 3.1 contains a discussion of damage and strain in all of the as-implanted Si, Ge, and Ge_xSi_{1-x}

samples. I then present in Section 3.2 a general discussion of the annealing behavior of these implanted samples. Unpublished data on arsenic-implanted Si and GeSi, as well as the results published in A1-A5 on Si^{28} and P^{31} implanted samples, will all be included in Chapter 3 for comparison and discussion. I would like to convince the readers that with some restrictions, the ion implantation technology may be used to effectively dope and process Si/GeSi heterostructures.

Table I.1: The ion species, doses, implantation temperatures, and annealing techniques used for the experimental results presented in this thesis

Ion	Ge content in Ge_xSi_{1-x}	Implantation temperature	Dose ($1x10^{13}/cm^2$)	Amorphization	Steady-state annealing	Rapid thermal annealing
Si	x=0 (Si), 0.10-0.22, 1 (Ge)*	RT-100°C	1-300	No	Yes	No
Si	x=0 (Si), 0.10-0.35, 1 (Ge)*	RT-60°C	20-100	Yes	Yes	No
P	x=0 (Si), 0.12-0.20	RT	1-20	No	Yes	Yes
P	x=0 (Si), 0.08-0.20	RT	20-150	Yes	Yes	Yes
As	x=0 (Si), 0.08, 0.16	RT	1	No	Yes	Yes
As	x=0 (Si), 0.08, 0.16	RT	150	Yes	Yes	Yes

*data included for relaxed GeSi films as well

References

1. See, for example, US News and World Report, p. 41, July 31, (1995); or M. Chang, Proc. Second Int'l Conf. Electron. Mater., Taiwan (1994).
2. R. Hull and J. C. Bean in *Strained-layer Superlattices : Materials Science and Technology*, edited by T. P. Pearsall, Ch. 1, pp. 1-72 (Academic Press, London, 1991).
3. D.L. Harame, J.H. Comfort, J.D. Cressler, E.F. Crabbé, J.Y.-C. Sun, B.S. Meyerson and T. Tice, IEEE Trans. Electron Devices, 42, 469 (1995).
4. F. Schäffler, Solid-State Electronics 37, 765 (1994).
5. Y.J. Mii, Y.H. Xie, E.A. Fitzgerald, D. Monroe, P.J. Silverman, J.M. Kuo, A.R. Kortan, F.A. Thiel and B.E. Weir, J. Vac. Sci. Technol. B10, 1807 (1992).
6. U. König, A.J. Boers, F. Schäffler and E. Kasper, Electron. Lett. 28, 160 (1992).
7. T.P. Pearsall, H. Temkin, J.C. Bean and S. Luryi, IEEE Electron Device Lett. 7, 330 (1986).
8. R.P.G. Karunasiri and K.L. Wang, J. Vac. Sci. Technol. B9, 2064 (1991).
9. E. Käsper and F. Schäffler, *Strained-layer Superlattices : Materials Science and Technology*, Semiconductors and Semimetals, Vol. 33, edited by T. P. Pearsall, Ch. 4 (Academic Press, London, 1991).
10. Y.H. Xie, E.A. Fitzgerald, D. Monroe, G. P. Watson and P.J. Silverman, Jpn. J. Appl. Phys. 33, 2372 (1994).
11. See, for example: M. D. Giles in *VLSI Technology*, edited by S.M. Sze, Ch. 8, p. 370 (McGraw-Hill, Singapore, 1988); or M.I. Current, I. Yamada, N.W. Cheung, P.L.F. Hemment, and K.J. Reeson in *Handbook of Ion Implantation Technology*, edited by J. F. Ziegler, pp. 363-433 (Elsevier Science Publishers, Amsterdam, 1992).
12. J. F. Gibbons, Proc. IEEE, 60, 1062 (1972).
13. C.A. King, J.L. Hoyt, and J.F. Gibbons, IEEE Trans. Electron Devices 36, 2093 (1989).
14. P.S. Peercy, B.W. Dodson, J.Y. Tsao, E.D. Jones, D.R. Myers, T.E. Zipperian, L.R. Dawson, R.M. Biefeld, J.F. Klem, and C.R. Hills, IEEE Electron Devices Lett. 9, 621 (1988).

15. R. Hull, J.C. Bean, J.M. Bonar, G.S. Higashi, K.T. Short, H. Temkin, and A.E. White, Appl. Phys. Lett. 56, 2445 (1990).

16. R. Hull and J. C. Bean in *Strained-layer Superlattices : Materials Science and Technology*, edited by T. P. Pearsall, Ch. 1, pp. 1-72 (Academic Press, London, 1991).

17. D. K. Nayak, K. Kamjoo, J. S. Park, J. C. S. Woo and K. L. Wang, 39, 56 (1992).

18. D. J. Eaglesham, J. M. Poate, D. C. Jacobson, M. Cerullo, L. N. Pfeiffer, and K. West, Appl. Phys. Lett. 58, 523 (1991).

19. D. Y. C. Lie, A. Vantomme, F. Eisen, T. Vreeland, Jr., M-A. Nicolet, T. K. Carns, and K. L. Wang, J. Appl. Phys. 74, 6039 (1993).

20. D. Y. C. Lie, A. Vantomme, F. Eisen, M.-A. Nicolet, V. Arbet-Engels, and K. L. Wang, Mat. Res. Soc. Symp. Proc. 262, 1079 (1993).

21. D. C. Paine, N. D. Evans, and N. G. Stoffel, J. Appl. Phys. 70, 4278 (1991).

22. Q. Z. Hong, J. G. Zhu, J. W. Mayer, W. Xia, and S. S. Lau, J. Appl. Phys. 71, 1768 (1992).

23. C. Lee, T. E. Haynes, and K. S. Jones, Appl. Phys. Lett. 62, 501 (1993).

24. D. Y. C. Lie, T.K. Carns, N.D. Theodore, F. Eisen, M-A. Nicolet, and K. L. Wang, Mat. Res. Soc. Symp. Proc. 321, 485 (1994).

25. D. Y. C. Lie, N.D. Theodore, J.H. Song, and M-A. Nicolet, J. Appl. Phys. 77, 5160 (1995).

CHAPTER 2: CHARACTERIZATION TECHNIQUES FOR ION-IMPLANTED Si/GeSi

There are various characterization techniques that allow one to analyze the materials or electronic properties of ion-implanted Si/GeSi. I shall briefly describe in this chapter the techniques that are most relevant to the results presented in this thesis.

2.1. Strain: X-ray Diffraction Techniques

Our ability to pseudomorphically grow epilayers on lattice-mismatched substrates is essential to the success of devices made with strained-layer heterostructures. As mentioned in Chapter 1, the presence of pseudomorphic strain in a heterostructure can change its electronic and optoelectronic properties; relaxation of the pseudomorphic strain is invariably accompanied by numerous defects that will degrade the performance of heterojunction devices [1-4]. Strain is thus a very important parameter for the characterization of Si/GeSi heterostructures. By definition, pseudomorphic growth means that the entire lattice mismatch is accommodated by the biaxial strain in the epilayers [5]. Ion channeling is a technique that has been used to measure strain (i.e., tetragonal distortion) in strained-layer heterostructures [5,6]. X-ray rocking curves can provide greater sensitivity and accuracy in measuring lattice parameters of epilayers than ion channeling can, and may also be less destructive [7-9]. I have used and aligned a double-crystal diffractometer and a double-channel-cut five-crystal x-ray diffractometer to study the strain states of Si/GeSi before/after implantation and annealing. The double-channel-cut five-crystal diffractometer has slightly better resolution than the double-crystal instrument because it contains one Si and one Ge crystal in series and the x-rays exiting from the tube will bounce twice within each channel of the crystal and become highly monochromatic before hitting the sample. To obtain a strong x-ray diffraction peak, the Bragg's condition $2d\sin\theta_B=n\lambda$ has to be satisfied, where d is the interplanar lattice spacing of the monocrystalline film or of the substrate, θ_B is the

diffraction angle, and λ is the wavelength of the incident x-ray beam. In the following paragraphs and throughout this thesis, unless otherwise specified, whenever we discuss the "strain" of a layer, we are referring to the values of "x-ray strain" of the film rather than of its "elastic strain." X-ray strain is defined as the change in the lattice parameter of a film normalized to that of the substrate, i.e., $\varepsilon = \Delta a_f/a_0$, where ε can be the in-plane strain (i.e., parallel strain, ε^{II}) or the perpendicular strain (i.e., $\varepsilon^{\perp}$), and a_f and a_0 are defined as the lattice parameters of the unstrained film and the substrate, respectively [6]. In general, x-ray rocking curves taken from non-symmetrical diffraction planes as well as from symmetrical ones are required to determine the strain state of a film. The set of equations valid for calculating both perpendicular and parallel strain in an arbitrarily strained film are given in Eqs. 1-2 [10],

$$-\Delta\theta = k_1\varepsilon^{\perp} + k_2\varepsilon^{II} \pm \xi \tag{1}$$

where

$$\begin{aligned} k_1 &= \cos^2\psi \tan\theta_B \pm \sin\psi\cos\psi, \\ k_2 &= \sin^2\psi \tan\theta_B \mp \sin\psi\cos\psi. \end{aligned} \tag{2}$$

$\Delta\theta$ (in units of radian) in Eq. 1 is the angular separation between the diffraction peaks of the epilayer and the substrate, which can be read directly from a rocking curve; ψ is the angle between the diffracting plane and the sample surface, θ_B is the Bragg angle of the substrate diffraction peak, and ξ is the component in the diffraction plane of the misorientation angle between the layer and the substrate. The plus sign in the last term of Eqs. 1-2 should be used when the angle of x-ray incidence with respect to the surface is θ_B-ψ and the minus sign is used when it is θ_B+ψ. For symmetrical diffraction planes, k_2=0 in Eqs. 1-2, and if we further assume that there is no misorientation (tilt) between the epilayers and the substrate (i.e., ξ=0), Eqs. 1-2 reduce to

$$\Delta\theta = -\tan(\theta_B)\varepsilon^{\perp} \tag{3}$$

Eq. 3 can be simply derived by the differentiation of Bragg's equation. If the in-plane strain of the epilayer is zero (i.e., $\varepsilon^{II}=0$), one only needs to record the rocking curves of symmetrical diffraction planes to obtain the perpendicular strain in the layers by using Eq. 3.

The electrons which are periodically distributed inside a crystal can scatter x-rays effectively. If we ignore second-order effects such as multiple scattering and absorption, the resulting scattering amplitude is negligible if $G \neq \Delta k$, where G is the reciprocal lattice vector of either the film or the substrate, and Δk is the change of the x-ray wave-vector after scattering [11]. The detailed interpretation of x-ray diffraction data would thus be best if one could first convert the spectra into a reciprocal-space representation, which can be done in a more elaborate triple-axis rocking curve setup [12]. In practice, however, it is easier to convert the positions and intensities of the peaks from a double-crystal rocking curve spectrum directly into a real-space strain profile by iterative computer simulation using either kinematic or dynamic x-ray diffraction theory [13-17]. The extraction of a unique depth profile for strain in a sample may not always be possible by using the fitting procedure. It is, however, usually possible to approximate the maximum strain values in a sample with good precision (~±5%) [14,15].

Even though the x-ray rocking curve technique actually measures the x-ray strain or effectively the in-plane and perpendicular lattice constants of a film, the interface misfit dislocation densities can still be estimated from a rocking curve spectrum. The total lattice mismatch $f=(a_f-a_0)/a_0$ at the interface is the sum of the in-plane strain, ε^{II}, and the misfit strain δ (i.e., $f = \varepsilon^{II}+\delta$) [9]. The interface dislocation spacing S can then be obtained by $S=b_{eff}/\delta$, where b_{eff} is the effective Burgers vector, which is the in-plane component of the Burgers vector in the direction of spacing S. Due to the fact that it takes a relatively large number of misfit dislocations to create a measurable change in the epilayer diffraction peak position, one also has to examine the sharpness and intensity of the diffraction peaks to detect minute amounts of strain relaxation. Once the heterostructure is relaxed, the misfit dislocations at the interface may cause diffuse scattering and thus broaden the diffraction peaks [18]. The detection limit for misfit dislocation densities for either double-crystal or five-crystal rocking curve techniques are at best ~10^6-10^7

dislocations/cm^2 [7]. Other characterization methods that are more sensitive to low dislocation densities ($\leq 10^4$/cm^2) such as x-ray topography, electron-beam-induced-current (EBIC), or etch-pits techniques are required to study the onset of strain relaxation [9].

2.2. Damage:

2.2.1. MeV ^{4}He Channeling Spectrometry

The thickness and composition of an epi-GeSi layer grown on Si can be directly obtained from the analysis of its backscattering spectrum [19]. MeV ^{4}He channeling has been a convenient tool for measuring implantation-induced defects in a single crystalline sample for decades, since defects can serve as scattering centers that produce significant amounts of "dechanneling" signal [20,21]. For a detailed tutorial guide to the physics of ion channeling, please refer to the books by Feldman *et al.* and Chu *et al.* [19,20]. In a first-order approximation, the "channeled" fraction of the incident beam only interacts with the atoms that are displaced out of the lattice sites, while the "random" fraction of the incident beam interact with all of the atoms in the sample. Therefore, one must be able to separate these two contributions in a RBS/Channeling spectrum to obtain the total number of displaced atoms created by implantation. If the effect of multiple scattering is ignored, the depth profile of implantation-induced damage can be obtained using an iterative procedure that extracts the dechanneling signals produced by the implantation-displaced atoms alone [20-22]. All extracted damage levels are relative to that of an amorphous sample, which has a "maximum relative damage" value equal to unity. The RBS/Channeling technique does not generally provide the microscopic nature of the defects that produce dechanneling signals. Techniques such as transmission electron microscopy or electron paramagnetic resonance are needed for more precise identifications of defects than the RBS/Channeling technique.

2.2.2. Transmission Electron Microscopy

Transmission electron microscopy is a powerful tool for investigating the microscopic nature of defect, such as dislocations in Si/GeSi heterostructures. For a practical introduction to this technique, please refer to the books by Edington *et al.* [23]. The physics of electron beam diffraction is similar to that of x-ray diffraction described in Sec. 2.1. However, unlike x-ray rocking curves, cross-sectional transmission electron microscopy provides depth resolution of defects and can easily resolve dense arrays of dislocations at interfaces. The limitations of transmission electron microscopy are that samples have to be mechanically and/or chemically thinned first to ≈ 0.15 μm to allow the e-beam to traverse the sample, and these destructive preparation procedures usually provide only small areas suitable for examination. The sensitivity of cross-sectional transmission electron microscopy for dislocation observation is at best ~ 10^5-10^6 /cm^2, which is similar to careful x-ray rocking curves measurements [9]. Plan-view transmission electron microscopy can have slightly better resolution of defects densities; however, depth information on these defects is not available in this case.

2.3. Dopant Activity and Carrier Mobility: Hall effect and Sheet Resistance Measurements

It is well-known that the electrical conductivity of a semiconductor can be increased by many orders of magnitude by incorporating dopants into substitional sites in the crystal lattice [24]. The carrier concentration of a semiconductor can be directly obtained by Hall effect measurements, which effect is caused by the movement of charged carriers in the presence of a magnetic field [11]. Van der Pauw demonstrated in 1957 how the Hall effect and the associated sheet resistance measurements could be made on thin samples of arbitrary shape [25]. The work of Johansson *et al.* discusses in detail how to apply Hall measurements to ion-implanted samples [26]. I have performed Hall effect measurements on the ion-implanted samples using the Van der Pauw technique. Resistance values are experimentally determined by making four-terminal measurements where a constant current is driven through two contacts while the voltage is

monitored across another pair of contacts. Since all of the ion-implanted GeSi samples possess junction depths less than 0.3 μm, I simply approximate the carrier concentration and the resistance of a doped region by its sheet values. The percentage of activated dopants is determined by normalizing the measured sheet carrier concentration to the implantation dose. The electron Hall coefficient for both heavily-doped GeSi and Si by n-type dopants (P or As) is assumed to be unity in this work [27,28].

References

1. R. Hull and J. C. Bean in *Strained-layer Superlattices: Materials Science and Technology*, edited by T. P. Pearsall, Ch. 1, pp. 1-72 (Academic Press, London, 1991).
2. C.A. King, J.L. Hoyt, and J.F. Gibbons, IEEE Trans. Electron Devices 36, 2093 (1989).
3. P.S. Peercy, B.W. Dodson, J.Y. Tsao, E.D. Jones, D.R. Myers, T.E. Zipperian, L.R. Dawson, R.M. Biefeld, J.F. Klem, and C.R. Hills, IEEE Electron Devices Lett. 9, 621 (1988).
4. D. K. Nayak, K. Kamjoo, J. S. Park, Jason C. S. Woo and K. L. Wang, 39, 56 (1992).
5. K. N. Tu, J. W. Mayer and L. C. Feldman, *Electronic Thin Film Science* (Macmillian Pubilishing Company, New York, 1992).
6. S.T. Picraux, B.L. Doyle, and J.Y. Tsao, *Strained-layer Superlattices: Materials Science and Technology*, Semiconductors and Semimetals, Vol. 33, edited by T. P. Pearsall, Ch. 3, pp. 139-222 (Academic Press, London, 1991).
7. J. M. Baribeau, T. E. Jackman, D. C. Houghton, P. Maigné, and M. W. Denhoff, J. Appl. Phys. 63, 5738 (1988).
8. E. A. Fitzgerald, Mater. Sci. Rep. 7, 81 (1991).
9. V. S. Sperioso, J. Appl. Phys. 52, 6094 (1981).
10. T. Vreeland, Jr., and B.M. Paine, J. Vac. Sci. Technol. A4, 3153 (1986).
11. C. Kittel, *Introduction to Solid State Physics*, 6th ed. John Wiley, New York.
12. D.A. Neumann, H. Zabel and H. Morkoc, Mat. Res. Sos. Symp. Proc. 37, 47 (1985).
13. C. R. Wie, T. A. Tombrello, and T. Vreeland, Jr., J. Appl. Phys. 59, 3743 (1986).
14. C. J. Tsai, A. Dommann, M.-A. Nicolet and T. Vreeland, Jr., J. Appl. Phys. 69, 2076 (1991).
15. T. Vreeland, Jr., and B. M. Paine, J. Vac. Sci. Technol. A4, 3153 (1986).
16. G. Bai and M.-A. Nicolet, J. Appl. Phys. 70, 649 (1991).
17. D.Y.C. Lie, J.H. Song, N.D. Theodore, A. Vantomme, M-A. Nicolet, T.K. Carns, and K.L. Wang, J. Appl. Phys. 77, 2329 (1995).
18. P. F. Fewster, J. Appl. Cryst. 25, 714 (1992).

19. W.K. Chu, J.W. Mayer, and M-A. Nicolet, *Backscattering Spectrometry*, Ch. 8, pp. 223-275 (Academic Press, New York, 1978).

20. L. C. Feldman, J. W. Mayer, and S. T. Picraux, "Materials Analysis by Ion Channeling" (Academic Press, London, 1982).

21. F. Eisen in *Channeling: Theory, Observation and Applications*, edited by D.V. Morgan, (Wiley, London, 1973). Ch. 14, p. 426.

22. G. Bai and M.-A. Nicolet, J. Appl. Phys. 70, 3551 (1991).

23. J.W. Edington, *Practical Electron Microscopy in Materials Science* (Philips, Eindhoven, 1974).

24. See, for example, J. Gyulai in *Ion implantaion: Science and Technology*, edited by J. F. Ziegler (Academic Press, Orlando, 1984), pp. 139-210.

25. L.J. van der Pauw, Philips Tech. Rev. 20, 220 (1958).

26. N.G.E. Johansson, J.W. Mayer, and O.J. Marsh, Solid State Electronics, 13, 317 (1970).

27. Fisful, *Heavily Doped Semiconductors* (Plenum Press, New York, 1969), p. 133.

28. T.K. Carns, S.K. Chun, M.O. Tanner, K.L. Wang, T.I. Kamins, J.E. Turner, D.Y.C. Lie, M-A. Nicolet, and R.G. Wilson, Trans. IEEE Elec. Devices, 41, 1273 (1994).

CHAPTER 3: SUMMARY AND DISCUSSION

My experimental data on ion-implanted GeSi are summarized in this chapter and the general features of the results are highlighted. Whenever possible, my data will be compared with those available in the literature. The underlying physical mechanisms that may govern the reported phenomena are discussed. I begin by discussing the behavior of implantation-induced damage and strain versus the ion dose for all of the as-implanted Si, Ge, and Ge_xSi_{1-x} samples in Sec. 3.1. A general discussion of the annealing behavior of these implanted samples is then provided in Sec. 3.2. I will conclude this chapter by suggesting some interesting areas for future experimental studies.

3.1. As-Implanted Samples

It is well-known that ion implantation can create both damage and strain in a target material, and that the residual amount of damage and strain after post-implantation annealing depends on those initially generated in the as-implanted samples [1-3]. To perform a systematic study of ion-implanted Si/GeSi, it is therefore logical to first investigate implantation-induced damage and strain in as-implanted samples. Recently, several research groups have reported results for ion-implanted GeSi [4-14]. When compared with data available for Si, significant damage enhancement has been observed in implanted strained Ge_xSi_{1-x} films, e.g., selective amorphization in Si/Ge_xSi_{1-x} strained-layer superlattices [7,8]. I will summarize in sections 3.1.1 and 3.1.2 the strain and damage induced in both pseudomorphic and relaxed Ge_xSi_{1-x} films by ion implantation, where the ion range is limited such that the $Si\text{-}Ge_xSi_{1-x}$ interface is not significantly damaged. The results are compared with those observed in Si(100) and Ge(100) single crystals. The possible reasons for the observed enhancement in induced damage and strain in as-implanted

GeSi versus Si will be discussed. The dependence of the induced damage and strain versus the ion dose and the implantation temperature will be presented in Sec. 3.1.3 and Sec. 3.1.4, respectively.

3.1.1. Implantation-Induced Damage

MeV ^{4}He channeling spectrometry was used to measure the implantation-induced damage in as-implanted Si, Ge, and Si/GeSi samples. There was no detectable increase in the channeling yield as a result of the ^{4}He implantation. All Si/GeSi samples were of excellent crystalline quality, with a minimum channeling yield of ~3 to 4 % in both Si and Ge signals. The profiles of "relative damage" were extracted from the channeling spectra using a numerical iterative fitting model as described in Chapter 2 [15,16]. A measured damage value is relative to that of an amorphous sample, in which case a relative damage value of 100% is reached. I will use the *maximum* relative damage values obtained from these extracted damage profiles for easy analysis of data.

Figure 3.1 shows the dependence of the maximum relative damage versus the ion dose for implanted Si(100), Ge(100) and pseudomorphic Si(100)/Ge_xSi_{1-x} ($0.10 \le x \le 0.50$). The implanted ions species include P, Si, As, and Sb. Some data points in Fig. 3.1 are taken from the literature [17-19]. My own experimental data are those implanted with Si ions (five cases, plotted in open symbols), as well as those implanted with P and As ions (three cases). The curves for bulk Si and Ge (dotted lines), as well as for Ge_xSi_{1-x} (solid line) in Fig. 3.1 all exhibit three damage regimes: (I) There is an initially slow increase of the maximum relative damage with dose; (II) the rate of increase for the maximum relative damage accelerates after a threshold damage level of ~ 10-20% is reached, and (III) finally amorphization of the sample is reached beyond a critical ion dose which is a function of the Ge content. One of the most striking features of Fig. 3.1 is that the damage levels introduced by a given dose of ions in Ge_xSi_{1-x} (of low x-values, $10\% \le x \le 20\%$) are significantly higher than those in pure silicon. For example, Fig. 3.1 shows that the dose required for Si ions to amorphize Ge(100) is ~6×10^{13}/cm^2, while it takes ~8×10^{14}/cm^2 to amorphize Si, and ~2.5×10^{14}/cm^2 for x=0.10. One cannot predict the amorphization dose of Ge_xSi_{1-x} by simply

using the linear interpolation of data obtained from bulk Si and Ge, since it yields a wrong dose of ~$7x10^{14}/cm^2$ for x=0.10. This three-fold reduction in the amorphization dose for x=0.10 versus Si shows that a small addition of Ge to Si significantly enhances the retention of implantation-induced damage at room temperature. Similar behavior in terms of strong damage enhancement has also been observed in GaAs when Al atoms are added to the lattice [8].

For GeSi samples implanted with $1x10^{14}/cm^2$ Si ions of similar energies (80-100 keV), Fig. 3.1 shows that the values of maximum relative damage introduced in pure Ge (open Down Triangles) is higher than that in x=0.50 (solid Down Triangle), which is in turn higher than those in x=0.35 (solid Up Triangle) and those in x=0-0.20. The damage introduced in x=0.20 by 100 keV $5x10^{13}$ P/cm^2 (solid diamond) is also considerably higher than that generated in x=0.12 (solid squares). Similar behavior is found for 100 keV $1x10^{13}$ Sb/cm^2 implanted x=0.18 (cross) and x=0.10 (star) as well. It thus appears that as more Ge atoms are added into Si, higher levels of implantation-induced damage are observed. The addition of germanium may increase the retained damage in Ge_xSi_{1-x} alloys by (1): increasing the average energy per ion deposited in the collision cascades, which increases the number of defects initially generated by the impact of an ion; and/or by (2): decreasing the mobility of simple defects in the cascades to impede them from out-diffusing, thereby increasing the fraction of defects still present after the implantation. I have discussed these two factors in more detail in Fig. 5 of A1 (appendix), where these two effects appear to have roughly equal contributions to the observed damage enhancement for $0.1 \leq x \leq 0.2$ with respect to pure silicon for room temperature Si implantation [20]. It might be speculated that the retardation of defect mobility in GeSi could be attributed to the preferential binding of point defects with Ge atoms, thus forming higher-order defects such as Ge-defect complexes during implantation [21]. However, experimental data are required to prove this hypothesis.

Another systematic trend observed in Fig. 3.1 is that the implantation-induced damage increases with the mass of the incident ions. For example, the damage introduced in x=0.10 by 100 keV Sb ions with a dose of $1x10^{13}/cm^2$ (star) is substantially higher than that produced by 100 keV Si ions (open square). Similarly, the damage induced by 100 keV P ions with a dose of

$5x10^{13}/cm^2$ for x=0.12 (solid square) appears to be higher than that generated by 100 keV Si with the same dose. This dependence of implantation-induced damage on the ion mass is consistent with the fact that at a given ion energy, more energy is deposited into the atomic displacement process if heavier ions are used [22,23].

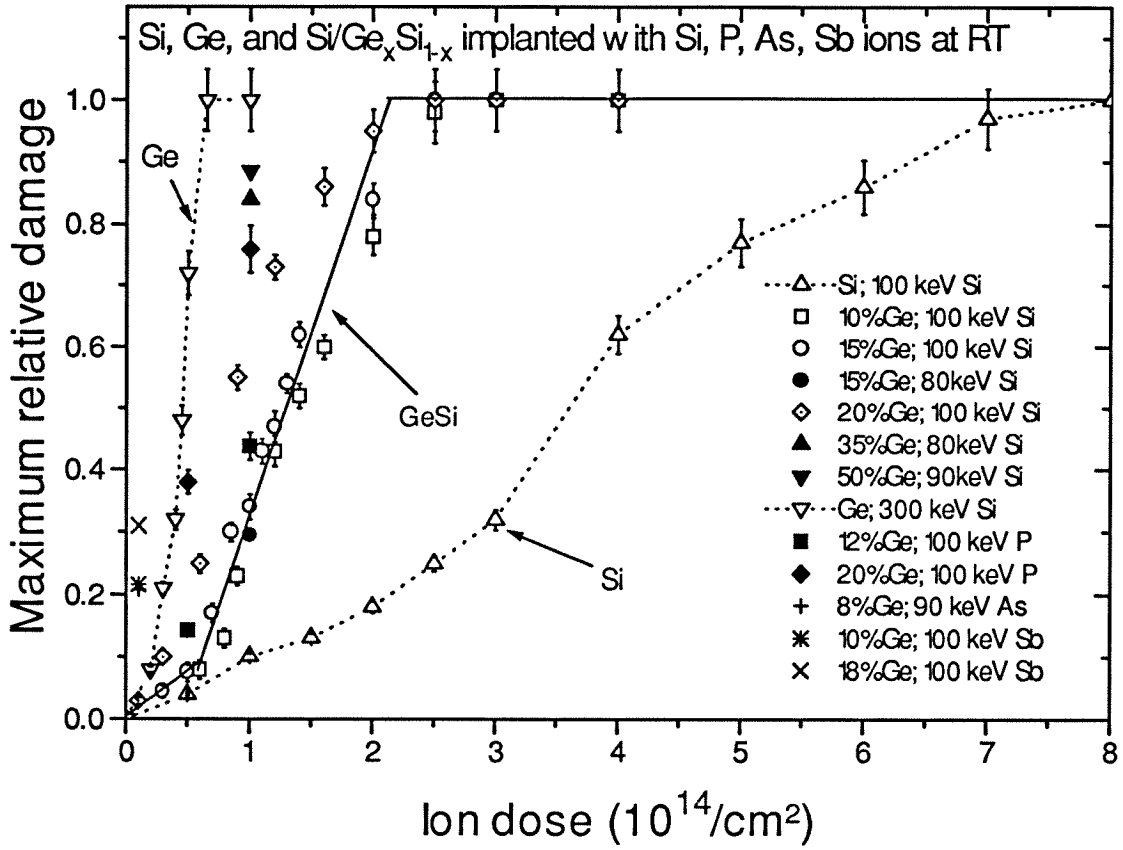

Figure 3.1. The values of maximum relative damage obtained from ^{4}He ion channeling spectra for Si, P, As, and Sb implanted Si(100), Ge(100) and pseudomorphic Si(100)/Ge_xSi_{1-x} ($0.10 \leq x \leq 0.50$) plotted versus the ion dose. A unity value in the maximum relative damage means that a continuous amorphous layer is formed in the implanted sample. A solid line is added as a guide to the eye to indicate the highly nonlinear nature of damage buildup as a function of incrementing ion dose in the Ge-Si system. Two dotted lines connect the data for bulk Si (open Up Triangles) and bulk Ge (open Down Triangles), respectively.

Detailed implantation parameters such as ion species, energy and Ge content can be found in the inserted legend. The data points for Sb implanted GeSi (star and cross) are taken from Ref. [17]. The data points that correspond to 80 keV Si implanted x=0.15 (solid circle), x=0.35 (solid Up Triangle), and 90 keV Si implanted x=0.50 (solid Down Triangle) are taken from Ref. [18,19]. All data are measured on samples implanted at room temperature with very low current densities ($\leq 0.2\mu A/cm^2$). The incident ion energies are selected such that the Si-GeSi interfaces of these samples are not noticeably damaged by the ion beams. The change in the ion energy from 100 keV for the case x = 0 (Si), 0.10, 0.13, 0.15, 0.20 to 300 keV for x = 1 (Ge) should be noted. This was done to maintain approximately similar values of average energy densities deposited in the collision cascade by the energetic ions.

All of the data points shown in Fig. 3.1 correspond to pseudomorphically strained GeSi alloys. One may wonder whether the intrinsic uniform strain in the epilayers affects the retained damage introduced by ion implantation. It is therefore of interest to examine whether implantation-induced damage differs in two samples identical except for their initial state of strain. I have quantitatively compared the damage produced by 100 keV Si ions at room temperature in both pseudomorphically strained and relaxed Ge_xSi_{1-x} layers of similar x for various Si ion doses (up to $2.5 \times 10^{14}/cm^2$). No significant difference in the implantation-induced damage is observed among these samples; these data points are plotted in Fig. 8 of A1. I propose that the reason the initial strain does not have a significant effect on the retained damage is because the elastic strain energy density in a GeSi film is small compared with the average energy density deposited into the atomic collision cascade by energetic ions [20,24-28]. For a cubic-structured GeSi film pseudomorphically grown on Si(100), the strain tensor ε_{ij} and the stress tensors σ_{ij} are related by the elastic constants, c_{ij}, where all stress tensor terms are zero except for the in-plane components $\sigma_{11} = \sigma_{22} = c_{11}\varepsilon_{11} + c_{12}(\varepsilon_{11} + \varepsilon_{33})$, and $\varepsilon_{33} = -2(c_{12}/c_{11})\varepsilon_{11}$ [29]. Therefore, the elastic strain energy per unit volume $U_{elastic} = \sigma_{11}\varepsilon_{11}$. The elastic constants are typically expressed in the unit of 10^{11} dynes/cm^2; and at 300°K, c_{11}=12.88, c_{12}=4.83 for Ge(100), while c_{11}=16.56, c_{12}=6.39 for Si(100) [29-30]. For x=0.10, interpolating the elastic constants between those of Ge(100) and

Si(100), we find that $U_{elastic}$ is less than 4% of the average energy density deposited in the collision cascade during a 100 keV Si implantation of the same film [20]. Therefore, the pre-existing pseudomorphic strain is unlikely to affect the retained damage very much. However, this argument comparing the average cascade energy density and strain energy density applies only to the part of damage formed promptly and locally within the cascade.

3.1.2. Implantation-Induced Strain

Both symmetrical (400) and asymmetrical (311) rocking curves were obtained at room temperature in air as little as one hour after implantation, as well as several months later. All epi-GeSi films discussed in this section have initial perpendicular strain values consistent with the values calculated from linear elasticity theory for the pseudomorphic films. The perpendicular strain in these as-implanted samples relaxes very little at room temperature (<0.01% in strain value in the experimentally accessible time frame, ranging from 1 hour to several months after implantation). The parallel strain $\varepsilon^{||}$ for all pseudomorphic samples considered here, implanted or not, is zero within the experimental sensitivity ($\sim 10^{-4}$). The perpendicular strain profiles were extracted by simulating the experimental rocking curves using dynamical x-ray diffraction theory [31-35]. The *induced* strain is defined by measuring the difference in the *total* strain values for a sample before and after ion implantation. Similar to the case of implantation-induced damage, the *maximum* values of these extracted perpendicular strain profiles are used for easy analysis and manipulation of data.

Figure 3.2 shows the values of the *induced* maximum perpendicular strain, plotted as a function of the ion dose for Ge, $0.10 \leq x \leq 0.20$ and Si. These values are always positive (compressive) in the Ge-Si system as-implanted with Si, P, and As ions. Although derived using a different analytical tool, the dose dependence of the implantation-induced perpendicular strain resembles that of the implantation-induced damage as shown in Fig. 3.1. Three dose regimes also exist here: first the induced strain increases slowly up to ~ 0.15-0.20 %, which value appears to be

a function of the Ge content in a sample; then the induced strain rises at a much faster pace and finally the samples are amorphized. The x-ray diffraction method becomes ineffective prior to amorphization due to the loss of x-ray diffraction intensity resulting from heavy damage introduced by the implantation.

If we look at the strain-dose dependence in Fig. 3.2 for GeSi and compare it with the dotted lines for bulk Si (open Up Triangles), it is clear that the presence of 10-20% of Ge atoms in the alloy substantially increases the amount of implantation-induced strain. One also observes that the strain values on the solid line are much higher than those obtained from linear interpolation of the values on the two dotted line for bulk Si and Ge. Examination of Fig. 3.2 further reveals that the implantation-induced strain in the Ge-Si system again increases with the mass of the incident ions and the content of Ge in the alloy, much like the case of implantation-induced damage (cf. Fig. 3.1).

It has been shown that the induced maximum perpendicular strain generated by Si ion implantation at room temperature in pure Ge and Si is approximately linearly related to the maximum relative damage, with a proportionality constant of ~ 0.013 [36,37]. This result was interpreted as meaning that in both bulk Si and Ge it is the damage that creates strain and that equal increments of damage produces roughly equal increments of strain. Since the uniform pseudomorphic strain in a non-implanted GeSi film does not create damage measurable by channeling, it has to be the implantation-induced damage that generates the additional strain in GeSi alloys as well [15]. However, the relationship between the induced damage and the induced strain in GeSi is more complicated than that in bulk Si and Ge. The data for induced damage versus the induced strain for both pseudomorphic and relaxed GeSi are plotted in Fig. 9 in appendix A1. Even though it is shown in Sec. 3.1 that the preexisting strain in epi-GeSi does not noticeably affect the implantation-induced damage as measured by channeling, the implantation-induced perpendicular strain in a pseudomorphic GeSi film is larger than that generated in a relaxed GeSi film of the same x and by the same implantation [20]. Since the ion channeling technique cannot provide microscopic details of these defects, it is possible that different

inventories of defects may cause the same amount of damage as determined by channeling analysis, thus generating different amount of strain [15,24]. This possibility will be discussed further in Sec. 3.2.1.

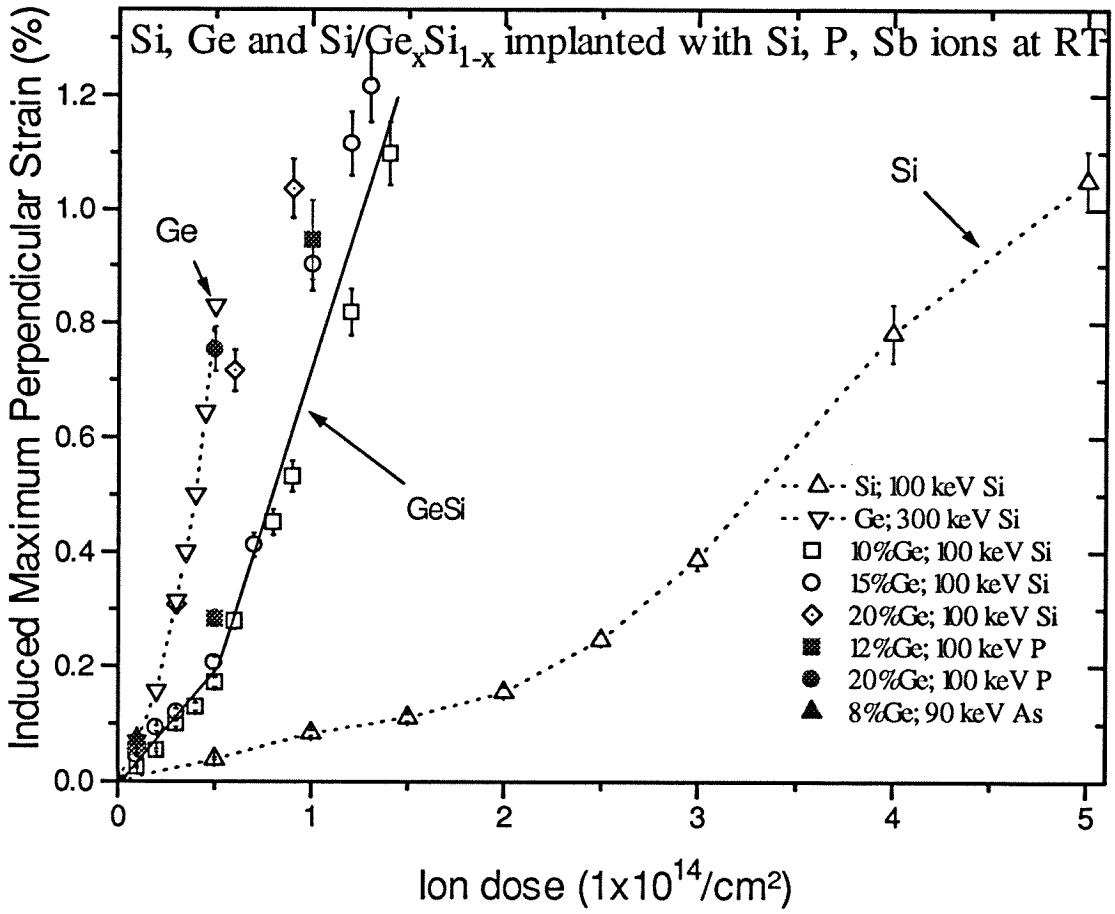

Fig. 3.2. The *induced* maximum perpendicular strain in ion-implanted Si(100), Ge(100) and pseudomorphic Si(100)/Ge_xSi_{1-x} ($0.10 \leq x \leq 0.20$) plotted versus the ion dose. The solid squares and solid circles correspond to 100 keV P implanted x=0.12 and x=0.20, respectively. The data for 90 keV As implanted x=0.08 is plotted as well (solid Up Triangle). Two dotted lines connect the data for bulk Si (open Up Triangles) and bulk Ge (open Down Triangles), respectively. A solid line is added as a guide to the eye to indicate the highly nonlinear nature of induced strain versus the ion

dose in the Ge-Si system. All implantations were performed at room temperature. Detailed implantation parameters such as ion species, energy and Ge content can be found in the inserted legend. The data points shown in Fig. 3.2 correspond to the same set of samples whose implantation-induced damage values are plotted in Fig. 3.1.

3.1.3. General Discussion of Induced Damage and Strain Versus Dose

Bai and Nicolet have reported almost identical nonlinear dependence of implantation-induced damage and strain versus dose for Si(100) as-implanted with F, Si, Ar, and Xe ions at various ion energies [16,36]. Both the implantation-induced damage and strain in that case first increase slowly with dose until a critical value of damage (~15%) is reached, and then rises rapidly until a continuous amorphous layer is formed. As shown in Figs. 3.1-3.2 for the as-implanted GeSi films, the implantation-induced damage and strain initially increase slowly with dose until a critical value of ~ 10-20% is reached, which value appear to be a function of the Ge content in the alloy. Holland *et al.* have observed a similar nonlinear relationship between the implantation-induced damage versus dose for Si(100) implanted with 100 keV ^{30}Si ions [38]. The initial slow increase of the damage and strain versus dose for the low dose regime in Figs. 3.1-2 is probably due to a considerable recombination of implantation-induced point-defects at room temperature, as proposed by both Holland *et al.* and by Bai and Nicolet [16,38].

Holland *et al.* also suggested that the "critical dose" for the onset of the transition from the initial slow increase of damage to the region of rapid buildup is at ~ $2x10^{14}$ Si/cm^2 for Si self-implantation [38]. They observed a sudden increase in the concentration of divacancy or higher-order vacancy clusters at this critical dose by comparing the results of single-alignment and double-alignment channeling measurements from the implanted Si before and after annealing. They further proposed that the rapid increase of implantation-induced damage right above the critical dose may be due to a cooperative process where preferential sinking of interstitial-like defects by regions of amorphous Si promotes the growth of vacancy-like defects in surrounding

regions, which in turn leads to further amorphization. On the other hand, Bai and Nicolet suggested that the retained defects generate perpendicular strain, and as the damage rises to the critical value (~10-20%), a large amount of energy is stored in the damaged region and additional defects created by the ion beam will cause the collapse of the damaged region into large disorder zones. They proposed that the c-a transformation should occur spontaneously as a cooperative process due to the overlapping of heavily damaged crystalline regions [16]. In general, c-a transformation is thought to take place spontaneously during implantation when the free energy of the damaged crystalline phase equals that of amorphous Si [39]. Numerous models exist for the process of ion-beam-induced c-a transformation, but a universal model that is capable of explaining data measured using a wide spectrum of techniques without controversy does not seem to be available yet [2,40,41]. Since the data presented in Figs. 3.1-2 does not provide the microscopic details of these implantation-induced defects, I shall not attempt to suggest which models might be more applicable to the case of ion-implanted GeSi.

3.1.4. Induced Damage and Strain Versus Implantation Temperature

I have described in the previous sections the induced damage and strain for Si, GeSi and Ge samples as-implanted at room temperature. Eriksson *et al.* reported that for bulk Si implanted at 150°C or at higher temperatures, the induced damage is greatly reduced as compared to a Si sample implanted at room temperature [42]. Morehead *et al.* have also reported that the dose required to amorphize Si at slightly elevated implantation temperatures (~100°C) may be an order of magnitude higher than that needed for room temperature implantation [43]. This increase in the amorphization dose is very likely caused by the increased mobility of point defects at elevated implantation temperature, which can facilitate the recombination of defects during implantation (i.e., "dynamic annealing") [44,45]. Picraux *et al.* have shown systematically that implantation-induced damage in Si is a strong function of the implantation temperature, and that the dynamic annealing occurring during implantation at a fixed temperature is not equivalent to post-

implantation annealing at that specific temperature [46,47]. Since as described the thermal budget permissible for annealing of implanted strained Si/GeSi is narrower than that of Si, one can try to minimize the induced damage and strain in as-implanted GeSi by performing implantation at elevated temperatures. If this succeeds, the demands on post-implantation annealing treatments may be significantly reduced in Si/GeSi. I therefore continued to investigate the induced damage and strain in strained Si/GeSi samples as-implanted at slightly elevated temperatures (up to 150°C) and published the results in A2 [48]. A discussion of the induced damage and strain in GeSi versus the implantation temperature is presented as follows.

Figure 3.3 plots the extracted maximum relative damage versus the implantation temperature for nearly pseudomorphically strained $Ge_{0.10}Si_{0.90}$ as-implanted with 320 keV Si ions for various doses (solid symbols and solid lines). At a fixed dose, the maximum relative damage always decreases with increasing implantation temperature. The most notable feature in this figure is that at sufficiently high temperatures of implantation, virtually all detectable damage, as measured by channeling spectrometry, disappears. The temperature at which this occurs increases with increasing dose. In terms of absolute temperature, the transition from full amorphization to a barely detectable amount of damage is very abrupt. For example, the maximum relative damage created in $Ge_{0.10}Si_{0.90}$ with a dose of 1 $x10^{15}$ Si^+/cm^2 reaches 100% (amorphization) at 60 °C, but it plunges to only ~2 % when the implantation temperature is increased to 100 °C.

Figure 3.3 also included three curves taken from work published by Haynes and Holland (open symbols and dotted lines), which data extend the systematic trend of damage enhancement with increasing Ge content in the alloys from RT implantation to elevated temperatures [18-20,49]. For example, the damage introduced with a dose of $1x10^{14}$ Si ions/cm^2 in x=0.35 is consistently much higher than that in x=0.15, which is still higher than that in x=0.10 from ~40-90 °C. These data of Haynes and Holland also show that the retained damage is a steep function of the implantation temperature. Our experimental data agree well with those of Haynes *et al.* in showing that the retained damage becomes quite small for implantation temperatures greater than ~ 100 °C. Haynes *et al.* have suggested that this abrupt reduction in the retained damage at higher

implantation temperature is a result of the increase in the point-defect mobility so that it is easier for the defects to diffuse out of the collision cascades [18,19].

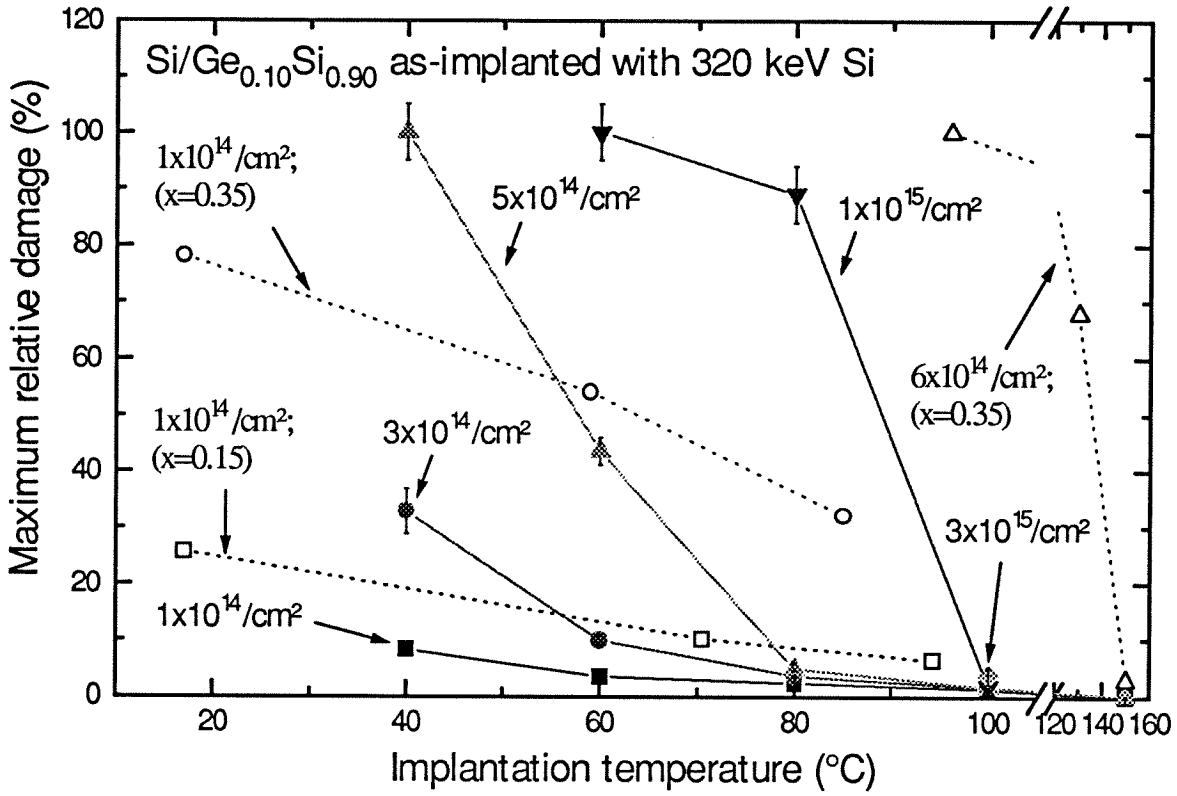

Fig. 3.3 The values of the maximum relative damage (extracted from the measured channeling spectra) plotted against the implantation temperature for as-implanted strained $Si/Ge_{0.10}Si_{0.90}$ with the dose of 320 keV Si ions as the parameter (solid symbols and solid lines). The data plotted as open symbols and dotted lines are taken from Refs. [18,19] for relaxed GeSi implanted with 80 keV Si ions at various temperatures.

A decrease in implantation-induced damage and/or strain with increasing implantation temperature has been reported for Si, Ge, relaxed GeSi, GaAs, and InP [18,19, 48-53]. Morehead and Crowder have proposed a simple model to estimate the temperature dependence of implantation-induced damage [43]. The model implies that the maximum relative damage created by implantation is linearly proportional to the ion dose. The model has been used in the past in connection with implantation-induced damage in Si, Ge, GaAs and unstrained Ge_xSi_{1-x} [18,19,49,50]. However, as shown in Fig. 3.1 and Fig. 3.3, the relationship between the maximum retained damage and the ion dose is clearly non-linear in general. Thus this particular model is not generally applicable because it fails in the present case.

For implantation performed at slightly elevated temperatures ($70°C<T_{imp}<150°C$), Haynes and Holland also showed that films with high Ge content (x=0.50-0.80) may even retain more implantation-induced damage than pure Ge [18,19]. Since the deposited energy density is higher in pure Ge than in GeSi, this phenomenon indicates that the deposited cascade energy is not the only important factor governing the amount of the retained damage as the implantation temperature increases. The higher fraction of retained damage in GeSi (over Ge) also suggests that the addition of Ge atoms to the Si matrix retards the mobility of implantation-induced defects very effectively, which effectiveness appears to be a strong function of substrate temperature and Ge content. I have discussed in Sec. 3.1.1 that the increased cascade-energy-density and the decreased mobility of defects in GeSi (compared to those in Si) make roughly equal contributions to the observed damage enhancement in $0.1\leq x\leq 0.2$ for room temperature Si implantation [20]. I suspect that the contribution from the cascade-energy-density factor will decrease in importance with increasing implantation temperature, however, as the recombination of defects becomes more important [54].

Besides the induced damage, implantation-induced perpendicular strain for pre-strained $Ge_{0.10}Si_{0.90}$ also decreases with increasing temperature of implantation, and becomes rather small for implantation at ~ 100 °C, as shown in Fig. 8 of appendix A2 [48]. Mantl *et al.* have observed that the strain in 10 nm-thick strained $Ge_{0.20}Si_{0.80}$ capped with a

10 nm Si layer relaxes during the 750 keV Si implantation at 240°C, and that the amount of strain relaxation increases with the ion dose [6]. Kringhøj *et al.* have recently reported that strain relaxation may be induced *in-situ* during MeV Si implantation into strained GeSi films at ~250°C, but no relaxation was observed for samples implanted at room temperature [55]. These findings suggest that there is a significant difference in the nature and/or mobility of defects between room-temperature implanted GeSi and those implanted at elevated temperatures.

3.2. Behavior of GeSi Annealed After Implantation

I will now discuss the annealing behavior of ion-implanted GeSi samples. The results of the removal of implantation-induced damage and strain by annealing of non-amorphized samples will be presented in Sec. 3.2.1. The behavior of solid-phase epitaxial regrowth for amorphized Si and GeSi will be discussed in detail in Sec. 3.2.2.1 and Sec. 3.2.2.2, respectively. Sec. 3.2.2.2 contains four subsections, which cover experimental data on solid-phase regrowth of strained GeSi, relaxed GeSi, and Si implanted with Si, P, or As ions. A general discussion and a mini-review of the available papers published on solid-phase epitaxy of GeSi in the literature is also included in Sec. 3.2.2.2.

3.2.1. Non-Amorphized Samples:

The annealing behavior of non-amorphized GeSi samples after Si-implantation is summarized in Fig. 3.4, which shows the induced maximum relative damage in a nearly pseudomorphic Si(100)/$Ge_{0.10}Si_{0.90}$ plotted versus the annealing temperature (solid symbols, solid lines). Data obtained from Ref. 2 for self-implanted Si is also presented in Fig. 3.4 (open symbols, dotted line). Figure 3.4 shows that the retained damage for both non-amorphized Si and GeSi

samples already decreases considerably after annealing at 300°C for 30 min. For self-implanted Si, it is reported that divacancies disappear after annealing in a temperature range of 200-300°C with a characteristic time of ~30 min [47,56]. Similar defect-removal mechanisms might be applicable for GeSi as well. The significant amount of residual damage left in both Si and GeSi at 300°C implies that the implantation-induced damage consists of a hierarchy of various defect structures of vacancies and interstitials [2]. For these non-amorphized samples, post-implantation furnace annealing at 550°C for 30 min can remove almost all of the damage measurable by ion channeling. The values of maximum relative damage in these samples decrease monotonically with the annealing temperature (from 200-550°C). Figure 3.4 demonstrates that the annealing behavior for non-amorphized GeSi is similar to that for Si, as revealed by simple isochronal annealing experiments.

The dependence of implantation-induced strain versus the annealing temperature is plotted in Fig. 9 of appendix A2, which indicates that if the sample is not amorphized, only a small amount of the induced maximum perpendicular strain is retained after 550 °C annealing for all doses. Similar behavior is observed in Fig. 3.4 for the implantation-induced damage. The strain recovery thus follows that of the damage. These facts can be simply interpreted by assuming that it is the induced damage that causes the strain. This notion has been stated before in Sec. 3.1.2 [20]. The total perpendicular strain in an implanted Si/GeSi never falls below its initial value after annealing at 550°C. Therefore, if the implantation does not amorphize Si/GeSi, induced damage and perpendicular strain are largely reversible, provided that no strain relaxation has taken place.

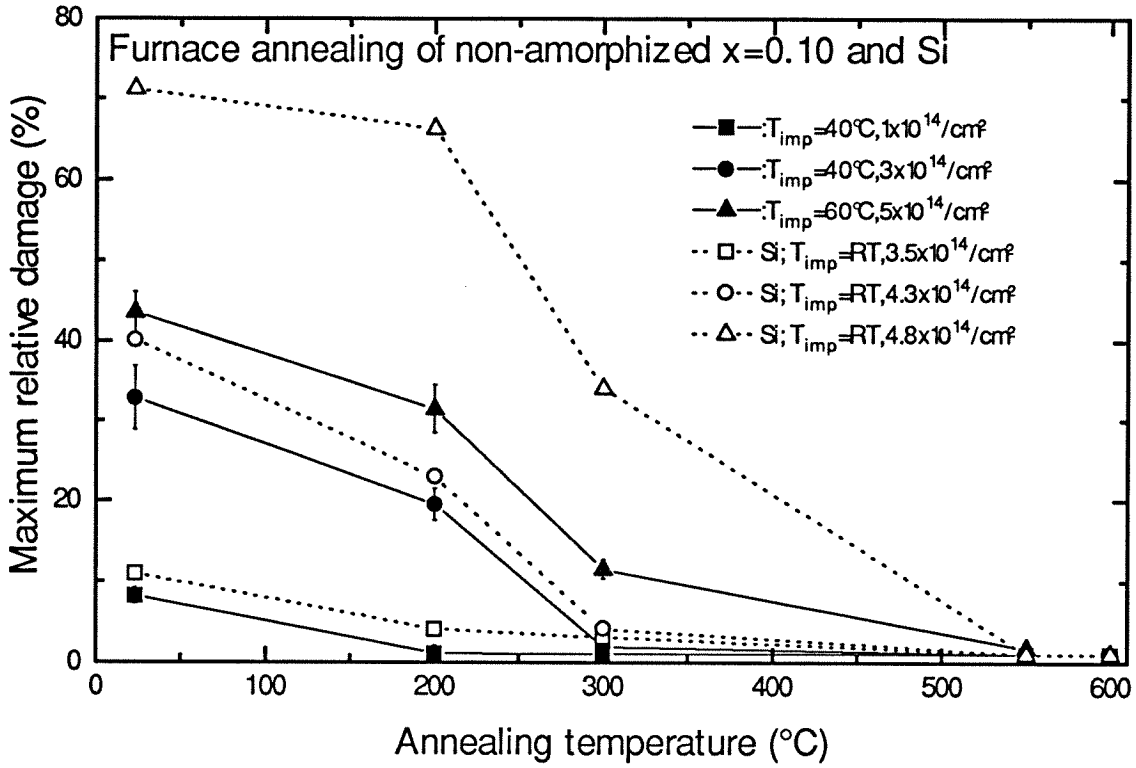

Fig. 3.4.: The values of maximum relative damage of nearly pseudomorphic Si(100)/$Ge_{0.10}Si_{0.90}$ samples implanted with 320 keV Si at 40 and 60°C plotted against the annealing temperature (solid symbols, solid lines). The data for room temperature self-implanted Si is obtained from Ref. 2 and is included for comparison (open symbols, dotted lines). All data shown here correspond to samples that do not have a continuous amorphous layer formed after the implantation ("non-amorphized samples"). All annealing experiments were performed in high vacuum (~$5x10^{-7}$ Torr) for a common duration of 30 min. The detailed implantation parameters can be found in the inserted legend.

It has been mentioned in Sec. 3.1.2 that channeling analysis determines damage in a microscopically unspecified way. Due to this, a single value of damage may correspond to different inventories of defects, and hence also to different amounts of induced strain [24]. After

the non-amorphized $Si/Ge_{0.10}Si_{0.90}$ samples are annealed from 200-500°C, the relationship between the induced maximum strain and the induced maximum relative damage at a given annealing temperature becomes very complicated, with data points scattering in a nearly random fashion. This result shows that the relationship between implantation-induced damage and strain in pre-strained GeSi differs from that in bulk Si and Ge and that it depends on the implantation and annealing temperatures as well. A deep understanding of the relationship between the implantation-induced damage and strain in GeSi requires a careful analysis of the microscopic nature of defects and their effects on the lattice strain profiles. Such analysis is expected to be very complex and difficult to achieve experimentally.

3.2.2. Amorphized Samples

Section 3.2.2 contains two subsections. I will first provide a short summary and introduction to the field of solid-phase epitaxy of Si and Ge in Sec. 3.2.2.1. It will be followed by a comparison and detailed discussion on the regrowth behavior of Si and GeSi in Sec. 3.2.2.2.

3.2.2.1. Solid-Phase Epitaxy of Si and Ge

Solid-phase epitaxy of amorphous Si on crystalline Si substrates has been studied extensively for more than two decades and several excellent review articles exist on this subject [57,58]. The driving force for solid-phase epitaxy is recognized as due to the bulk free energy of c-Si being lower than that of a-Si (by ~ 0.1 eV/atom at 300 K) [59]. Because of this free energy difference, random nucleation and growth of small crystalline Si clusters in the amorphous phase can take place at a given temperature; if these crystallite are not all well-oriented with each other, the resulting phase will be poly-Si instead of crystalline Si [57]. Unless this process of random nucleation and growth of crystalline Si nuclei is suppressed and the growth is confined to a layer-by-layer fashion at the crystalline-amorphous interface, defect-free regrowth of amorphous Si into crystalline Si cannot be realized [1]. Solid-phase epitaxy can occur when an amorphous layer is in direct contact with an atomically clean substrate, which then serves as a template for the ordered

crystalization of the amorphous film in a layer-by-layer fashion at temperatures near or well below its melting point [29,58]. This atomically clean substrate does not have to be atomically sharp for solid-phase epitaxy to take place [60]. The kinetics of solid-phase epitaxial regrowth of Si has been studied thoroughly, compared to few papers being available in the literature for Ge [47,57,61,62]. It has been shown that during solid-phase epitaxial regrowth, the velocity of interface movement (i.e., "regrowth velocity" or "solid-phase epitaxy rate") for intrinsic Si and Ge are characterized by unique thermal activation energies of 2.68 eV and ~2.1 eV, respectively, and this velocity depends on the crystallographic orientation of the substrates and the impurity concentration in the amorphous layers [29,57,58]. Spaepen devised a model based on Si(111) substrates that regards solid-phase epitaxy as a simple process of bond rearrangement which begins with single bond-breaking events and proceeds as a defect moves along a crystalline ledge [63]. That model was later extended to Si(100) and the single activation energy for solid-phase epitaxy was explained as the sum of the energy required for bond-breaking at the a-c interface and the increased energy for bond distortion [64]. The orientation dependence of the solid-phase epitaxy rate can be explained geometrically by assuming the rearrangement of bonds propagate along the (111) planes [29,65]. Other models for solid-phase epitaxy kinetics that involve diffusion and capturing of defects such as charged dangling bonds or self-interstitials from the amorphous film to the crystalline substrate have also been proposed [66,67]. These models for the kinetics and the origin of the activation energy for solid-phase epitaxy differ primarily on the microscopic natures of defects. It remains very difficult experimentally to directly differentiate among these microscopic types of defects during regrowth.

Dopants such as phosphorus or boron can enhance the solid-phase epitaxy rate in Si and Ge over a wide range of temperatures [61,62,68,69]. This effect was hypothesized to be caused by the increased charged vacancy concentration at the a/c interface, which can be a strong function of the position of Fermi level [61]. If both n-type and p-type dopants are present in the film with comparable concentration, dopant compensation effect is observed where solid-phase epitaxy rate is brought back close to its value of an intrinsic Si layer [69]. Williams and Elliman

further proposed that the kinetics of solid-phase epitaxy is controlled by creating and moving kink-like steps on (110) ledges at the a/c interface [58,70]. According to that model, addition of dopants can decrease the migration energy of kinks and/or increase the concentration of charged kinks. Even though the dopant-induced change in the regrowth velocity is apparently controlled by the electronic properties at the a/c interface, these models that used kink-sites or vacancy concentration cannot explain the regrowth behavior at high temperatures when the doped films become nearly intrinsic [57]. Thus even though solid-phase epitaxial regrowth of Si is routinely used in the IC industry today, Olson and Roth suggested that a detailed and well-accepted atomistic model that could satisfactorily explain the kinetics of solid-phase epitaxy did not appear to be available as yet [57].

Recently, Aziz has suggested that solid-phase epitaxy of Si may be well-described by an alternative two-stage mechanism, each having an activation energy separated by less than 1.0 eV [71]. Aziz and Lu *et al.* also proposed that they have ruled out the possibility of any regrowth mechanisms in which a *single* rate-limiting step occurs in the bulk of either crystalline or amorphous phase [71,72]. If this proposal of two-stage or multi-stage rate-limiting processes for solid-phase epitaxy is true, then measuring the precise value of the activation energy for a given material may not be very meaningful [73]. Therefore, no serious attempt is made in this thesis work to measure the precise values of the activation energies for the solid-phase epitaxy of Ge_xSi_{1-x}.

3.2.2.2. Solid-Phase Epitaxy of GeSi

In section 3.2.2.2, which contains four subsections, I will continue to discuss the behavior of solid-phase epitaxial regrowth of epi-GeSi on Si(100) substrates and compare it with that of Si. Since my study on solid-phase epitaxy of P-implanted GeSi has been published in papers A3 and A4 in the appendix, I will only briefly summarize the P-implanted work here, while discussing more of the data for arsenic-implanted GeSi and Si (Sec. 3.2.2.2.1 and Sec. 3.2.2.2.2). The results

on the clean regrowth of a fully relaxed GeSi is reported in Sec. 3.2.2.2.3. A mini-review and a general discussion of the field of solid-phase epitaxy of GeSi is presented in Sec. 3.2.2.2.4.

3.2.2.2.1. Degraded Crystallinity for Metastable GeSi

To heavily dope Si by ion implantation, it is common practice to amorphize the sample and subsequently anneal it so that solid-phase epitaxy can take place [1,2]. However, for metastable strained Ge_xSi_{1-x} layers, numerous reports indicate that implantation-induced amorphization and solid-phase epitaxy result in relaxed GeSi of poor crystalline quality [4-7]. To demonstrate the difference between the solid-phase epitaxial regrowth of Si and GeSi, I have selected two metastable pseudomorphic Si/Ge_xSi_{1-x} samples (x=0.08, 0.16) of a common thickness of 145±10 nm and amorphized them with high-dose arsenic implantation. Several arsenic-implanted Si reference samples, together with these epi-GeSi layers, are subsequently annealed under either steady-state or rapid thermal annealing conditions. Since I found that the general regrowth behavior in GeSi and Si is insensitive to the annealing techniques, only the results of samples annealed under steady-state conditions will be shown here in Sec. 3.2.2.2.1 and 3.2.2.2.2. A report on the regrowth behavior of arsenic-implanted GeSi and Si after rapid-thermal annealing can be found in Ref. 74. Figures 3.5(a)-(c) show three sets of <100> channeling spectra for Si(100), x=0.08 and x=0.16 implanted with $1.5x10^{15}/cm^2$ arsenic ions at 90 keV before and after furnace annealing, respectively. The peak concentration of As ions is roughly $3x10^{20}/cm^3$, as estimated from both the backscattering spectra and TRIM simulations. For all as-implanted samples, the backscattering yields that correspond to the near-surface portions of the layers reach the levels of their random spectra, which indicates that the top ~125 nm of these 145 nm-thick samples are amorphized after implantation. The original Si-GeSi interfaces for the as-implanted x=0.08 and x=0.16 remain sharp and undamaged within the sensitivity of cross-sectional transmission electron microscopy. The amorphous/crystalline fronts in Figs. 3.5(a)-(c) all move toward the surface after annealing at 500°C for 30 min, which indicates that solid-phase epitaxy

has taken place in all Si/Ge_xSi_{1-x} samples (x=0,8%,16%), resulting in thinner amorphous regions. After annealing at 550-800°C for 30 min, the backscattering yields of the entire amorphized layers decrease further, suggesting the completion of solid-phase epitaxial regrowth [61,62,65,75]. The channeling spectra of amorphized Si after solid-phase epitaxy are indistinguishable from that of a virgin sample; however, the spectra for amorphized GeSi after solid-phase epitaxy show a step-like increase in yields at and below ~1.1 MeV. The step-like increase in the backscattering yields for the regrown GeSi has been observed before, and can be explained by the formation of numerous dislocations at and near the Si/GeSi interface that are responsible for the strain relaxation of epi-GeSi [74-77]. The channeling minimum yields for these regrown GeSi are ~6-8%, which values are considerably higher than those of the as-deposited Ge_xSi_{1-x} (~3-4%) [15,80]. The channeling spectra indicate that a regrown GeSi is inferior to that of an as-deposited film in crystalline quality, while the regrown Si has excellent crystallinity comparable to that of bulk Si. The reason for this difference between regrown Si and GeSi will be discussed later in detail at Sec. 3.2.2.2.4. A similar phenomenon of degraded crystallinity for metastable GeSi after solid-phase epitaxy has also been reported for Si, P and Sb amorphized Ge_xSi_{1-x} [6,12-14,75-77].

Olson and Roth have showed that the solid-phase epitaxy velocity of undoped Si(100) at 500°C is ~0.57 nm/min, and Paine *et al.* have reported that this velocity at 500°C for undoped x=0.054 is ~0.20 nm/min, and for undoped x=0.17 is ~0.24 nm/min [57,78]. My data in Fig. 3.5 show that the solid-phase epitaxy velocity at 500°C is fastest in arsenic-implanted Si (~3.5 nm/min), while it is ~1.6 nm/min for x=0.16 and slowest in x=0.08 (~0.58 nm/min). Compared with the data in the literature, the regrowth velocities for arsenic-implanted Si and GeSi as shown in Fig. 3.5 both increase considerably over those of undoped Si and GeSi, and this enhancement appears to be dependent on the Ge content in the Ge-Si system [74]. Acceleration of regrowth velocity in arsenic-implanted Si has also been reported, and the results in Fig. 3.5 is consistent with those in the literature [57,68]. A similar enhancement in the velocity of solid-phase epitaxy is also reported for phosphorus-implanted GeSi and Si [65,75]. However, it should be pointed out that in the case of arsenic-implanted Si, the regrowth velocity is a complicated function of the

arsenic ion dose, where velocity enhancement as well as retardation, precipitation of dopants and dopant-induced random nucleation and growth have all been observed [57].

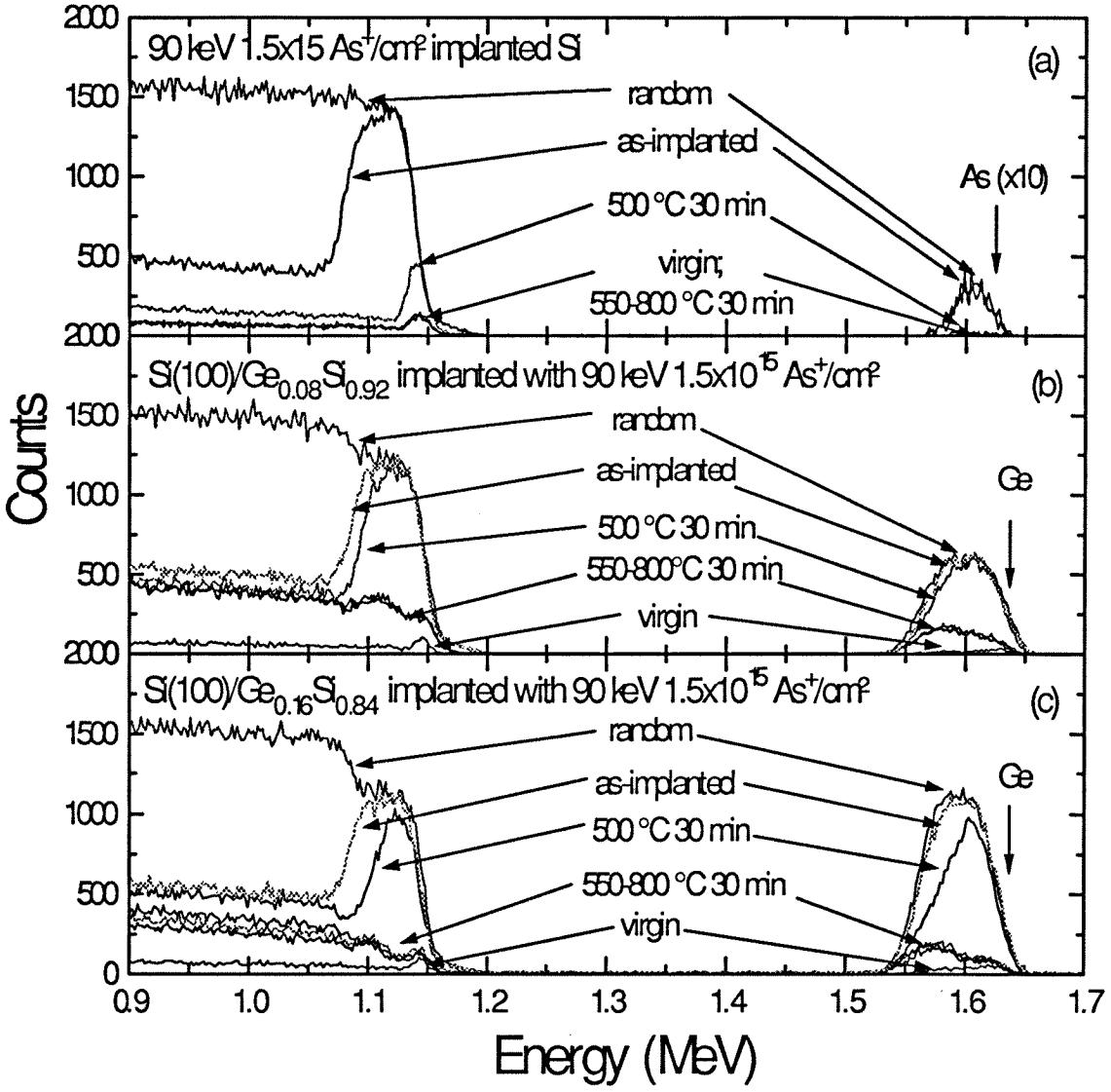

Fig. 3.5. 2 MeV ^{4}He ion channeling analysis along the [100] direction for (a): bulk Si(100); (b): x=0.08; and (c): x=0.16 before/after implantation with 1.5×10^{15} As/cm^2 at room temperature and subsequently annealed in a high-vacuum (~5×10^{-7} Torr) furnace at 500-800°C for 30 min at each temperature. The two epi-GeSi films have a common thickness of 145±10 nm. The channeling and the random spectra of

unimplanted samples before annealing are also plotted for reference. The arsenic signal in Fig. 3.5(a) is magnified ten times. The detector angle is 170° with respect to the direction of the incident ^{4}He beam.

3.2.2.2.2. Strain Relaxation for Metastable GeSi After Solid-Phase Epitaxy

Figure 3.6 shows the x-ray rocking curves for arsenic-implanted Si (Fig. 3.6(a)), x=0.08 (Fig. 3.6(b)), and x=0.16 (Fig. 3.6(c)) after 30-min furnace annealing at 500-800°C. The rocking curves in Fig. 3.6 and the channeling spectra in Fig. 3.5 correspond to the identical batch of arsenic-implanted and annealed samples. The rocking curve of the as-implanted Si in Fig. 3.6(a) is almost indistinguishable from that of a virgin Si sample because the implantation-induced amorphous Si layer produces insignificant coherent x-ray diffraction signals. After the implanted Si is annealed at 550-800°C for 30 min, the amorphous Si regrows completely by solid-phase epitaxy (cf. Fig. 3.5(a)), and two weak peaks are observed on both sides of the Si substrate peak. These weak signals as well as the small broadening found on the left-hand-side of the Si substrate peak are possibly caused by residual defects remaining after solid-phase epitaxy [81-83]. The rocking curves of the as-implanted GeSi samples in Figs. 3.6(b)-(c) do not contain noticeable GeSi diffraction signals arising from the non-amorphized bottom crystalline strained GeSi (of ~10-20 nm thickness) partly because the layer is too thin and partly because the diffraction intensity is severely weakened by the implantation-induced damage. After the implanted GeSi samples are annealed at 500°C for 30 min, weak diffraction signals appear in Figs. 3.6(b)-(c) near their pseudomorphic peak positions. This phenomenon can be attributed to the partially regrown amorphous GeSi (Figs. 3.5(b)-(c)) and to the removal of some defects in the bottom non-amorphized region. After the implanted $Ge_{0.16}Si_{0.84}$ samples are annealed at 550°C-800°C for 30 min (Fig. 3.6(c)), the rocking curves exhibit two distinctly different peaks: the first is very broad and centered roughly around ~ -0.25°, which corresponds to the Bragg angle of a fully relaxed $Ge_{0.16}Si_{0.84}$ film. Judging from the position and the intensity of this broad peak, we infer that the regrown layer is fully relaxed and has a crystalline quality inferior to that of the as-grown sample. The second peak is

located at ~ -0.42°, roughly where the Bragg angle of a pseudomorphic $Ge_{0.16}Si_{0.84}$ film is. This indicates that the lower crystalline portion of the GeSi film remains almost fully strained after furnace annealing at 800°C for 30 min. Similar results have also been observed in P-implanted x=0.12 after regrowth [75]. For the epi- $Ge_{0.08}Si_{0.92}$ film, the two diffraction peaks resulting from both regrown and non-amorphized bottom portions of the GeSi layer are not clearly separated in Fig. 3.6(b), possibly because these peaks are too close to be clearly resolved (cf. Fig. 3.6(c)).

I have also performed rocking curve measurements on 150 nm-thick pseudomorphic $Ge_{0.08}Si_{0.92}$ on Si(100) implanted and amorphized by 20 keV $1.5x10^{15}$ P/cm^2 and subsequently annealed under both steady-state furnace annealing and rapid-thermal annealing conditions. The common phenomena observed for metastable GeSi are such that once they are amorphized by Si, P, or As ions, the pseudomorphic strain of the regrown GeSi films cannot be preserved using either annealing technique. This behavior is very different from that of the non-amorphized case (Sec. 3.2.1). Cross-sectional transmission electron micrographs of these amorphized and regrown GeSi samples reveal that high densities of dislocations (10^{10}-10^{11}/cm^2) are always present in these films [75,77,84]. I therefore conclude that for metastably strained GeSi films, the initial pseudomorphic strain is lost and the crystalline quality of GeSi is considerably degraded after solid-phase epitaxial regrowth.

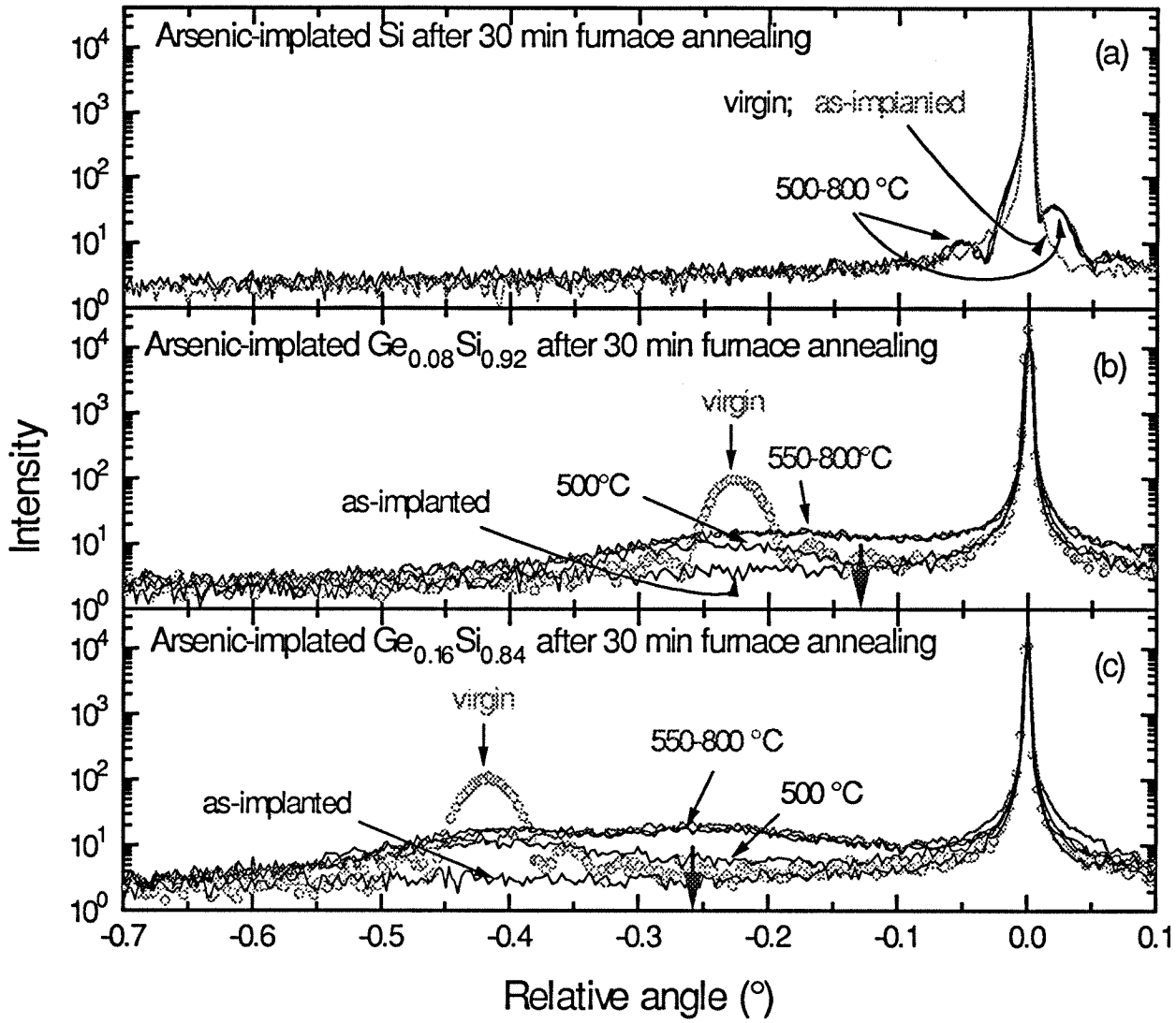

Fig. 3.6. Double-channel-cut five-crystal x-ray rocking curves of (400) symmetrical diffraction for (a): bulk Si(100); (b): x=0.08; and (c): x=0.16 before/after implantation with 1.5×10^{15} As/cm^2 at room temperature and subsequently annealed in a high-vacuum furnace at 500-800°C for 30 min, respectively. The origin of the abscissa in Figs. 3.6(a)-(c) is placed at the Bragg angle of a Si substrate (θ_B=34.575°; λ =1.541Å). The arrows on the abscissae of Fig. 3.6(b) and 3.6(c) indicate the signal position of the fully relaxed x=0.08 and x=0.16 epilayers, respectively.

3.2.2.2.3. Clean Regrowth of Fully Relaxed GeSi

I have just shown that the solid-phase epitaxy of metastably strained GeSi films on Si(100) are always accompanied by numerous defects. It is therefore interesting to investigate whether a thermally stable GeSi can regrow cleanly as in the case of Si(100). Figure 3.7 shows a thermally stable, fully-relaxed $Ge_{0.35}Si_{0.65}$ film on Si(100) after amorphization by Si implantation followed by solid-phase epitaxial regrowth under 30-min steady-state annealing in vacuum at 550°C. The regrown GeSi is of the same crystallinity as the virgin non-implanted film, within the sensitivity of channeling spectrometry and cross-sectional transmission electron micrographs (not shown). Similar clean regrowth in fully relaxed GeSi has also been independently reported by several groups, in clear contrast from those observed in metastable films [13,60,85]. For example, the regrowth velocities for strained Ge_xSi_{1-x} are found to be lower than that of Si, while those of strain-relaxed film is higher than that of Si [13,60,78]. The solid-phase epitaxy of a GeSi film seems to be very much dependent on its strain state. Chilton *et al.* have reported that the pseudomorphic strain and crystallinity of a 30 nm-thick $Ge_{0.16}Si_{0.84}$ film is preserved after solid-phase epitaxy, but not for a $Ge_{0.29}Si_{0.71}$ film of similar thickness, if measured by ion channeling technique [5]. Solid-phase epitaxial regrowth of a thin pseudomorphic $Ge_{0.10}Si_{0.90}$ film (~100Å) after Si implantation does not show detectable damage within the sensitivity of cross-sectional transmission electron microscopy, while numerous defects are observed for thicker films of similar x-value [13,14,75,86]. The regrowth behavior of epi-GeSi on Si(100) is thus influenced by its film thickness, its strain state, and the Ge content in the alloy. These data suggests that solid-phase epitaxy of GeSi is a complicated process which depends on several parameters, as will be discussed in greater detail in the next section.

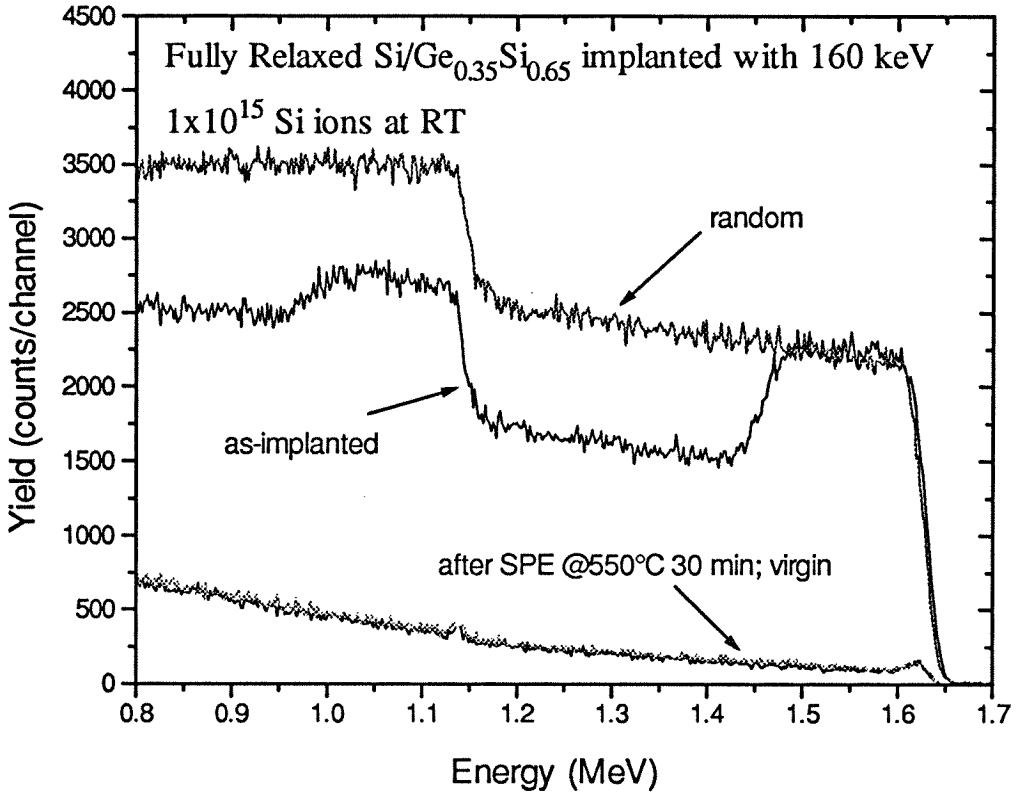

Fig. 3.7 <100> axial channeling spectra from a fully relaxed $Si/Ge_{0.35}Si_{0.65}$ implanted with 160 keV $1x10^{15}$ Si/cm² at room temperature before/after vacuum furnace annealing at 550°C for 30 min. The epi-$Ge_{0.35}Si_{0.65}$ (~ 1μm in thickness) was deposited on a 3μm-thick GeSi graded buffer layer and the as-deposited sample contains $\leq 10^8$ dislocations/cm² [87]. A random and a channeling spectrum of this as-deposited virgin sample are also plotted.

3.2.2.2.4. General Discussion of Solid-Phase Epitaxy of GeSi

Next, I would like to provide a general discussion of the behavior of solid-phase epitaxial regrowth of GeSi on Si(100). I have shown in the previous sections some experimental data on the regrowth behavior of both GeSi and Si. The major difference between the solid-phase epitaxy

of amorphous Si and GeSi films on Si substrates arises from the intrinsic strain introduced by the lattice mismatch between GeSi and Si [13,60,78,88]. Hydrostatic stress as well as non-hydrostatic stress have been shown to affect the rate of solid-phase epitaxy for pure Si and Ge [88-90]. For example, Aziz *et al.* have reported that the solid-phase epitaxy rate for a-Si grown on the tensilely-strained side is greater than that on the compressive side of elastically bent Si wafers [88]. Since considerable compressive biaxial stresses can be developed during solid-phase epitaxy of GeSi on Si, it is not surprising that the stresses in GeSi may also affect its regrowth kinetics, as will be discussed later.

Figure 11 of appendix A2 shows that the solid-phase epitaxial regrowth of a metastably-strained epi-GeSi results in extensive residual damage in the regrown layer [20]. There is, however, a distinct region of regrown GeSi about 20-30 nm thick with good crystalline quality lying right on top of the Si substrate. Similar results have been reported by Hong *et al.* and Lee *et al.* for Si-implanted x=0.10 and x=0.12, where they found a ~30-40 nm GeSi of good crystallinity sandwiched between the original a/c interface and the defective GeSi after the completion of solid-phase epitaxy [13,14]. These results suggest that an amorphous GeSi layer may regrow defect-free and pseudomorphically up to its "equilibrium critical thickness"; above this thickness, the regrown layer relaxes with a high density of defects. The data of Elliman *et al.*, Kringhøj *et al.* and Paine *et al.* all support the above suggestion by showing that a thermally-stable GeSi film with a thickness smaller than that of its critical thickness remains pseudomorphic and defect-free after solid-phase epitaxy [60,78,91,92]. A general definition of the equilibrium critical thickness is given as the pseudomorphic layer thickness at which the work done by the layer stresses during defect formation equals the work that is required to introduce the defects [78,93]. Since the solid-phase epitaxy of metastable GeSi results in highly defective films that should be avoided for electronic applications, an accurate model that can predict the crystalline quality and strain of *any* GeSi films after regrowth is of great interest for the practical design of GeSi devices. I will therefore carefully examine the models available in the literature for solid-phase epitaxial regrowth

of GeSi. These models will be used to fit my data as well as all available data in the literature. The limitations of these models will be discussed.

More than a dozen papers have been published so far on the solid-phase epitaxial regrowth of GeSi. A chronological collection of relevant publications on solid-phase epitaxy of strained GeSi is listed in Table 3.1, where the ion species, film thicknesses, Ge content, and the crystalline qualities and strain states of both as-deposited and regrown GeSi samples are tabulated for each study. A popular model for the solid-phase epitaxy of GeSi was proposed by Paine *et al.* [60,78]. They carried out detailed calculations of the critical thickness of regrown GeSi for specific types of strain-relieving defects (i.e., 60° dislocations and 90° partial plus stacking faults) based on a modification of Matthews' theory (from the strain energy approach). This is the most quantitative model existing today for the critical thickness of GeSi during solid-phase epitaxy. They also performed extensive experimental studies on the detailed regrowth kinetics of GeSi. For GeSi alloys with large lattice mismatch ($x \geq 11.6\%$), it is shown that planar defects such as 90° partial and stacking faults can be generated during regrowth to relieve the stress. This relaxation process is accompanied by faceting of the a/c interface during solid-phase epitaxy [6,60,78,93-95]. After a GeSi layer reaches its critical thickness, this model predicts that the regrowth front will facet from planar to a V-shaped sawtooth morphology to relieve the stress, which changes the regrowth surface from (100) planar growth to {111} facet growth. I have also observed significant sawtooth-like faceting during the regrowth of P-implanted x=0.12 at 500°C (see Fig. 2(d) of A3) [75]. Similar faceting of regrown fronts during solid-phase epitaxy of metastable GeSi have also been reported by Lee *et al.*, Wong *et al.* and Elliman *et al.* [14,92,96]. However, Paine *et al.* have also stated that the above critical-thickness model unrealistically ignores the kinetic barriers for defect nucleation, and that the predicted critical thickness values may be strongly dependent on the value chosen for the stacking fault energy [78]. The critical thickness values predicted from that model may thus have large discrepancies from values experimentally observed for GeSi films with relatively higher Ge content ($x \geq 0.12$) [78].

The work summarized in Table 3.1 suggests that the critical thickness for x=0.04 to regrow coherently should be no greater than ~1700Å, and that of x=0.16 is probably ~350 Å. These values appear to be a steep function of the Ge content in the alloys, and they are generally larger than the critical thickness values calculated by Paine *et al.* [62,78]. Besides the fact that this model ignores the kinetic barriers for defect nucleation and is dependent on the stacking fault energy values, the difference between the calculated and the experimentally observed critical thickness values may also be related to the sensitivity limits of instrumentation [97]. The experimental techniques used for most publications in Tab. 3.1 are ion channeling, time-resolved reflectivity measurements and transmission electron microscopy, As previously described in Chapter 2, channeling actually measures the tetragonal distortion of the film and is not as sensitive to strain relaxation as x-ray rocking curves, which have about the same sensitivity to dislocations as transmission electron microscopy (~10^6/cm^2). Tools of higher detection resolution to defects and hence to the strain relaxation process, such as x-ray topography and etch pits techniques, are preferred for checking the supposedly "defect-free" GeSi films after solid-phase epitaxy. The major experimental difficulty that prevents us from easily achieving this goal is that the thickness of thermally-stable GeSi may be very thin. For example, the critical thickness of x=0.35 as predicted by the model of Paine *et al.* is only ~30-50Å, making accurate thickness measurements and analysis of defects quite challenging.

After the completion of solid-phase epitaxy for metastable GeSi films, high densities of dislocations (10^{10}-10^{11}/cm^2) are observed in Si-implanted x=0.10, phosphorous-implanted x=0.12, and arsenic-implanted x=0.08 and x=0.16 samples [13,74,75]. Hong *et al.* have proposed that the critical thickness for the coherent regrowth of GeSi may not be determined solely by the thermal equilibrium critical thickness model predicted by Matthew and Blakeslee or by Paine *et al.* [60,93], but rather by the kinetic competition between the processes of solid-phase epitaxy as well as dislocation nucleation [13]. If the regrowth velocity V is assumed to be constant, they hypothesize that a "delay time" τ may exist for the nucleation of threading dislocations to take place in GeSi, resulting in a thin defect-free region of a thickness equal to $V \cdot \tau$ after solid-phase

epitaxy [13]. A ~400Å thick defect-free layer after solid-phase epitaxial regrowth of GaAs has also been observed by Grimaldi *et al.*, where they hypothesize that the growing crystal front can only accumulate local defects to a maximum distance of ~400Å before the defects begin to precipitate in clusters [98]. In that case the effect of biaxial stress during the regrowth of GaAs is not considered to be important. However, for the case of solid-phase epitaxial regrowth of GeSi, successful critical thickness models must seriously consider the strain energy of epi-GeSi during the regrowth process. Besides the built-in stress in the regrown epilayer, implantation-induced defects may also affect the kinetics of the regrowth process. Dopant incorporation is shown to also affect the regrowth kinetics in GeSi, as in the cases of Si and Ge [12,57,74-77].

One may wonder that since the growth temperature for both molecular beam epitaxy and solid-phase epitaxy of GeSi are about the same in my study (~550°C), why then can the samples grown by molecular beam epitaxy exceed their equilibrium critical thickness by more than an order of magnitude, but the samples grown by solid-phase epitaxy can not? One obvious explanation has been suggested by Kringhøj *et al.* [91] who argued that during molecular beam epitaxy the GeSi alloy grows at an atomically sharp crystalline/vacuum interface, whereas the crystallization during solid-phase epitaxy occurs at a rugged amorphous/crystalline interface. The rugged amorphous/crystalline interface could enhance defect-nucleation. Hong *et al.* have also suggested that the strain relaxation happening during solid-phase regrowth of metastable GeSi may be related to a lowered nucleation barrier for dislocation formation caused by implantation-induced defects near the a-c interface. Since the exact kinetic barriers for defect nucleation during solid-phase regrowth of GeSi are unknown and likely to be complex, both stress and defect induced effects may be important in causing the difference between the critical thickness values of GeSi samples grown by molecular beam epitaxy and solid-phase epitaxy.

It is reported that the activation energy for solid-phase epitaxy of strained GeSi varies from 2.8 to 3.3 eV, which values are substantially larger than the interpolated values obtained from those of Si and Ge [13,14,60,78]. The activation energy of strain-relaxed GeSi films of x values ≤ 0.31, however, is rather close to that of Si, i.e., ~2.68±0.12 eV, as reported by several

different groups [73,85,99]. To explain the increase in the activation energy for the solid-phase epitaxy of strained versus relaxed GeSi, Hong *et al.* used the concept of activation-strain tensor and proposed that the compressive stress in GeSi would increase the kinetic activation barrier of solid-phase epitaxy and thus retard the regrowth velocity [Hong, Aziz]. On the other hand, Paine *et al.* and Elliman *et al.* suggested that the larger activation energy may typically be associated with {111} faceting and the change of regrowth habit from (100) to {111} to relieve the stress [78, 91-92, 94-96]. The stress-induced increase in the activation energy for metastable GeSi films may be directly related to the change of regrowth habit during solid-phase epitaxy, but more experimental data are needed to support this relationship [92].

Table 3.1. Chronological list of papers on solid-phase epitaxy of strained GeSi: values of film thickness, composition and crystallinity before/after regrowth

Ge content	Thickness (Å)	Ion	Initial crystallinity	Crystallinity after solid-phase epitaxy	Strain preserved ?	Authors
16%	~350	As	χ_{min}= 4%	χ_{min}= 4%	Yes	Chilton *et al.* [5]
30%	870	Si	with misfit dislocations	many planar defects (stacking faults) but few dislocations	No	Paine *et al.* [6]
16%	275 (three pairs of Si/GeSi)	Si	χ_{min}= 4%	χ_{min}= 6%	Yes	Vos *et al.* [7]
5.4%, 11.6%, 17.0%	2100, 1770, 2040	Si	N/A; most likely excellent	few defects for 5.4%; many stacking faults for 11.6% and 17.0%	Yes (5.4%); No (11.6%; 17.0%)	Paine *et al.* [78]
4-12%	3300-4200	Si	χ_{min}= 4% for x=0.04; χ_{min}= 6% for x=0.10 with many defects at Si-GeSi interface; N/A for the rest	fully recovered for Ge_xSi_{1-x} with x < 8%; for x=0.10, χ_{min}=12% with many dislocations after regrowth; the first ~300 Å defect-free	No for x=0.10; N/A for all others	Hong *et al.* [13]
4%, 9%, 13%	1700	Si	N/A	increased χ_{min} for all samples	No for all samples	Bai and Nicolet [3]
8%	3000	Sb	χ_{min}= 3%	χ_{min}= 11%	N/A	Atzmon *et al.* [17]
12%	2000	Si	N/A; most likely excellent	many dislocations and stacking faults	No	Lee *et al.* [14]
10%	2000	Si	N/A; most likely excellent	many defects; first 200 Å regrown GeSi defect-free	No	Paine [60]
8%	3000	Sb	χ_{min}=3%	N/A; most likely excellent	Yes (?)	Atzmon *et al.* [100]
12%	2650	P	χ_{min}=3-4%	χ_{min}= 6%; numerous dislocations	No	Lie *et al.* [75,77]

8.5%, 17%	1200	Si	N/A; most likely excellent	good for 8.5%; strain-relieving defects for 17%	Yes for 8.5%; No for 17%	Elliman *et al.* [92]
10%	3700	Si	χ_{min}= 4%	χ_{min}= 6%; numerous dislocations; first ~200 Å regrown GeSi defect-free	No	Lie *et al.* [48]
8%, 16%	1500	As	χ_{min}=3-4%	χ_{min}= 6%; numerous dislocations	No	Lie *et al.* [74]

3.2.3. Enhanced Strain Relaxation Due to Implantation-Induced Damage

Strain relaxation of pseudomorphic GeSi can degrade the electronic performance of Si/GeSi heterojunction devices and should therefore be avoided for practical applications [101-104]. Pseudomorphic Si/GeSi typically shows significant strain relaxation at furnace annealing temperatures roughly 100-200°C higher than their growth temperatures, which are usually ~ 500-700 °C [105]. Since implantation introduces defects in Si/GeSi, it is interesting to investigate whether these defects will have an effect on the unwanted strain relaxation process. Figure 3.8 shows the rocking curves of x=0.20 annealed at 800°C for 30 min before/after 100 keV P implantation with various doses. The epi-GeSi peak for an as-deposited virgin x=0.20 clearly broadens and moves slightly towards the Si substrate peak after annealing at 800°C, which shows that the strain in the layer just starts to relax and is far from being fully relaxed yet. After the sample is amorphized with a dose of 1.5×10^{15} P/cm^2 (cf. Fig. 3.1) and annealed at 800°C, the weakened epi-GeSi peak further broadens and moves significantly toward 0°; the epi-GeSi is thus fully relaxed [75,76]. It is evident that the strain relaxation process is enhanced after implantation, and that the enhancement increases with the ion dose. The dose-dependence of the enhancement of strain relaxation can be hypothetically explained as follows: since the number of implantation-induced defects increases with dose, these defects may act as nucleation sites to form strain-relieving defects (e.g., dislocations) in GeSi. Hull *et al.* have observed a similar enhancement of

strain relaxation in a strained Si/GeSi/Si implanted with either B or As below their amorphization doses [106]. They also postulate that the defects created by implantation can serve as nucleation sites for the formation of incipient dislocation loops, which then lead to the relaxation of strain in GeSi. My results thus further demonstrate that implantation-induced damage, which is a monotonic function of the ion dose, can substantially enhance the strain relaxation of both amorphized and non-amorphized Si/GeSi [20,76]. For an implantation dose of $1x10^{13}/cm^2$, no enhancement of strain relaxation is observed in Fig. 3.8, within the sensitivity of x-ray analysis, which is probably due to the low density of implantation-induced defects (cf. Fig. 3.1).

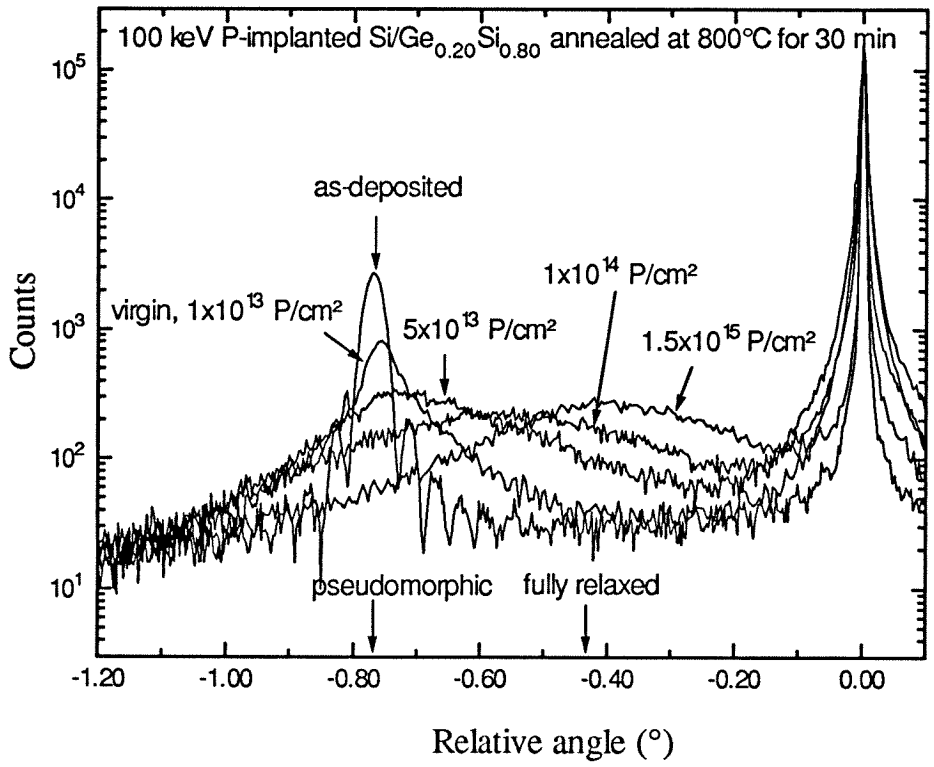

Fig. 3.8 : Double-crystal x-ray rocking curves of (400) symmetrical diffraction for pseudomorphic $Si(100)/Ge_{0.20}Si_{0.80}$ annealed in vacuum at 800°C for 30 min for both implanted and non-implanted samples. All implantation was performed at room temperature at 100 keV with P ions. The origin of the abscissa is placed at the Bragg angle of a Si substrate (θ_B=45.475°; λ=1.936Å, Fe$k\alpha_1$ radiation). The

arrows on the abscissa indicate the peak positions of the fully strained ("pseudomorphic") and fully relaxed $Ge_{0.20}Si_{0.80}$, respectively.

To show the effect of implantation-induced damage on the strain relaxation process in a more presentable fashion, I plot in Fig. 3.9 the values of the *induced* maximum perpendicular strain in P-implanted x=0.12 against the annealing temperature. For samples annealed below 600°C, implanted GeSi show induced positive perpendicular strain that increases with the ion dose (e.g., dotted line, open Down Triangles for a dose of $2x10^{14}/cm^2$). The implantation-induced strain still exists up to 600°C, probably due to residual damage that cannot be removed at this relatively low annealing temperature (cf. Figs. 1-2 of A4) [76]. The strain in a virgin non-implanted sample starts to relax at 600°C (solid line, solid squares), but it relaxes less substantially than implanted GeSi, similar to what is shown in Fig. 3.8. The dotted line and the solid line in Fig. 3.9 start crossing each other at a temperature lower than 700°C. This behavior suggests that when samples are annealed at 700°C or at higher temperatures, the enhancement of strain relaxation in implanted GeSi (over non-implanted GeSi) has already taken place. The relaxation process is evidently facilitated by the residual defects in the epi-GeSi, since GeSi samples implanted with a higher dose always relax more than those implanted with lower doses. When the implanted sample is amorphized and fully regrown (solid diamond), the epi-GeSi is again completely relaxed (cf. Fig. 3 of A3; Fig. 3.8) [75]. Similar enhancement of strain relaxation is also observed for Sb implanted x=0.10 [100].

Another interesting observation on the kinetics of strain relaxation process for implanted GeSi is worth special attention. I have shown in Fig. 2 of A3 bright-field transmission electron micrographs for 100 keV P-implanted x=0.12 [75]. The as-implanted GeSi is amorphized to a depth of ~190 nm, which is roughly 75% of the film thickness, and the Si-GeSi interface appears unaffected by the ion bombardment. After the completion of solid-phase epitaxial regrowth, the amorphous portion of the layer becomes crystalline again but strain relaxed, while the bottom non-amorphized epi-GeSi remains fully strained (cf. Fig. 2(e) and Fig. 3 of A3) [75]. As the

implanted sample is annealed at 700°C for 30 min, Fig. 2(g) of A3 shows that the threading arm of a dislocation half-loop extends through the regrown region down to the Si-GeSi interface. Based on this evidence, I hypothesize that at 700°C dislocation half-loops first form at the bottom of the regrown GeSi layer during annealing, and then glide down upon {111} planes until parts of the loops intersect the Si-GeSi interface. Each dislocation loop can then open out, leaving a segment of misfit dislocation lying at the Si-GeSi interface. This hypothesis suggests that if significant amounts of defects are present near or within a strained GeSi film, these defects may attack the Si-GeSi interface to relieve the intrinsic strain at high enough annealing temperatures. This hypothesis might even be applicable to thermally-stable GeSi films, which will need to be verified experimentally.

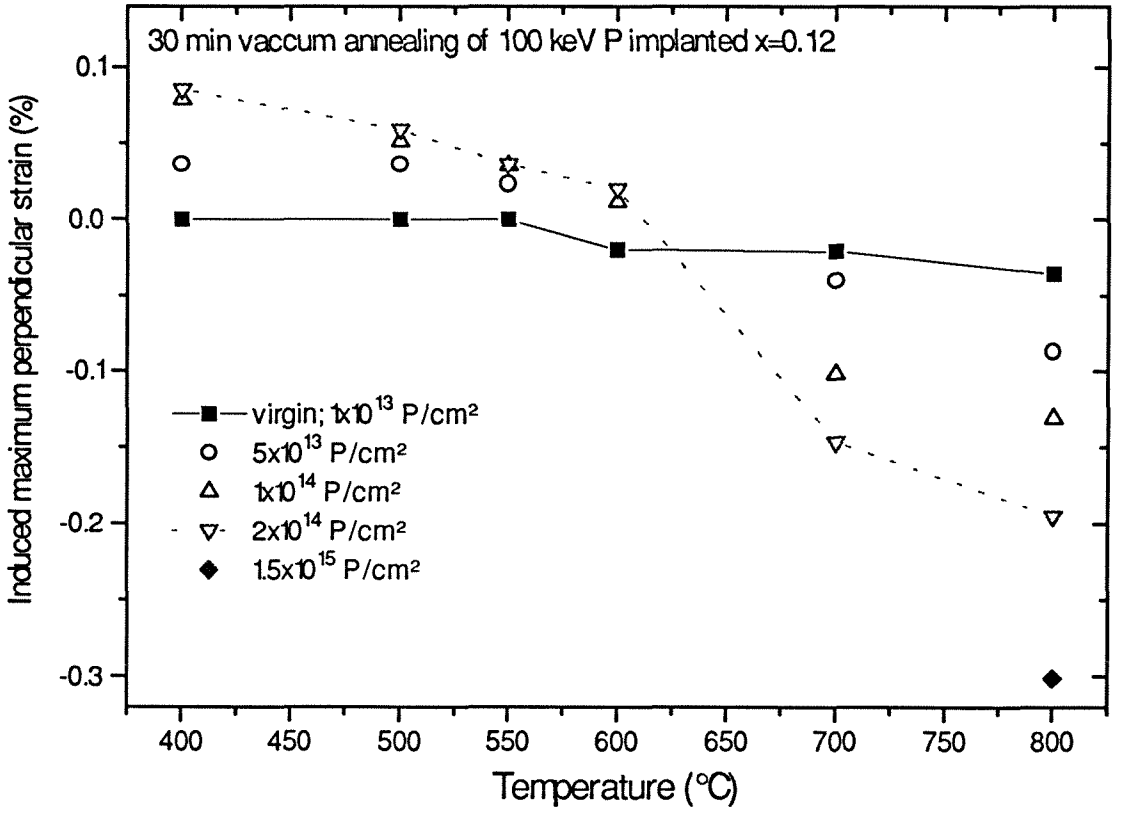

Fig. 3.9 The values of the induced maximum perpendicular strain in x=0.12 implanted with 100

keV P ions at room temperature for various doses are plotted versus the annealing temperature. The duration of annealing is 30 min each. The detailed implantation parameters are inserted as legends. The annealing curve for a virgin non-implanted x=0.12 is also plotted (solid squares and solid line). The case for the sample implanted with a dose of $2x10^{14}$ P/cm^2 (crosses) is connected by a dotted line to show the trend of strain evolution.

3.2.4. Electrical Activation for Dopant-Implanted GeSi

The percentage of electrically active dopants after implantation and annealing is one of the most important parameters for the practical application of ion implantation technology to the semiconductor industry. I will next present data on both Si and GeSi implanted with n-type dopants (P, As) after both steady-state (Sec. 3.2.4.1) and rapid-thermal annealing (Sec. 3.2.4.2). Discussion and comparison of the dopant activation behavior in Si and GeSi will also be made.

3.2.4.1. Steady-State Furnace Annealing

The fractions of activated dopants for P-implanted x=0.12 are plotted in Fig. 3.10 versus the steady-state furnace annealing temperatures (solid symbols and solid lines). These values are compared with data obtained from Ref. 43 for P-implanted Si (open symbols and dotted line). Figure 3.10 shows that if the GeSi is not amorphized (doses of 1,5, and $10x10^{13}$/cm^2), nearly complete activation of ~90-100% cannot be achieved unless the samples are annealed at temperatures $\geq$ 700°C, where significant amount of strain relaxation has already taken place (see Figs. 1-2 of A4) [76]. Comparing these three non-amorphized cases for P-implanted GeSi, one can see that the electrical activity decreases as the ion dose increases if the samples are annealed below 700°C. Examination of data in Fig. 3.10 for the non-amorphized cases of P-implanted Si also reveals a similar trend of decreased activity versus dose. A possible explanation is that the

heavier damage at higher dose is more difficult to remove by annealing and thus may impede or compensate the activation of P ions [2,47].

For amorphized x=0.12, Fig. 3.10 shows that about 50% of the phosphorus ions is activated after 500°C annealing, and almost 100% is activated after 550°C (solid Down Triangles). Figure 2 of A3 also shows that solid-phase epitaxial regrowth of this amorphized x=0.12 is roughly halfway complete at 500°C and becomes entirely complete at 550°C, which correlates very well with the electrical data [75]. This good correlation suggests that nearly all of the P ions are located on substitutional sites of the crystalline lattice after solid-phase epitaxial regrowth. Since dopant activation for non-amorphized GeSi remains poor after annealing at 550°C, it is evident that layer-by-layer solid-phase epitaxial regrowth of P-implanted GeSi enhances the dopant activation process, as it does for Si and Ge [1,2,47]. The dopant activation curve for this pseudomorphic GeSi layer implanted with 1.5×10^{15} P ions/cm^2 is very similar to that of Si implanted with 5×10^{15} P ions/cm^2, probably due to the similar extent of amorphization introduced by the ions [23,77,107]. The sheet electron mobility values for the regrown GeSi layers are about 20-30% lower than those obtained from a Si sample implanted and annealed at identical conditions, which are also plotted in Fig. 4 of A3. For heavily doped semiconductors, it is known that ionized impurity scattering is the dominant scattering process for electron transport [108-111]. Alloy scattering at room temperature is expected to significantly contribute to this reduction of mobility in GeSi over that in Si [111]. Furthermore, the scattering by a high density of dislocations in the regrown GeSi layers may also lower the electron mobility in GeSi over that in Si [110]. For $T_{ann} \geq 550$°C, our maximum mobility values are more than 10% higher than those reported by Atzmon *et al.*, where Sb ions were used [17].

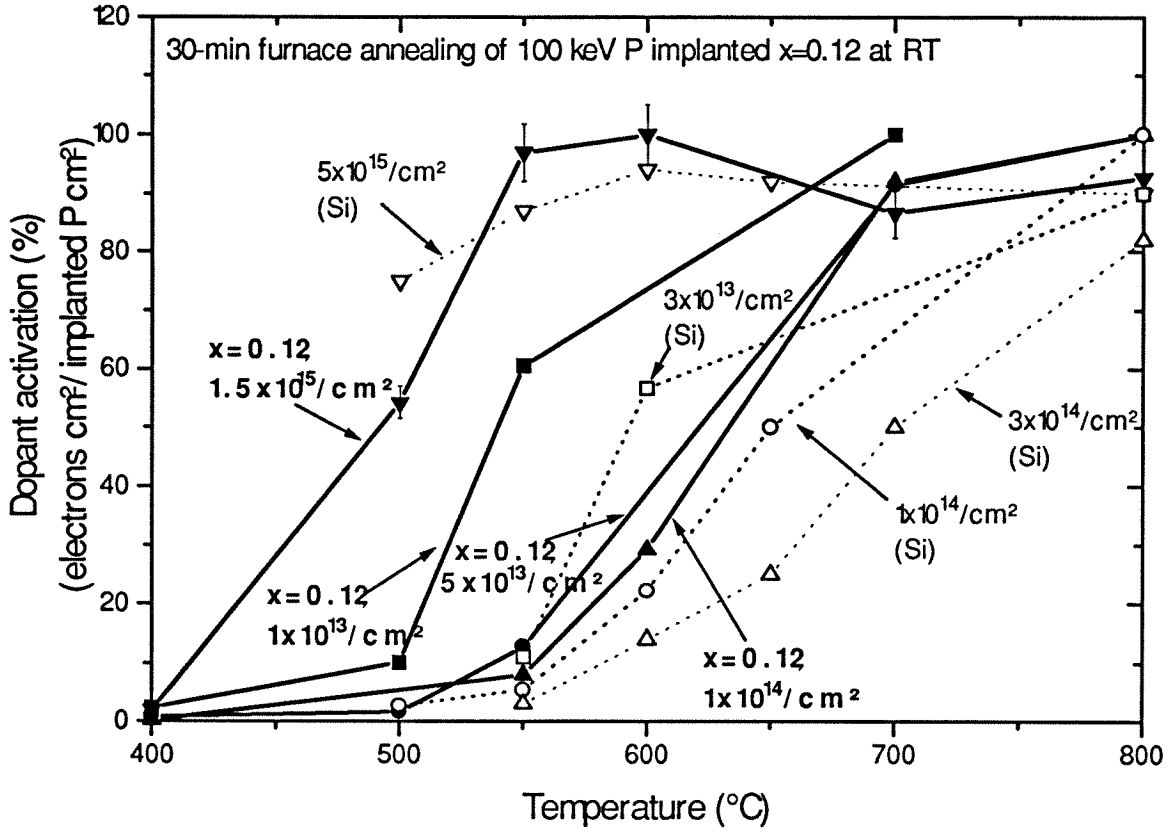

Fig. 3.10 The ratio in % of electrons/cm² obtained from Hall measurements to implanted P atoms/cm² for x=0.12 implanted with $1x10^{13}$ P/cm² (solid squares), $5x10^{13}$ P/cm² (solid circles), $1x10^{14}$ P/cm² (solid Up Triangles) and $1.5x10^{15}$ P/cm² (solid Down Triangles) at 100 keV as a function of annealing temperature. The implantation was performed at room temperature and the duration of annealing at each temperature was 30 minutes. Corresponding data obtained from Hall measurements for 280 keV P implanted Si are plotted for comparison (open squares for $3x10^{13}$ P/cm²; open circles for $1x10^{14}$ P/cm²; open Up Triangles for $3x10^{14}$ P/cm²; and open Down Triangles for $1.5x10^{15}$ P/cm², from Ref. 43).

Arsenic is one of the most important n-type dopants for future ULSI devices since it has high solubility and small diffusion constant in Si [44]. I will next present the behavior of dopant

activation for arsenic-implanted samples after steady-state furnace annealing. Figure 3.11 shows data for the percentage of electrically activated arsenic ions in x=0.08 and in Si for a high-dose (amorphizing) As implantation at room temperature. The corresponding backscattering channeling spectra are plotted in Fig. 3.5(a) in Sec. 3.2.2.2.1. The arsenic signals for random and channeled ^{4}He beam incidence of the as-implanted Si are almost equal. This close resemblance indicates that after room temperature implantation the majority of the as-implanted arsenic ions are not located at Si lattice sites [12,47]. After annealing at 500-800°C for 30 min, Fig. 3.5(a) indicates that the entire arsenic peak disappears. The disappearance of the arsenic signal shows that the arsenic atoms move from random positions in the lattice to specific substitutional sites as a result of solid-phase epitaxy; they can therefore become electrically active [1,47,112]. The As activation presented in Fig. 3.11 for the high dose implanted Si supports the above interpretation by an independent observation. The percentage of active dopants is negligible at 500°C when the solid-phase epitaxy rate is slow, but increases to ~80% right after the completion of the solid-phase regrowth at 550°C (cf. Fig. 3.5(b)). Solid-phase epitaxial regrowth thus facilitates the activation of implanted arsenic ions in GeSi and Si, similar to the case of P-implanted samples [74-77].

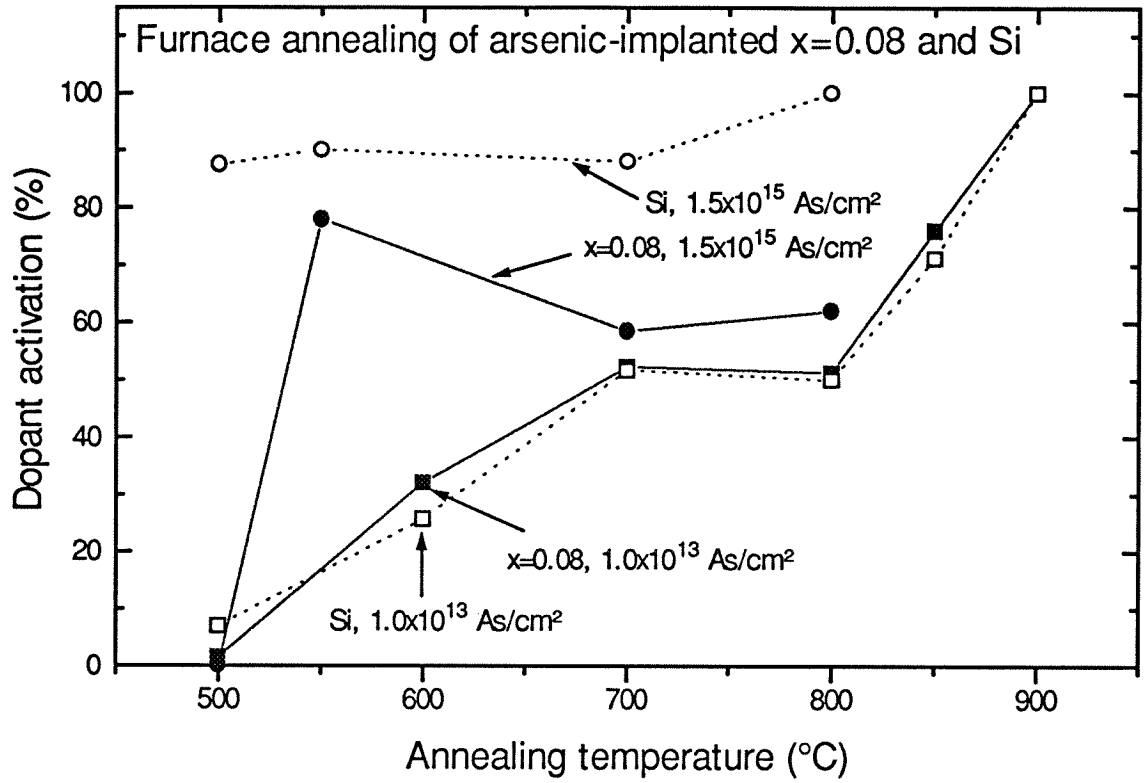

Fig. 3.11: The percentage of activated arsenic ions for x=0.08 and Si(100) implanted with $1x10^{13}$ As/cm² (solid and open squares, respectively) and $1.5x10^{15}$ As/cm² (solid and open circles, respectively) at 90 keV plotted as a function of the annealing temperature. The implantation was performed at room temperature and the annealing was performed in high vacuum (~$5x10^{-7}$ Torr) at each temperature for 30 minutes each.

The percentage of activated arsenic ions in Si is consistently higher than that in x=0.08 for high-dose ($1.5x10^{15}$/cm²) implanted samples, possibly due to the difference of the solid-solubility limit of arsenic atoms in GeSi and Si [12,77,84]. For both P and As implanted GeSi samples, the fractions of the activated dopants reach their maximum values right after the completion of solid-phase epitaxial regrowth, and then decrease slightly if annealed for longer times or at higher temperatures (cf. Figs. 3.10-3.11). Atzmon *et al.* have also found a similar trend in Sb implanted

strained GeSi [17]. They proposed that it is because the concentration of substitutional Sb exceeds its solid solubility immediately after regrowth; further annealing results in the system moving towards thermal equilibrium with Sb being rejected into non-substitutional sites. Similar explanations might be applicable for both P and As implanted GeSi.

For the low-dose ($1x10^{13}/cm^2$) implanted samples, the activated percentage of arsenic ions in x=0.08 is very similar to that in Si under all steady-state annealing conditions studied here. The activated percentage stays around 60% at 700-800°C, and reaches complete activation at 900°C, where significant strain relaxation has already taken place. Mayer *et al.* have reported that in almost every case they have studied in ion-implanted Si where a continuous amorphous layer is *not* present, annealing temperatures of at least 700-750°C are required for the dopant activation to reach its maximum [47]. The dopant activation curves shown in Figs. 3.10-3.11 for the non-amorphized GeSi and Si are rather similar in terms of this "threshold" annealing temperature required to produce the maximum activation. This similarity might suggest the possibility that defect centers exist up to that temperature for both Si and GeSi, as proposed by Mayer and Marsh [47].

3.2.4.2. Rapid-Thermal Annealing Versus Steady-State Furnace Annealing

Processing steps that produce shallow junction depths and high throughputs are preferred for the fabrication of semiconductor devices in the ULSI era. It has been suggested that the advantages of rapid-thermal annealing over the traditional steady-state furnace annealing are primarily due to the single wafer processing nature of the operation and its ability of selecting one desired process over another unwanted one [113]. I will therefore discuss in this section the dopant activation data obtained from implanted GeSi annealed under rapid thermal conditions. A comparison will be made with the electrical data presented in Sec. 3.2.4.1. to see which annealing technique is preferable for processing ion-implanted GeSi samples.

Figures 3.10-3.11 have shown that for steady-state furnace annealed GeSi, temperatures ≥ 700°C are required to achieve good activation. At these temperatures the GeSi layers may have relaxed considerably, resulting in high dislocation densities (e.g., Figs. 1-2 of A5) [114]. Data presented in Figs. 3.8-3.9 also demonstrate that implantation-induced defects may enhance the strain relaxation process for Si/GeSi [75,76]. To avoid strain relaxation yet activate dopants, transient annealing techniques which reduce the annealing time of the sample may be good alternatives to traditional steady-state furnace annealing techniques [115]. For example, it is shown in Fig. 3 of A5 that for x=0.12 implanted with $5x10^{13}$ P/cm^2 (non-amorphized case), annealing at 700°C for only 40 s is sufficient to activate all the dopants and preserve the strain; prolonged annealing to 30 min introduces unwanted strain relaxation [114]. In this particular case, the advantage of rapid-thermal annealing may be explained as that strain relaxation process for implanted Si/GeSi requires annealing times longer than 40 s at 700°C; the activation process, on the other hand, is rapid enough that the movement of implanted phosphorus atoms into substitional sites can take place within this short time frame [113]. This case of ion-implanted metastable GeSi seems to provide a classic example which demonstrates the advantage of using rapid-thermal annealing to select or enhance a desired process (i.e., dopant activation), while avoiding or retarding another slower process (i.e., strain relaxation). Rapid-thermal annealing is shown in A.5 to be superior to steady-state furnace annealing for processing P-implanted x=0.12 with a dose of $5x10^{13}$/cm^2 [114]. This advantage of rapid-thermal annealing is expected to also exist for x=0.12 implanted with lower ion doses, since less damage will be introduced in the implanted layers and hence the enhancement of strain relaxation should be less significant (cf. Figs. 3.1 and 3.9).

For non-amorphized GeSi implanted with arsenic ions, I also found that rapid-thermal annealing is the preferred technique for post-implantation annealing. For example, for annealing at 800°C, the implanted GeSi shows significant strain relaxation after 30 min steady-state annealing, but not within 40 s or less of rapid-thermal annealing. The fraction of the activated arsenic ions in x=0.08 after rapid-thermal annealing for 40s at 800°C is ~90%, considerably higher than the

~50% obtained for x=0.08 after 30-min steady-state annealing at 800°C. The activation percentage of arsenic ions in GeSi is generally lower for that in P-implanted GeSi. This phenomenon has also been observed in the case of P and As implanted Si [1,47].

It is shown in Figs. 3.10-3.11 that solid-phase epitaxial regrowth of GeSi can facilitate dopant activation if the implanted samples are annealed under steady-state conditions. The regrown GeSi, however, is relaxed and full of defects. It is also of interest to know whether solid-phase epitaxial regrowth of GeSi that takes place during rapid-thermal annealing conditions can also enhance dopant activation or possibly recover the pseudomorphic strain. I have therefore amorphized Si and x=0.08 using 20 keV P ions or 90 keV As ions with a common dose of $1.5x10^{15}/cm^2$ and performed rapid-thermal annealing on them from 600-800°C for 10-40s. Right after the completion of solid-phase epitaxial regrowth, the percentage of the activated dopants always lies at 80-100%, which proves that solid-phase epitaxy can facilitate dopant activation of P and As ions in GeSi, much as the cases in bulk Si and Ge, insensitive to the annealing technique used. Atzmon *et al.* also reported that activation of implanted Sb ions in regrown GeSi is significantly better than the cases of non-amorphized GeSi [12]. However, for amorphized GeSi samples, the advantage of rapid-thermal annealing over steady-state annealing no longer exists. The original pseudomorphicity and crystallinity of a regrown metastable GeSi is always lost after either steady-state furnace annealing or rapid-thermal annealing. More studies are therefore needed to find out whether rapid-thermal annealing still outperforms furnace annealing under various other implantation conditions.

3.3. Conclusions and Suggestions for Future Work

(1) The nonlinear increase of the implantation-induced maximum relative damage with dose is a general property of the Ge-Si system (see Sec. 3.1.1, Sec. 3.1.3, Sec. 3.1.4).

(2) Increasing the Ge content in Ge_xSi_{1-x} strongly enhances the implantation-induced damage. This enhancement in the retained damage is due to both an increase in the average energy density per ion deposited in the collision cascade and a retardation in the mobility of point defects. At higher temperatures of implantation, the mobility factor is expected to be more important (see Sec. 3.1.1, Sec. 3.1.4).

(3) The preexisting strain in epi-GeSi does not noticeably affect the implantation-induced damage, as measured by the ion channeling technique. This may be so because the elastic strain energy in the film is quite small compared with the average energy density deposited by energetic ions in the collision cascade (see Sec. 3.1.1).

(4) Both the implantation-induced maximum relative damage and maximum perpendicular strain increase with the dose and the mass of ions, as well as the Ge content in the Ge-Si system. It is the implantation-induced damage that produces additional strain in pre-strained GeSi, but not vice versa. The relationship between the induced damage and strain in GeSi, however, is more complicated that in bulk Si and Ge. A deep understanding of the relationship between the implantation-induced damage and strain in GeSi requires a careful analysis of the microscopic natures of defects and thus is expected to be very complex (see Sec. 3.1.2, Sec. 3.2.1).

(5) If the implantation dose is not sufficient to amorphize the epi-GeSi, the induced damage and perpendicular strain in Si/GeSi are largely reversible, provided that no strain relaxation has taken place (see Sec. 3.2.1).

(6) The solid-phase epitaxial regrowth of metastably-strained GeSi always results in strain relaxation and degraded crystallinity under both steady-state and rapid-thermal annealing conditions. Implantation-induced amorphization must be avoided for practical applications (see Sec. 3.2.2). Fully relaxed GeSi, however, can regrow cleanly (see Sec. 3.2.2.2.3).

(7) An amorphous GeSi layer may regrow defect-free and pseudomorphically up to its equilibrium critical thickness; above this thickness, the strain in the regrown layer relaxes and the layer develops a high density of defects. This critical thickness value is a steep function of the Ge content in the alloys, and it agrees with that calculated by Paine *et al.* within an order of magnitude [78] (see Sec. 3.2.2.2.4).

(8) Enhancement of the strain relaxation process in ion-implanted metastable epi-GeSi films on Si(100) is observed, and the enhancement increases with ion dose. This dose-dependence of the strain relaxation process may be interpreted as follows: Since the number of implantation-induced defects increases with dose, these defects may act as nucleation sites to form strain-relieving defects (e.g., dislocations) in GeSi (see Sec. 3.2.3).

(9) Solid-phase epitaxial regrowth of implanted GeSi facilitates the electrical activation of n-type dopants (i.e., P, As, Sb), independent of the annealing techniques used in this study. This phenomenon is similar to the case of dopant-implanted Si (see Sec. 3.2.4).

(10) For non-amorphized metastably-strained GeSi implanted with P or As ions, rapid-thermal annealing outperforms steady-state furnace annealing in preservation of the pseudomorphic strain and in improved activation of dopants. However, for amorphized GeSi samples, there is no advantage in using rapid-thermal annealing over steady-state annealing; they both fail to recover the strain and crystallinity after regrowth (see Sec. 3.2.4.2).

(11) Since hot implantation at ~100°C can effectively suppress the induced damage and strain in GeSi and can thus prevent amorphization, such hot implantation may be preferable (over room temperature implantation) for the case of high-dose implanted metastable epi-GeSi. The enhancement of strain relaxation after post-implantation annealing may also be less serious for the

case of ~100°C implanted GeSi than for room temperature implanted materials since the induced damage in GeSi is minimal at ~100°C (see Sec. 3.2.3). A combination of hot-implant and rapid thermal annealing may be able to avoid amorphization in metastable GeSi while capable of effectively activating dopants. This conclusion is based on damage and strain considerations only. Experiments that involve dopant implantation at elevated temperatures are required to justify the advantage of hot implantation over room temperature implantation for doping epi-GeSi layers [44,47].

(12) If numerous implantation-induced defects are present inside a pre-strained metastable GeSi film, these defects can eventually attack the original Si-GeSi interface to relieve the intrinsic strain at high annealing temperatures (see Fig. 2 of A3; Sec. 3.2.3). I further hypothesize that this phenomenon might even happen to GeSi films that are thermally stable. Further experimental work will be needed to verify this hypothesis. If this is true, it may become a potential reliability problem for Si/GeSi devices.

(13) A database on the *exact* critical thickness values for solid-phase epitaxial regrown Ge_xSi_{1-x} films should be generated for the optimal design of Si/GeSi devices. These values obtained from careful measurements should help us to refine the existing models and significantly improve our understanding of solid-phase epitaxy in the Ge-Si system.

(14) Having studied the material and electrical properties of epi-GeSi films implanted with n-type dopants, it would therefore be logical and interesting to extend this study to GeSi layers implanted with p-type dopants (e.g., boron).

(15) Carbon implantation into Si or strained GeSi can form tensilely-strained Si or high-quality strain-compensated GeSiC layers that may be useful for novel device applications [116]. It is

therefore of interest to further study the strain evolution and dopant activation behavior in these implanted samples under various annealing treatments.

Based on the results presented in this thesis, I would like to restate in the end that the mature ion-implantation technology can be used to effectively dope and process Si/GeSi heterostructures, provided that the processing parameters and techniques are carefully selected and controlled. This general research area of Si-based strained-layer heterostructures should become more and more important as we approach the "post-shrink" era for Si ULSI technology [105,117-119].

References

1. J. Gyulai in *Ion implantation: Science and Technology*, edited by J. F. Ziegler (Academic Press, Orlando, 1984), pp. 139-210.
2. J. F. Gibbons, Proc. IEEE, 60, 1062 (1972).
3. G. Bai and M.-A. Nicolet, J. Appl. Phys. 71, 4227 (1992).
4. S. Mantl, B. Holländer, W. Jäger, B. Kabius, H. J. Jorke, and E. Käsper, Nucl. Instr. Meth. B 39, 405 (1989).
5. B. T. Chilton, B. J. Robinson, D. A. Thompson, T. E. Jackman, and J.-M. Baribeau, Appl. Phys. Lett. 54, 2 (1989).
6. D. C. Paine, D. J. Howard, N. G. Stoffel, and J. H. Horton, J. Mater. Res. 5, 1023 (1990).
7. M. Vos, C. Wu, I. V. Mitchell, T. E. Jackman, J.-M. Baribeau and J. P. McCaffrey, Appl. Phys. Lett. 58, 951 (1991).
8. D. J. Eaglesham, J. M. Poate, D. C. Jacobson, M. Cerullo, L. N. Pfeiffer, and K. West, Appl. Phys. Lett. 58, 523 (1991).
9. T. E. Haynes and O. W. Holland, Appl. Phys. Lett. 61, 61 (1992).
10. M. Vos, C. Wu, I. V. Mitchell, T. E. Jackman, J.-M. Baribeau, and J. P. McCaffrey, Nucl. Instr. and Meth. B 66, 361 (1992).
11. G. Bai and M.-A. Nicolet, J. Appl. Phys. 71, 4227 (1992).
12. Z. Atzman, M. Eisenberg, Y. Shacham-Diamand, J. W. Mayer, and F. Schäffler, J. Appl. Phys. 75, 377 (1994).
13. Q. Z. Hong, J. G. Zhu, J. W. Mayer, W. Xia, and S. S. Lau, J. Appl. Phys. 71, 1768 (1992).
14. C. Lee, T. E. Haynes, and K. S. Jones, Appl. Phys. Lett. 62, 501 (1993).
15. L. C. Feldman, J. W. Mayer and S. T. Picraux, "Materials Analysis by Ion Channeling" (Academic Press, London, 1982).
16. G. Bai and M.-A. Nicolet, J. Appl. Phys. 70, 3551 (1991).

17. Z. Atzmon, M. Eisenberg, P. Revesz, J. W. Mayer, S. Q. Hong, and F. Schaffer, Appl. Phys. Lett. 60, 2243 (1992).

18. T. E. Haynes and O. W. Holland., Appl. Phys. Lett. 61, 61 (1992).

19. T. E. Haynes and O. W. Holland., Nucl. Instrum. Methods, B 81, 901 (1993).

20. D. Y. C. Lie, A. Vantomme, F. Eisen, T. Vreeland, Jr., M-A. Nicolet, T. K. Carns, and K. L. Wang, J. Appl. Phys. 74, 6039 (1993).

21. J. J. Goubet, D. Stievenard, D. Mathiot, and M. Zazoui, Phys. Rev. B46, 10113 (1992).

22. J. F. Ziegler in *Ion implantaion: Science and Technology*, edited by J. F. Ziegler (Elsevier Science Publishers, Netherland, 1992), p. 43.

23. S. M. Sze, *VLSI Technology* (McGraw-Hill, Singapore, 1988).

24. D. Y. C. Lie, A. Vantomme, F. Eisen, T. Vreeland Jr., M-A. Nicolet, V. Arbet-Engels, and K. L. Wang, J. Electronic Mater. 23, 369 (1994).

25. D. A. Thompson and R. S. Walker, Rad. Eff. 36, 91 (1978).

26. K. B. Winterbon, "Ion Implantation Range and Energy Deposition Distributions" (Plenum Press, New York, 1975), Vol. 2.

27. R. S. Walker and D. A. Thompson, Rad. Eff. 37, 113 (1978).

28. D. A. Thompson, R. S. Walker, and J. A. Davies, Rad. Eff. 32, 135 (1977).

29. K. N. Tu, J. W. Mayer, and L. C. Feldman, *Electronic Thin Film Science* (Macmillian Pubilishing Company, New York, 1992).

30. "Handbook of Semiconductor Silicon Technology," ed. W.C. O'Mara, R.B. Herring and L.P. Hunt (Noyes Publications, New York, 1990).

31. C. R. Wie, T. A. Tombrello, and T. Vreeland, Jr., J. Appl. Phys. 59, 3743 (1986).

32. C. J. Tsai, A. Dommann, M.-A. Nicolet, and T. Vreeland, Jr., J. Appl. Phys. 69, 2076 (1991).

33. T. Vreeland, Jr., and B. M. Paine, J. Vac. Sci. Technol. A4, 3153 (1986).

34. V. S. Sperioso and T. Vreeland, Jr., J. Appl. Phys. 56, 1591 (1984).

35. V. S. Sperioso, J. Appl. Phys. 52, 6094 (1981).

36. G. Bai and M.-A. Nicolet, J. Appl. Phys. 70, 649 (1991).

37. D. Y. C. Lie, A. Vantomme, F. Eisen, M.-A. Nicolet, V. Arbet-Engels, and K. L. Wang, Mat. Res. Soc. Symp. Proc. 262, 1079 (1993).

38. O. W. Holland, S. J. Pennycook, and G. L. Albert, Appl. Phys. Lett. 55, 2503 (1989).

39. M.L. Swanson, J.R. Parsons, and C.W. Hoelke, Radiat. Eff. 9, 248 (1971).

40. J.R. Dennis and E.B. Hale, 30, 219 (1976).

41. G. Carter, M. J. Nobes, and R. G. Elliman, Vacuum, 45, 1197 (1994).

42. L. Eriksson, J.A. Davies, N.G.E. Johassson, and J.W. Mayer, J. Appl. Phys. 40, 842 (1969).

43. B. L. Crowder, and F. F. Morehead, Jr., Appl. Phys. Lett., 14, 313 (1969).

44. J. Gyulai in *Ion implantaion: Science and Technology*, edited by J. F. Ziegler (Elsevier Science Publishers, Netherland, 1992).

45. T.P Sorjeen, O. W. Holland, M. K. El-Ghor, and C. W. White, Mat. Res. Soc. Symp. Proc. 128, 593 (1989).

46. S.T. Picarux, J.E. Westmoreland, J.W. Mayer, R.R. Hart, and O.J. Marsh, Appl. Phys. Lett. 14, 7 (1969).

47. J. W. Mayer, L. Eriksson, and J. A Davis, *Ion Implantation in Semiconductors* (Academic Press, New York, 1970).

48. D.Y.C. Lie, J.H. Song, N.D. Theodore, A. Vantomme, M-A. Nicolet, T.K. Carns, and K.L. Wang, J. Appl. Phys. 77, 2329 (1995).

49. O. W. Holland and T. E. Haynes, Appl. Phys. Lett. 61, 3148 (1992).

50. T. E. Haynes and O. W. Holland, Appl. Phys. Lett. 59, 452 (1991).

51. A. Vantomme, J. H. Song, D. Y. C. Lie, F. Eisen, M.-A. Nicolet, V. Arbet-Engels, and K. L. Wang, Mat. Res. Soc. Symp. Proc. 326, 121 (1994).

52. U. G. Akano, I. V. Mitchell, F. R. Shepherd, and C. J. Miner, Can. J. Phys. 70, 789 (1992).

53. F. Eisen, J. S. Harris, B. Welch, R. D. Pashley, D. Sigurd, and J. W. Mayer in *Ion Imaplantation in Semiconductors and Other Materials*, edited by B. L. Crowder (Plenum, New York, 1974), p. 631.

54. T. Haynes, private communications.

55. P. Kringhøj, J. M. Glasko, and R. G. Elliman, Nucl. Instrum. Methods (in press, 1995).

56. H. J. Stein, F. L. Vook, and J. A. Borders, Appl. Phys. Lett. 14, 328 (1969).

57. G. L. Olson and J. A. Roth, Mater. Sci. Rep. 3, 1 (1988).

58. J. S. Williams in *Surface Modification and Alloying*, edited by J. M. Poate and G. Foti (Plenum Press, New York, 1983).

59. E. P. Donovan, F. Spaepen, D. Turnbull, J. M. Poate, and D. C. Jacobson, J. Appl. Phys. 57 1795 (1985).

60. D. C. Paine, JOM-J. Miner. Metal. Mater. Soc. 2, 55 (1993).

61. L. Csepregi, J. W. Mayer, and T. W. Sigmon, Phys. Lett. A54, 157 (1975).

62. I. Suni, G. Goltz, M-A. Nicolet, and S. S. Lau, Thin Solid Film, 93, 171 (1982).

63. F. Spaepen, Acta Metall. 26, 1167 (1978).

64. T. Saito and I. Ohdomari, Phil Mag. B43, 673 (1981).

65. S. S. Lau and W. F. Van der Weg, *Thin Films: Interdiffusion and Reactions*, edited by J. M. Poate, K. N. Tu and J. W. Mayer (Wiley-Interscience, New York, 1978), Ch. 12.

66. P.J. Germain, M.A. Paesler, D.E. Sayers, and K. Zellama, Mat. Res. Soc. Symp. Proc. 13, 135 (1983).

67. J. Narayan, J. Appl. Phys. 53, 8607 (1982).

68. I. Suni, G. Goltz, M. G. Grimaldi, M-A. Nicolet, and S. S. Lau, Appl. Phys. Lett, 40, 269 (1982).

69. A. Lietolia, A. Wakita, T. W. Sigmon, and J. F. Gibbons, J. Appl. Phys. 53, 4399 (1982).

70. J. M. Poate and. J. S. Williams in *Ion Implantation and Beam Processing* (Academic Press, New York, 1984), pp. 13-57.

71. M. J. Aziz in *Crystallization and Related Phenomena in Amorphous Materials: Creamics, Metals, Polymers and Semiconductors*, edited by M. Libera, P. Cebe, T. Haynes and J. Dickson, Mat. Res. Soc. Symp. Proc. (in press).

72. G.-Q. Lu, E. Nygren and M. J. Aziz, J. Appl. Phys. 70, 5323 (1991).

73. P. Kringhøj and R. G. Elliman, Phys. Rev. Lett. 73, 858 (1994).

74. D.Y.C. Lie, J.H. Song, M-A. Nicolet, N.D. Theodore, J. Candelaria, M.O. Tanner, S. Thomas, and K.L. Wang, Mat. Res. Soc. Symp. Proc. (in press).

75. D. Y. C. Lie, N.D. Theodore, J.H. Song, and M-A. Nicolet, J. Appl. Phys. 77, 5160 (1995).

76. D. Y. C. Lie, J.H. Song, M-A. Nicolet, and N.D. Theodore, J. Electron. Mater. (in press).

77. D. Y. C. Lie, T.K. Carns, N.D. Theodore, F. Eisen, M-A. Nicolet, and K. L. Wang, Mat. Res. Soc. Symp. Proc. 321, 485 (1994).

78. D. C. Paine, N. D. Evans, and N. G. Stoffel, J. Appl. Phys. 70, 4278 (1991).

79. S. Q. Hong, Q. Z. Hong, and J. W. Mayer, J. Appl. Phys. 72, 3821 (1993).

80. W.K. Chu, J.W. Mayer, and M-A. Nicolet, *Backscattering Spectrometry*, Ch. 8, pp. 223-275 (Academic Press, New York, 1978).

81. F. Cemballi, M. Servidori, E. Gabilli, and R. Lotti, Phys. stat. sol. A87, 225 (1987).

82. P. F. Fewster, J. Appl. Cryst. 25, 714 (1992).

83. J. Klappe, Ph.D. thesis, University of Twente, Netherlands, 1994.

84. D.Y.C. Lie, J.H. Song, M-A. Nicolet, N.D. Theodore, M.O. Tanner, S. Thomas, and K.L. Wang, to be submitted to J. Appl. Phys.

85. T.E. Haynes, M.J. Antonell, C.A. Lee and K.S. Jones, Phys. Rev. B51, 7762 (1995).

86. N.D. Theodore and D.Y.C. Lie, unpublished data.

87. E. A. Fitzgerald, Y.-H. Xie, D. Monroe, P. J. Silverman, J. K. Kuo, A. R. Kortan, F. A. Thiel , and B. A. Weir, J. Vac. Sci. Technol. B 10, 1807 (1992).

88. M.J. Aziz, P.C. Sabin, and G.-Q. Lu, Phys. Rev. B44, 9812 (1991).

89. G.-Q. Lu, E. Nygren, M. J. Aziz, D. Turnbull, and C.W. White, Appl. Phys. Lett. 54, 2583 (1989).

90. J. Fratello, J.F. Hays, and D. Turnbull, J. Appl. Phys. 51, 4718 (1980).

91. P. Kringhøj, R. G. Elliman, and J. L. Hansen, Mat. Res. Soc. Symp. Proc. 321, 461 (1994).

92. R. G. Elliman, W.-C. Wong, and P. Kringhøj, Mat. Res. Soc. Symp. Proc. 321, 375 (1994).

93. J. W. Matthews and A. E. Blakeslee, J. Cryst. Growth 27, 118 (1974).

94. D. C. Paine, D. J. Howard, and N. G. Stoffel, J. Electronic Mater. 20, 735 (1991).

95. D. J. Howard, W. E. Bailey, and D. C. Paine, Appl. Phys. Lett. 63, 2893 (1993).

96. W.-C. Wong and R.G. Elliman, Mat. Res. Soc. Symp. Proc. 321, 491 (1994).

97. E. A. Fitzgerald, Mater. Sci. Rep. 7, 81 (1991).

98. M. G. Grimaldi, B. M. Paine, M-A. Nicolet, and D. K. Sadana, J. Appl. Phys. 52, 4038 (1981).

99. S.Y. Shiryaev, M. Fyhn, and A. N. Larsen, Appl. Phys. Lett. 63, 3476 (1993).

100. Z. Atzmon, M. Eisenberg, E. Zolotoyabko, S. Q. Hong, and J.W. Mayer, Nucl. Instr. Meth B80/81, 751 (1993).

101. R. Hull, J.C. Bean, J.M. Bonar, G.S. Higashi, K.T. Short, H. Temkin, and A.E. White, Appl. Phys. Lett. 56, 2445 (1990).

102. C.A. King, J.L. Hoyt, and J.F. Gibbons, IEEE Trans. Electron Devices 36, 2093 (1989).

103. P.S. Peercy, B.W. Dodson, J.Y. Tsao, E.D. Jones, D.R. Myers, T.E. Zipperian, L.R. Dawson, R.M. Biefeld, J.F. Klem, and C.R. Hills, IEEE Electron Devices Lett. 9, 621 (1988).

104. D. K. Nayak, K. Kamjoo, J. S. Park, J. C. S. Woo, and K. L. Wang, 39, 56 (1992).

105. R. Hull and J. C. Bean in *Strained-layer Superlattices: Materials Science and Technology*, edited by T. P. Pearsall, Ch. 1, pp. 1-72 (Academic Press, London, 1991).

106. R. Hull, J.C. Bean, J.M. Bonar, G.S. Higashi, K.T. Short, H. Temkin, and A.E. White, Appl. Phys. Lett. **56**, 2445 (1990).

107. W. P. Maszara and G. A. Rozgonyi, J. Appl. Phys. 60, 2310 (1986).

108. G. Masetti, M. Severi, and S. Solmi, IEEE, Trans. Electron Devices, 30, 764 (1983).

109. T. Manku and A. Nathan, IEEE Trans. Electron Dev., 39, 2082 (1992).

110. Fisful, *Heavily Doped Semiconductors* (Plenum Press, New York, 1969), p. 133.

111. See, for example, T.K. Carns, S.K. Chun, M.O. Tanner, K.L. Wang, T.I. Kamins, J.E. Turner, D.Y.C. Lie, M-A. Nicolet, and R.G. Wilson, Trans. IEEE Elec. Devices, 41, 1273 (1994); or M. Glicksman, Phys. Rev. 111, 125 (1958).

112. N.G.E. Johansson, J.W. Mayer, and O.J. Marsh, Solid State Electronics, 13, 317 (1970).

113. T.O. Sedgwick, Mat. Res. Soc. Symp. Proc. 92, 3 (1987).

114. D.Y.C. Lie, J.H. Song, M-A. Nicolet, and N.D. Theodore, Appl. Phys. Lett. 66, 592 (1995).

115. S. Tatsuta, T. Inata, S. Okamura, and S. Hiyamizu, Jap. J. Appl. Phys. 23, L147 (1984).

116. See, for example, J.W. Strane, H.J. Stein, S.R. Lee, B.L. Doyle, S.T. Picraux, and J.W. Mayer, Appl. Phys. Lett. 63, 2786 (1993).

117. D.L. Harame, J.H. Comfort, J.D. Cressler, E.F. Crabbé, J.Y.-C. Sun, B.S. Meyerson, and T. Tice, IEEE Trans. Electron Devices, 42, 469 (1995).

118. F. Schäffler, Solid-State Electronics 37, 765 (1994).

119. B.S. Meyerson, Proc. IEEE, 80, 1592 (1992).

APPENDIX

Some of the most representative papers published by the author are enclosed here in the appendix. They are:

A1. "Damage and strain in epitaxial Ge_xSi_{1-x} films irradiated with Si," **D.Y.C. Lie**, A. Vantomme, F. Eisen, T. Vreeland, Jr., M-A. Nicolet, T.K. Carns, V. Arbet-Engels, and K.L. Wang, J. Appl. Phys. 74, 6039 (1993).

A2. "Dependence of damage and strain on the temperature of Si-irradiation in epitaxial $Ge_{0.10}Si_{0.90}$ films on Si(100)," **D.Y.C. Lie**, J.H. Song, A. Vantomme, F. Eisen, M-A. Nicolet, N.D. Theodore, T.K. Carns, and K.L. Wang, J. Appl. Phys. 77, 2329 (1995).

A3. "Solid phase epitaxial regrowth and dopant activation of P-implanted metastable pseudomorphic $Ge_{0.12}Si_{0.88}$ on Si(100)," **D.Y.C. Lie**, N.D. Theodore, J.H. Song, and M-A. Nicolet, J. Appl. Phys. 77, 5160 (1995).

A4. "Strain evolution and dopant activation in P-implanted metastable pseudomorphic $Si(100)/Ge_xSi_{1-x}$," **D.Y.C. Lie**, J.H. Song, M-A. Nicolet, and N.D. Theodore, J. Electron. Mater. (in press).

A5. "Advantage of rapid thermal annealing over furnace annealing for P-implanted metastable $Si(100)/Ge_{0.12}Si_{0.88}$," **D.Y.C. Lie**, J.H. Song, M-A. Nicolet, and N.D. Theodore, Appl. Phys. Lett. 66, 592 (1995).

Appendix 1

Damage and strain in epitaxial Ge_xSi_{1-x} films irradiated with Si

D. Y. C. Lie, A. Vantomme,[a] F. Eisen, T. Vreeland, Jr., and M.-A. Nicolet
California Institute of Technology, Pasadena, California 91125

T. K. Carns, V. Arbet-Engels, and K. L. Wang
Department of Electrical Engineering, University of California, Los Angeles, California 90024

(Received 3 May 1993; accepted for publication 28 July 1993)

The damage and strain induced by irradiation of both relaxed and pseudomorphic Ge_xSi_{1-x} films on Si(100) with 100 keV ^{28}Si ions at room temperature have been studied by MeV ^4He channeling spectrometry and x-ray double-crystal diffractometry. The ion energy was chosen to confine the major damage to the films. The results are compared with experiments for room temprature Si irradiation of Si(100) and Ge(100). The maximum relative damage created in low-Ge content films studied here ($x=10\%$, 13%, 15%, 20%, and 22%) is considerably higher than the values obtained by interpolating between the results for relative damage in Si-irradiated single crystal Si and Ge. This, together with other facts, indicates that a relatively small fraction of Ge in Si has a significant stabilizing effect on the retained damage generated by room-temperature irradiation with Si ions. The damage induced by irradiation produces positive perpendicular strain in Ge_xSi_{1-x}, which superimposes on the intrinsic positive perpendicular strain of the pseudomorphic or partially relaxed films. In all of the cases studied here, the induced maximum perpendicular strain and the maximum relative damage initially increase slowly with the dose, but start to rise at an accelerated rate above a threshold value of ~0.15% and 15%, respectively, until the samples are amorphized. The pre-existing pseudomorphic strain in the Ge_xSi_{1-x} film does not significantly influence the maximum relative damage created by Si ion irradiation for all doses and x values. The relationship between the induced maximum perpendicular strain and the maximum relative damage differs from that found in bulk Si(100) and Ge(100).

I. INTRODUCTION

Heterostructures of Ge_xSi_{1-x} on Si (Si/Ge_xSi_{1-x}) are of great technological interest today because the carrier mobilities in Ge_xSi_{1-x} are higher than those in Si and such heterostructures are compatible with Si integrated-circuit technology. They have been studied for applications to heterojunction bipolar transistors, modulation-doped field effect transistors, bipolar inversion-channel and field effect transistors, bipolar and complementary metal-oxide-semiconductor circuits, infrared superlattice detectors, and mixed tunneling transistors.[1-5]

Ion implantation is one of the key processing steps in doping and processing semiconductor devices. Recently, several studies have been made on implantation or irradiation of Si/Ge_xSi_{1-x} heterostructures.[6-14] When compared with the data for Si, significant damage enhancement in strained Ge_xSi_{1-x} films has been observed, such as the selective amorphization for ion-bombarded Ge_xSi_{1-x} strained-layer superlattices.[9,10] Haynes *et al.*[11] have also reported a similar damage enhancement for relaxed Ge_xSi_{1-x} layers, and Vos *et al.*[12] have qualitatively compared the damage found in Si, Ge, pseudomorphic and relaxed Ge_xSi_{1-x} layers.

Strain is of primary importance for the stability of practical devices fabricated from lattice-mismatched Si/Ge_xSi_{1-x} heterostructures, and it has been reported that ion irradiation will induce further strain in the pseudomorphically strained Ge_xSi_{1-x} layers.[13,14] The goal of this study is to investigate the strain and damage induced in pseudomorphic and relaxed Ge_xSi_{1-x} films by ion irradiation when the ion range is limited such that the $Si\text{-}Ge_xSi_{1-x}$ interface is not significantly damaged. The results are compared with those observed in Si(100) and Ge(100) single crystals. The relationships of irradiation-induced strain and damage versus the Si ion dose are reported for Si, Ge, and for both pseudomorphic and relaxed Ge_xSi_{1-x} films. We also make quantitative comparisons between the damage produced in fully strained and relaxed Ge_xSi_{1-x} layers for a range of irradiation doses with the same Ge composition.

For the sake of brevity, unless otherwise specified, we will use expressions such as $x=0.10$ to replace pseudomorphic $Si/Ge_{0.10}Si_{0.90}$ while fully relaxed $x=0.10$ will refer to fully relaxed $Si/Ge_{0.10}Si_{0.90}$ films.

II. EXPERIMENTAL PROCEDURES

Pseudomorphic films of Ge_xSi_{1-x} on Si(100) substrates were grown by conventional ultrahigh vacuum molecular-beam epitaxy at the University of California at Los Angeles (UCLA). The sample growth temperatures, minimum yields, pseudomorphic strain values, and thickness for $x=0.10$, 0.13, 0.15, and 0.20 are summarized in Table I. All samples are of excellent crystalline quality, with a minimum channeling yield of ~3% to 4% in both

[a]On leave from Instituut voor Kern- en Stralingsfysika, Catholic University of Leuven, Belgium, Senior Research Assistant, N.F.W.O. (National Fund for Scientific Research, Belgium).

 0021-8979/93/74(10)/6039/7/$6.00 © 1993 American Institute of Physics

TABLE I. Basic information about the pseudomorphic Si/Ge_xSi_{1-x} samples used in this article.

x (Ge content)	T_{growth} (°C)	$\epsilon^{\perp}_{exp}$ (%)	$\epsilon^{\perp}_{theo.}$ (%)	χ_{min} (%)	Thickness (Å)
0.10	~450	0.72	0.74	~4	2450
0.13	~450	0.95	0.95	~3	2350
0.15	~400	1.10	1.08	~4	2400
0.20	~400	1.38	1.45	~4	2000

Si and Ge signals. Film thickness was determined by MeV ^{4}He backscattering spectrometry. High-resolution double-crystal x-ray rocking curves evidence the pseudomorphic nature of the heterostructures, with a parallel strain equal to zero within the experimental sensitivity ($\sim 10^{-4}$). All of the strain values refer to the difference in lattice constant with respect to those of the substrates. These measured strain values are consistent with the predictions of linear elasticity theory for the pseudomorphic films.

Another $x=0.10$ layer~3 μm thick, also grown by molecular beam epitaxy at UCLA, was shown by x-ray rocking curve analysis to have a lattice constant of 5.454 Å, which is that of a fully relaxed film. A 600-nm-thick layer with $x=0.22$ was grown at the Institute of Thin Film and Ion Technology (ISI) in Jülich, Germany, where strain measurement with MeV ^{4}He ions channeled parallel to an inclined [110] axis yielded a tetragonal distortion of 4.9×10^{-3} for that sample. We confirmed the thickness by backscattering spectrometry. X-ray rocking curves yielded strain values equivalent to a tetragonal distortion of 5.0×10^{-3}, in agreement with the channeling experiments. This sample is therefore partially relaxed, with residual strain about 17% of that of a pseudomorphic film. Both this partially relaxed $x=0.22$ and the fully relaxed $x=0.10$ films are of rather good crystalline quality, with minimum channeling yields of ~4% and ~5% in the Si and Ge signals, respectively.

All of the $Si(100)/Ge_xSi_{1-x}$ epilayers described above, as well as Si(100) and Ge(100) wafers, were irradiated at room temperature in high vacuum ($\sim 10^{-7}$ Torr) with 100 keV ^{28}Si ions to doses ranging from 10^{13} to 10^{15} Si/cm^2. All samples were chemically cleaned before loading into the implanter (10 min each in ultrasonic baths of trichloroethane, acetone, and methanol, followed by a dip in 0.1% HF solution until a hydrophobic surface was obtained, finally rinsed in de-ionized water, and then blown dry with nitrogen gas). During irradiation, the sample normal was tilted by 7° with respect to the incident beam to minimize channeling. The beam current was limited to $\leqslant 0.1\ \mu$A/cm^2 and kept fairly steady to limit beam heating or dose-rate effects. The ion doses reported here are within ±5% accuracy.

X-ray double crystal diffractometry was used to monitor the strain in the implanted layer. Both symmetrical (400) and asymmetrical (311) rocking curves were taken at room temperature in air as little as 1 h after irradiation, as well as several months later. The strain profiles as a function of depth were extracted by simulating the experimental rocking curves using the dynamical x-ray diffraction theory.[15] MeV ^{4}He channeling spectrometry was used to measure relative damage in the implanted layers.[16] There was no detectable increase in the channeling yield as a result of the He irradiation. The relative damage profiles were extracted from these channeling spectra using a numerical, iterative fitting model.[17]

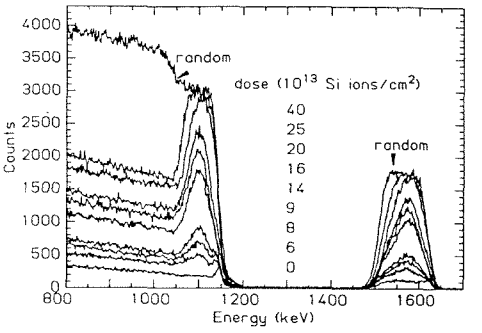

FIG. 1. The ^{4}He axial channeling spectra along the [100] direction of $x=0.10$ irradiated with 100 keV Si to various doses at room temperature. The detector angle is 170° with respect to the direction of the incidence ^{4}He beam.

We have utilized an ion energy of 100 keV for irradiation of Ge_xSi_{1-x} films in order to limit the damage at the interface. The change in the ion energy from 100 keV for the case $x=0$ (Si), 0.10, 0.13, 0.15, 0.20 to 300 keV for $x=1$ (Ge) should be noted. This was done to maintain approximately similar values of average energy densities deposited in the collision cascade by the energetic ions.

III. RESULTS AND DISCUSSION

A. Damage and strain

Figure 1 shows the 2 MeV ^{4}He [100] axial channeling spectra for $x=0.10$ irradiated with various doses of Si, together with the spectrum for random beam incidence. For both Ge and Si signals, the irradiation causes damage peaks that rise with increasing Si ion dose, until they reach the level of the random incidence spectrum. We have used the Si signals in these spectra to extract profiles of damage.

Figure 2 shows a set of selected x-ray rocking curves from symmetrical (400) diffraction for $x=0.10$. The negative angular shift of the epilayer signal with respect to that of the substrate at 0° indicates a positive perpendicular strain of the film, $\epsilon^{\perp}$, which clearly increases with the irradiation dose. The perpendicular strain relaxes very little at room temperature (<0.01% in strain value in the experimentally accessible time frame of 1 h to many months after irradiation). The parallel strain, $\epsilon^{\parallel}$, of all pseudomorphic samples considered here, irradiated or not, is zero within the experimental sensitivity (<0.01%). Because of the damage created by the ion irradiation, the intensity of the x-ray diffraction peak from the irradiated layer decreases as the dose rises.

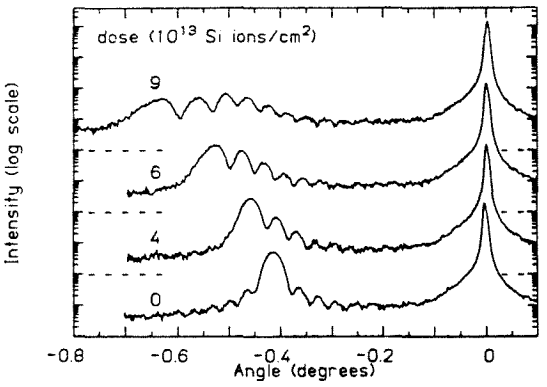

FIG. 2. The x-ray rocking curves from symmetrical (400) diffraction of $x=0.10$ irradiated with 100 keV Si to various doses at room temperature. The samples for 6 and 9×10^{13} Si ions/cm^2 in Fig. 1 and here are identical. The origin of the abscissa is placed at the Bragg angle $\theta_B=45.475°$ of the Si substrate.

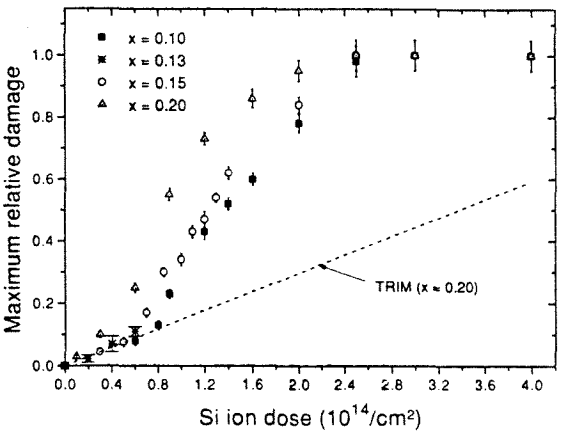

FIG. 4. The maximum relative damage in $x=0.10$, 0.13, 0.15, and 0.20 irradiated at room temperature by 100 keV Si. The dashed line is the TRIM calculation of the number of displaced atoms in an amorphous $x=0.20$ irradiated by 100 keV Si at 0 K.

B. Dose dependence of damage

The maximum values of the relative damage profiles for Ge, $x=0.10$ and Si are plotted in Fig. 3 as a function of irradiation dose. All curves in Fig. 3 exhibit three damage regimes: (I) there is an initially slow increase of the maximum relative damage with dose; (II) the rate of increase of the maximum relative damage accelerates after a threshold level of $\sim15\%$ is reached, and (III) finally amorphization of the sample is reached beyond a critical dose, $\phi_c(x)$, which is a function of the Ge content. In the case of $x=0.10$, $\phi_c\sim2.5\times10^{14}$/cm^2, which is a third of that for Si self-irradiation ($\sim7\times10^{14}$/cm^2), even though there is only 10 at. % Ge in the film. It thus appears that a small addition of Ge to Si significantly enhances the retention of irradiation-induced damage. Such an effect can be explained either by an increase in the number of defects initially generated by the impact of an ion or by an increase in the fraction of the defects still present after irradiation. These possibilities are discussed further below. A recent article also showed the existence of these three regimes for the case of Si in an almost identical irradiation experiment.[18] An earlier article on damage in Si produced by 230 keV Si ions also reported a nonlinear increase of damage with dose.[19]

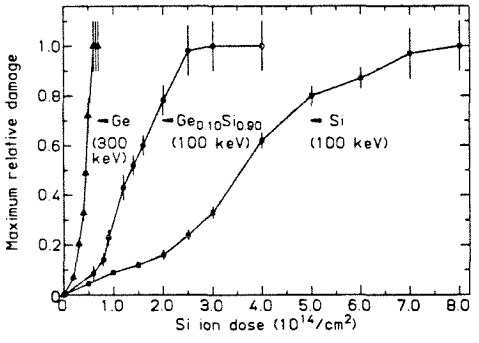

FIG. 3. The maximum relative damage in Si(100) and $x=0.10$ irradiated by 100 keV Si, and in Ge(100) irradiated by 300 keV Si, plotted vs the Si ion dose. All irradiations were done at room temperature.

The maximum relative damage obtained from the channeling measurements for $x=0.10$, 0.13, 0.15 and 0.20 is reported in Fig. 4. We see that all curves exhibit three regimes similar to those identified in Fig. 3. It is thus clear that a nonlinear rise of damage with dose is a general feature of the way damage builds up in the Ge-Si system, under the irradiation conditions applied here. Figure 4 also shows how the maximum relative damage rises with the dose of 100 keV ^{28}Si ions as predicted by the TRIM90 simulation code[20] for an amorphous target of $x=0.20$ at 0 K. A binding energy of 1 eV and a threshold displacement energy of 15 eV were used as input parameters for the simulation. The computed relative damage does not correctly represent the highly nonlinear data. By concept, TRIM simulation will predict a linear dose dependence because it does not include interactions of defects. The nonlinear dose dependence of the experimental results shows that these interactions are very important. This conclusion is consistent with results reported for pure Ge and Si.[14,21] Thus, TRIM does not serve as a relevant predictor of the retained maximum damage versus dose.

The data in Figs. 3 and 4, as well as the results of other workers,[6–14] show that the retained damage introduced by a given dose of silicon ions increases rapidly with the addition of a relatively small amount of germanium (10%–20%) to pure silicon. It will be demonstrated in Sec. III D below that this increase in retained damage is not related to the initial pseudomorphic strain in the alloy film. The presence of germanium might increase the retained damage in Ge_xSi_{1-x} alloys by increasing the average energy per ion in the collision cascades, and/or by decreasing the mobility of the defects in the cascades, resulting in higher damage re-

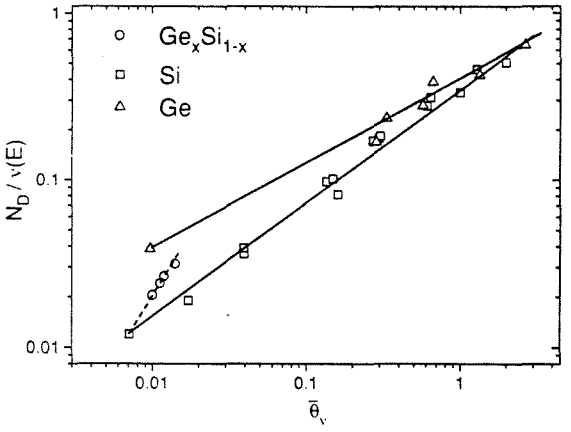

FIG. 5. The total number of displaced atoms, N_D, divided by $\nu(E)$, the component of ion energy dissipated in elastic collisions, is plotted vs the averaged energy density deposited into the collision cascade per atom, $\bar{\theta}_\nu$ (eV/atom). The two solid straight lines were drawn using the least-mean-square fitting over all data points for bulk Ge (above), or for bulk Si (below). The dashed line is to indicate the trend as x increases in 100 keV Si irradiated $x=0.10$, 0.13, 0.15, and 0.20.

tention at a given bombardment temperature, as discussed in the remainder of this section.

Thompson and Walker have shown that in a given material the stability of ion bombardment damage is dependent on $\bar{\theta}_\nu$, the average energy density per atom in the collision cascades produced by the bombarding ions.[22] This quantity is given by

$$\bar{\theta}_\nu = 0.2\nu(E)/N_V V_R. \quad (1)$$

$\nu(E)$ is the component of ion energy dissipated in elastic collisions, which can be evaluated using the results of Winterbon.[23] N_ν is the number of atoms contained within a spheroid defined by the longitudinal and transverse straggling of the statistical damage distribution, which can also be calculated using Winterbon's tables. V_R is the ratio of an individual cascade volume to the transport cascade volume. This quantity can be estimated by using the results in Fig. 4 of Ref. 24.

We have calculated values of $\bar{\theta}_\nu$ for 100 keV Si ions incident on silicon and on Ge_xSi_{1-x} alloy for $x=0.10$, 0.13, 0.15, and 0.20. The value of $\bar{\theta}_\nu$ increases from 0.0072 eV/atom in pure silicon to 0.0142 eV/atom when $x=0.20$. In order to assess the effect that this increase in $\bar{\theta}_\nu$ may have on damage in these materials, we have plotted data obtained in the present work together with data from Thompson and Walker and Davies[25] in Fig. 5. N_D in this figure is the number of displaced atoms per incident ion determined in samples in which only a few percentages of the atoms have been displaced. N_D was obtained by integrating the damage profiles extracted from the channeling spectra. In the present work this corresponds to the low dose regime I. Straight lines have been drawn using a least square fit in the figure to indicate the trend of the data for pure silicon and pure germanium. These lines give a good representation of the damage retained in silicon or germanium bombarded at room temperature using a variety of different ions and bombarding energies. If the only effect of a small percentage of germanium were to increase the density of retained defects as a result of the increase in the value of $\bar{\theta}_\nu$, the points for $x=0.10$, 0.13, 0.15, and 0.20 would be expected to fall very near to the line through the silicon data points. However, the points for the Ge_xSi_{1-x} alloys fall significantly above this line indicating that the effect of the germanium in the alloys is to both increase the damage as a result of the increase in $\bar{\theta}_\nu$ and to reduce the mobility of the defects in the collision cascades resulting in an increase in damage retention. Inspection of Fig. 5 suggests that these two effects make roughly equal contributions to the observed damage increases with respect to pure silicon.

A dashed line has been drawn in Fig. 5 to indicate the trend of the points as x increases. The extension of the dashed line intersects the line drawn for the germanium data points at a $\bar{\theta}_\nu$ value corresponding to $x=0.35$. It is interesting to note that Haynes and Holland[11] found that for $x=0.50$ the alloy accumulates damage at about the same rate as pure germanium. These results suggest that the incremental damage accumulation decreases with increments of x above $x=0.20$.

It is worth pointing out, as has been done in Ref. 25, that the ordinate in Fig. 5 can also be given a scale corresponding to an effective threshold energy, E_d^{eff}, by using the modified Kinchin–Pease formulation[26]

$$N_D = 0.42\nu(E)/E_d^{\text{eff}}. \quad (2)$$

Application of this formula to the silicon data points in Fig. 5 yields an effective threshold energy ranging from about 35 eV for the data point at the lowest value of $\bar{\theta}_\nu$ to 0.65 eV at the point with the highest value of $\bar{\theta}_\nu$. This wide variation in effective threshold is a further indication of the inadequacy of damage calculation programs, such as TRIM, which make use of a single value for the displacement energy.

C. Perpendicular strain versus dose

Figure 6 shows the maximum values of the perpendicular strain, $\epsilon_{\text{max}}^{\perp}$, plotted as a function of the Si ion dose for Ge, $x=0.10$ and Si. The dashed line is the component of the strain in the pseudomorphic film that is added to the initial strain as a result of the Si irradiation. Although derived from a different analytical method, the dose dependence of the irradiation-induced perpendicular strain resembles that of the damage shown in Fig. 3. Three dose regimes exist here too: first the induced perpendicular strain builds up slowly up to ~0.15%; then the induced strain rises at an accelerated rate; finally samples are amorphized. The x-ray method becomes ineffective prior to amorphization due to the loss of x-ray diffraction intensity resulting from the damage.

Figure 7 shows the maximum perpendicular strain for $x=0.10$, 0.15, 0.20 versus the Si irradiation dose. In all three cases the dependence of maximum perpendicular strain on dose has the same characteristics as displayed for

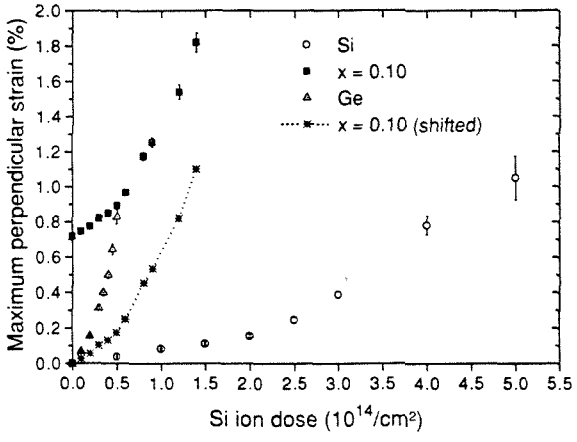

FIG. 6. The maximum perpendicular strain in Si(100) and in $x=0.10$ irradiated by 100 keV Si, and in Ge(100) irradiated by 300 keV Si, plotted vs the Si ion dose. The shifted dashed line shows the *induced* maximum perpendicular strain of the 100 keV Si irradiated $x=0.10$. All irradiations were performed at room temperature.

pure Si and Ge in Fig. 6. We thus conclude that in general the perpendicular strain rises nonlinearly with the dose in the Ge-Si system in much the same way as does the damage (previous section, Figs. 3 & 4).

D. Damage versus strain

We have shown in the previous sections and in Refs. 14 and 21 that the irradiation-induced perpendicular strain and damage are related. Also, the uniform strain in an unirradiated pseudomorphic film does not create damage measurable by channeling. These facts strongly suggest that it is the retained damage that induces the strain.

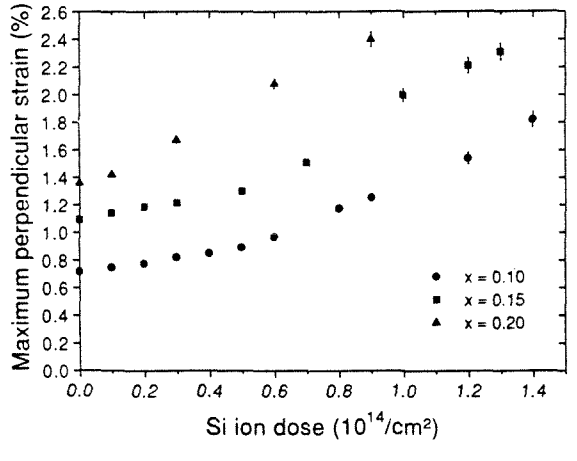

FIG. 7. The maximum perpendicular strain plotted vs Si ion dose of $x=0.10$, 0.15, and 0.20, all irradiated by 100 keV Si at room temperature.

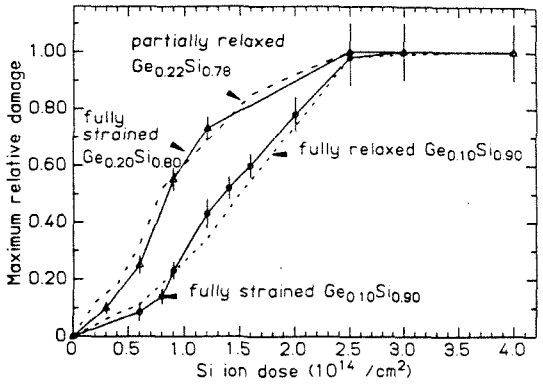

FIG. 8. The maximum relative damage of $x=0.10$ and $x=0.20$ irradiated by 100 keV Si at room temperature were plotted vs the Si ion dose (solid lines). The maximum relative damage of a fully relaxed $x=0.10$ and a partially relaxed $x=0.22$, both irradiated at the same condition as described above, were also plotted here (dashed lines) for comparisons.

1. Influence of initial strain

We now consider how the uniform strain, present initially in epitaxial films, affects the retained damage generated by Si irradiation. Epitaxial Ge_xSi_{1-x} films with different amounts of strain relaxation offer a convenient opportunity to investigate this question. We have done so using samples of $x=0.10$ for both fully relaxed and fully strained layers, and with partially relaxed and fully strained samples of almost the same composition ($x=0.22$ and 0.20, respectively). Figure 8 shows that the initially uniform strain of the Ge_xSi_{1-x} samples does not alter the induced damage levels significantly. For both pseudomorphic and fully relaxed $x=0.10$ layers, the curves of maximum relative damage versus the Si ion-dose are similar. The damage-dose relationships among pseudomorphic $x=0.20$ and partially related $x=0.22$ films are close to each other as well.

We suggest that the reason the initial strain does not play an important role here is because the elastic energy density in the film is small compared with the average energy density per atom deposited into the atomic collision cascade by the energetic ions. To see this quantitatively, the elastic energy density of an elastically isotropic material is given by

$$U_{\text{elastic}}=2\mu\epsilon_0^2(1+\nu)/(1-\nu), \tag{3}$$

where μ is the elastic shear modulus, $\epsilon_0\approx -0.042x$ is the elastic mismatch of the strained film, and ν is its Poisson ratio. For $x=0.10$ and taking μ about 70 Gpa,[27] Eq. (3) gives

$$U_{\text{elastic}}\approx 5\times 10^{-4}\ \text{eV/atom},$$

which is about 5% of the average energy density deposited in the collision cascade during 100 keV Si irradiation of the same film. Thus the pre-existing pseudomorphic strain is unlikely to strongly affect the defect accumulation/

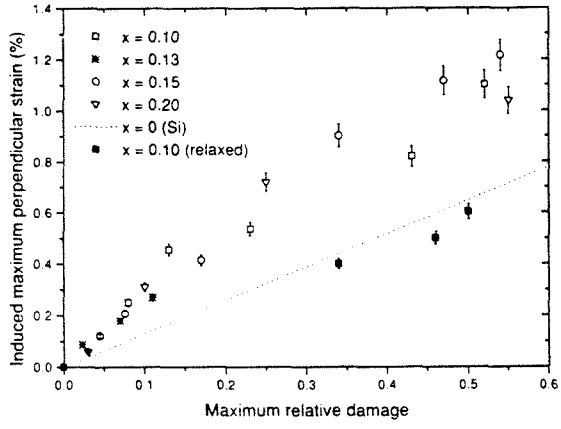

FIG. 9. The induced maximum perpendicular strain is plotted vs the maximum relative damage for $x=0.10$, 0.13, 0.15, and 0.20 irradiated with 100 keV Si (both fully strained and fully relaxed). The dashed line is the relationship between the maximum perpendicular strain and the maximum relative damage for bulk Si irradiated with 100 keV Si.

annihilation mechanism. Vos *et al.*[12] have also suggested that the initial strain of the film may not result in damage enhancement in Ge_xSi_{1-x}.

2. Damage versus induced strain

The results presented in Sec. III D 1 show that a uniform pseudomorphic strain has little effect on the retained damage measured in Ge_xSi_{1-x} at room temperature. This does not prove (in general) that a nonuniform strain will not affect the retained damage. It has been shown that in pure Ge and Si the maximum perpendicular strain generated by Si ion irradiation at room temperature is approximately linearly related to the maximum relative damage, with a proportionality constant of ~ 0.013.[14] This result was interpreted as meaning that in both Si and Ge it is the damage that creates strain and that equal increments of damage produces roughly equal increments of strain.[14,19] It is interesting therefore to relate the measured maximum perpendicular strain with the maximum relative damage for Ge_xSi_{1-x} as well (Fig. 9). The significant dislocation density in the initially relaxed layers broadens their diffraction peaks and makes the maximum radiation-induced strain difficult to determine. Therefore, only three data points at high doses are plotted for the fully relaxed $x=0.10$ film. Also shown is the linear dependence for the 100 keV Si sample self-irradiated at room temperature.

There is a significant difference in Fig. 9 between the points for pseudomorphic Ge_xSi_{1-x} and the dotted line for Si. Because of the scatter in the data points for Ge_xSi_{1-x} it is not possible to determine whether or not there is a consistent dependence of the relation between strain and damage on the value of x. It is clear however that for values of x as small as 0.10, there is significantly higher strain per unit damage in the alloy than in pure silicon. It is possible that this increased strain is associated with the stabilization of defects by Ge discussed in Sec. III B, but the present work does not permit any conclusions about the details of such an association.

The points for the fully relaxed film with $x=0.10$ fall significantly below those for the unrelaxed alloy films and slightly below the linear relation for pure Si. A fully relaxed layer has dislocations that are absent in its pseudomorphic counterpart (and whose density is approximately $8\times 10^8/cm^2$ for $x=0.10$).[28] The difference in strain accumulation with damage between pseudomorphic and relaxed films may be associated with this difference in the initial dislocation density of the sample, but speculations on detailed mechanisms are not warranted at the present time.

IV. CONCLUSIONS

(1) The nonlinear increase of the maximum relative damage with dose is a general property of the Ge-Si system irradiated with Si ions at room temperature.

(2) Increasing the Ge content in the film strongly enhances the damage.

(3) The increase in relative damage with Ge content in the films is due to both an increase in the average energy density per ion deposited in the collision cascade and a stabilization of the damage, in roughly equal proportions.

(4) As the relative damage increases with the dose and Ge content, so does the induced maximum perpendicular strain.

(5) There is greater induced maximum perpendicular strain in pseudomorphic Ge_xSi_{1-x} films than in Si or Ge for the same maximum relative damage, but not in relaxed Ge_xSi_{1-x} films.

ACKNOWLEDGMENTS

This work was supported by the Semiconductor Research Corporation under a coordinated research program at Caltech and at UCLA, contract no. 93-SJ-100. D. Y. C. Lie would like to express deep appreciation to Dr. Holländer at ISI, Jülich, Germany for providing the $x=0.22$ sample. The authors would also like to thank Dr. C. J. Tsai and Dr. G. Bai for providing the simulation programs; Dr. T. Workman, R. Gorris, M. Easterbrook for help in maintaining and repairing equipment, and Professor W. L. Johnson, Professor T. Christman, and Dr. M. Li for illuminating discussions.

[1] R. People, IEEE J. Quantum Electron. **22**, 1696 (1986).
[2] C. A. King, J. L. Hoyt, and J. F. Gibbons, IEEE Trans. Electron Devices **36**, 2093 (1989).
[3] D. K. Nayak, J. C. S. Woo, J. S. Park, and K. L. Wang, IEEE Electron Device Lett. **12**, 154 (1991).
[4] S. C. Jain and W. Hayes, Semicond. Sci. Technol. **6**, 547 (1991).
[5] K. P. MacWilliams and J. D. Plummer, IEEE Trans. Devices **38**, 2619 (1991).
[6] S. Mantl, B. Holländer, W. Jäger, B. Kabius, H. J. Jorke, and E. Kasper, Nucl. Instrum. Methods B **39**, 405 (1989).
[7] B. T. Chilton, B. J. Robinson, D. A. Thompson, T. E. Jackman, and J.-M. Baribeau, Appl. Phys. Lett. **54**, 2 (1989).
[8] D. C. Paine, D. J. Howard, N. G. Stoffel, and J. H. Horton, J. Mater. Res. **5**, 1023 (1990).

[9] M. Vos, C. Wu, I. V. Mitchell, T. E. Jackman, J.-M. Baribeau, and J. P. McCaffrey, Appl. Phys. Lett. **58**, 951 (1991).
[10] D. J. Eaglesham, J. M. Poate, D. C. Jacobson, M. Cerullo, L. N. Pfeiffer, and K. West, Appl. Phys. Lett. **58**, 523 (1991).
[11] T. E. Haynes and O. W. Holland, Appl. Phys. Lett. **61**, 61 (1992).
[12] M. Vos, C. Wu, I. V. Mitchell, T. E. Jackman, J.-M. Baribeau, and J. P. McCaffrey, Nucl. Instrum. Methods B **66**, 361 (1992).
[13] G. Bai and M.-A. Nicolet, J. Appl. Phys. **71**, 4227 (1992).
[14] D. Y. C. Lie, A. Vantomme, F. Eisen, M.-A. Nicolet, V. Arbet-Engels, and K. L. Wang, Mater. Res. Soc. Symp. Proc. **262** (1993).
[15] C. J. Tsai, A. Dommann, M.-A. Nicolet, and T. Vreeland, Jr., J. Appl. Phys. **69**, 2076 (1991).
[16] L. C. Feldman, J. W. Mayer, and S. T. Picraux, *Materials Analysis by Ion Channeling* (Academic, London, 1982).
[17] G. Bai and M.-A. Nicolet, J. Appl. Phys. **70**, 3551 (1991).
[18] O. W. Holland, S. J. Pennycook, and G. L. Albert, Appl. Phys. Lett. **55**, 2503 (1989).
[19] G. Bai and M.-A. Nicolet, J. Appl. Phys. **70**, 649 (1991).
[20] J. F. Ziegler, J. P. Biersack, and U. Littmark, *The Stopping and Range of Ions in Matter* (Pergamon, London, 1985).
[21] G. Bai and M.-A. Nicolet, J. Appl. Phys. **70**, 3551 (1991).
[22] D. A. Thompson and R. S. Walker, Radiat. Eff. **36**, 91 (1978).
[23] K. B. Winterbon, *Ion Implantation Range and Energy Deposition Distributions* (Plenum, New York, 1975), Vol. 2.
[24] R. S. Walker and D. A. Thompson, Radiat. Eff. **37**, 113 (1978).
[25] D. A. Thompson, R. S. Walker, and J. A. Davies, Radiat. Eff. **32**, 135 (1977).
[26] P. Sigmund, Appl. Phys. Lett. **14**, 114 (1969).
[27] *Handbook of Semiconductor Silicon Technology,* edited by W. C. O'Mara, R. B. Herring, and L. P. Hunt (Noyes, New York, 1990).
[28] G. Bai, Ph. D. thesis, California Institute of Technology, 1991, Chap. 2.

Appendix 2

Dependence of damage and strain on the temperature of Si irradiation in epitaxial $Ge_{0.10}Si_{0.90}$ films on Si(100)

D. Y. C. Lie,[a] J. H. Song,[b] A. Vantomme,[c] F. Eisen, and M.-A. Nicolet
California Institute of Technology, Pasadena, California 91125

N. D. Theodore
Motorola, Inc., MD-M360, 2200 West Broadway Road, Mesa, Arizona 85202

T. K. Carns and K. L. Wang
University of California, Los Angeles, California 90024

(Received 11 August 1994; accepted for publication 5 December 1994)

Damage and strain produced in a 370-nm-thick strained epitaxial $Ge_{0.10}Si_{0.90}$ film on Si(100) by irradiation with 320 keV $^{28}Si^+$ ions at fixed temperatures ranging from 40 to 150 °C and for doses from 1 to $30\times10^{14}/cm^2$ have been measured by MeV ^4He channeling spectrometry, transmission electron microscopy, and high-resolution x-ray diffractometry. The ion energy was chosen so that the maximum damage created by irradiation occurs very near the GeSi-Si interface. For all temperatures, the retained damage and the perpendicular strain induced by the irradiation are significantly greater in the GeSi epilayer than in the Si substrate. For all doses the retained damage and the induced perpendicular strain become small above 100 °C. Both rise nonlinearly with increasing ion dose. They are related to each other differently in GeSi than in bulk Si or Ge irradiated at room temperature. Postirradiation furnace annealing can remove a large portion of the induced damage and strain for nonamorphized samples. Amorphized samples regrow by solid-phase epitaxy after annealing at 550 °C for 30 min; the regrown GeSi is, however, highly defective and elastically relaxed. A consequence of this defectiveness is that irradiation-induced amorphization in metastable GeSi is undesirable for applications where good crystalline quality is required. Ion implantation above room temperature can prevent amorphization. © *1995 American Institute of Physics.*

I. INTRODUCTION

Si/Ge_xSi_{1-x} heterostructures have been widely studied because of their suitability for advanced electronic and optical devices.[1–3] Ion implantation is the dominant method used for introduction of precise amounts of dopants into near-surface regions of semiconductors for integrated-circuit applications. Implantation creates damage and modifies strain in implanted materials.[4–8] A few groups have recently reported that both the irradiation-induced damage and the strain in GeSi differ considerably from those in bulk Si and Ge.[9–17] For example, preferential amorphization of strained GeSi layers in Si/GeSi superlattices has been observed.[14,16] Strong enhancement of implantation-induced damage has been found in both relaxed and strained GeSi over that in Si under otherwise unchanged conditions.[10–17] Lie *et al.* further reported that the initial strain of Si-irradiated GeSi at room temperature has an insignificant effect on the irradiation-induced damage measured by ion channeling spectrometry; the initial strain does, however, alter the induced strain.[9,10] Haynes and Holland investigated the damage generated by Si irradiation in fully relaxed Ge_xSi_{1-x}, Si, and Ge for various irradiation temperatures and concluded that the presence of Ge in the Si matrix retards short-range mobilities of point defects and thus causes the observed damage enhancement in GeSi over Si.[12,13] Lie *et al.* later independently showed that for mildly damaged Ge_xSi_{1-x} irradiated at room temperature, the increase in cascade energy density and the reduction of the defect mobility contribute roughly equally to the observed enhancement of damage in GeSi.[9]

To heavily dope Si by ion implantation, it is common practice to amorphize the sample and to subsequently anneal it to take advantage of solid-phase epitaxial regrowth.[18,19] For bulk Si and Ge, amorphization followed by layer-by-layer epitaxial regrowth minimizes channeling tails of dopants, improves electrical activation, and reduces the density of implantation-induced residual defects. For the case of Si/GeSi heterostructures, however, if the implantation introduces amorphization, the regrown GeSi can contain high densities of defects.[15,17,20–31] The detailed regrowth behavior of a GeSi film depends on its Ge content and its strain state. Regrowth of Si/GeSi is reported to be very different from regrowth of bulk Si or Ge. It is known that critical implantation temperatures exist for bulk Si and Ge above which the materials do not amorphize unless very high current densities and doses are used.[15,32] It is therefore of scientific interest and also technological significance to investigate whether performing implantation at elevated substrate temperatures can prevent the amorphization of strained GeSi layers.

The thermal instability of strained Si/GeSi is another potential barrier for the successful application of ion implantation for fabrication of Si/GeSi heterostructures. To effectively remove residual defects, postimplantation furnace annealing at temperatures on the order of 900–1000 °C is

[a]E-mail: donald@iago.caltech.edu
[b]On leave from Yonsei University, Seoul 120-749, Korea.
[c]On leave from Instituut voor Kern- en Stralingsfysika, Catholic University of Leuven, Belgium.

 0021-8979/95/77(6)/2329/10/$6.00 © 1995 American Institute of Physics

required in the case of ion-implanted Si.[5,18] At such high annealing temperatures, strain relaxation and interdiffusion take place in metastable Si/Ge_xSi_{1-x} heterostructures.[2,32–34] The annealing window for implanted strained Si/Ge_xSi_{1-x} is thus narrower than in the case of Si. A possible solution to this problem is to minimize the induced damage and strain in the as-implanted sample by performing implantation at elevated temperatures; if this succeeds, the demands on postimplantation annealing treatments will be reduced. Therefore, there is a need to study the effects of annealing on the damage and strain generated by hot implantation into strained Si/GeSi.

The goal of this work is to investigate experimentally how damage and strain induced by 320 keV ^{28}Si irradiation into a nearly pseudomorphic $Si(100)/Ge_{0.10}Si_{0.90}$ layer change with sample temperatures ranging from 40 to 150 °C for various doses, and how damage and strain further evolve upon subsequent annealing.

II. EXPERIMENTAL PROCEDURE

Strained epitaxial $Ge_{0.10}Si_{0.90}$ films were grown on (100) Si substrates by ultrahigh-vacuum molecular-beam epitaxy at ~500 °C at the University of California at Los Angeles. 2 MeV ^4He channeling spectrometry gives a minimum ⟨100⟩ channeling yield of 3%–4% for the as-grown films, which indicates rather good crystalline quality. The thickness of the films is 370±50 nm, as measured by both cross-section transmission electron microscopy and the MeV ^4He backscattering spectrometry. The strains present in the films were measured using a high-resolution x-ray diffractometer with a monochrometer using two double-channel-cut Si and Ge crystals in series. X-ray rocking curves of both (400) symmetrical and (311) asymmetrical diffractions were obtained at room temperature in air. The value of the perpendicular strain measured from the x-ray rocking curves for as-grown GeSi is $(6.6\pm0.2)\times10^{-3}$. The calculated value for the strain of a pseudomorphic film is $(7.5\pm0.5)\times10^{-3}$. The as-grown $Ge_{0.10}Si_{0.90}$ films are therefore nearly pseudomorphic, with a strain value of ~90% that of a fully strained sample. To estimate the initial dislocation density in an as-grown sample, we assume that the broadening in the x-ray-diffraction peak for GeSi is only due to the presence of threading dislocations and the film's finite thickness. We can then roughly estimate the dislocation density using the equation $\rho_t=(W_d)^2/9b^2$, where W_d is the full width at half-maximum of the GeSi film peak broadened by dislocations only, and b is the Burgers vector of the dislocations.[35] By this method, an as-grown sample is estimated to have a dislocation density of $\sim5\times10^6/cm^2$. The dislocation density measured using plan-view transmission electron microscopy is $\sim10^7/cm^2$, which is consistent with the x-ray results. X-ray rocking curves of the heterostructure are simulated using a computer code based on dynamical x-ray-diffraction theory[8,36] to extract depth profiles of the perpendicular strain and of the random lattice displacement (i.e., static Debye–Waller factor).

After chemical cleaning, the samples were mounted with silicone heat paste to the holder of a 400 keV ion implanter. The sample normal was tilted by 7° away from the incident beam in order to minimize channeling during irradiation. The $^{28}Si^+$ ion flux was maintained around 60 nA/cm^2 to minimize beam heating and dose rate effects. The irradiations were performed using 320 keV $^{28}Si^+$ ions at fixed temperatures ranging from 40 to 150 °C and with doses ranging from 1 to $30\times10^{14}/cm^2$. The silicone paste on the backside of the samples established thermal contact with the carousel holder. The temperatures of irradiation quoted in this article refer to equilibrium temperatures of the holder as measured by a thermocouple immediately prior to the irradiation. The increase in the sample temperature due to beam heating effects is estimated to be less than 1 °C. The projected range in $Si/Ge_{0.10}Si_{0.90}$ for 320 keV $^{28}Si^+$ obtained from the TRIM-92 simulation code[37] is ~480 nm, i.e., significantly beyond the GeSi film thickness of 370 nm. The damage peak obtained from the same simulation was located at ~370±60 nm, i.e., roughly at the Si-GeSi interface. The irradiation-induced damage in the samples was characterized using MeV ^4He backscattering/channeling spectrometry; the induced strain was measured using x-ray rocking curves with both (400) and (311) diffraction. After these measurements, the as-irradiated samples were annealed in high vacuum (~10^{-7} Torr) for 30 min at 200 °C first; the same sample was then annealed at 300 °C for 30 min, and later at 550 °C for 30 min. Selected samples were further annealed at higher temperatures ranging from 600 to 800 °C.

III. RESULTS

A. Irradiation-induced damage

Figure 1 shows two sets of 2 MeV ^4He channeling spectra obtained along the ⟨100⟩ axial direction for Si/GeSi samples as irradiated with 320 keV Si ions to doses of 5×10^{14} (bottom) and 1×10^{15} Si^+/cm^2 (top) at temperatures of 40–150 °C. Also shown in Fig. 1 as reference are the spectra for a ⟨100⟩ direction (labeled "as grown") and for a randomly oriented beam incidence on a virgin sample (labeled "random"). The detector angle is 170° with respect to the direction of the incident ^4He beam. The surface energies for Si and Ge signals are indicated by arrows. The energy corresponding to the projected range of 320 keV Si ions is labeled as R_p. Figure 1 shows that considerably more damage is retained in GeSi than in Si. For example, the backscattering yield of a GeSi film irradiated at 40 °C with a dose of 5×10^{14} Si^+/cm^2 reaches the height of the spectrum taken with a random beam incidence (labeled "random"), which indicates that a buried amorphous layer is formed in the epi-GeSi. This is not so for the Si substrate, because the channeling yield there (at 0.8–0.95 MeV) falls considerably below the random level, even though the Si has received at least as much implanted ions as the adjacent GeSi. Several groups have observed similar enhancement of damage in strained GeSi over that in Si with irradiations performed at temperatures no higher than ~50 °C.[14,16] The results in Fig. 1 confirm these reports and extend the existence of this effect to yet higher temperatures.

We extracted the irradiation-induced maximum relative damage in the epi-GeSi from such channeling spectra using a straight-line approximation.[38,39] The data extraction proce-

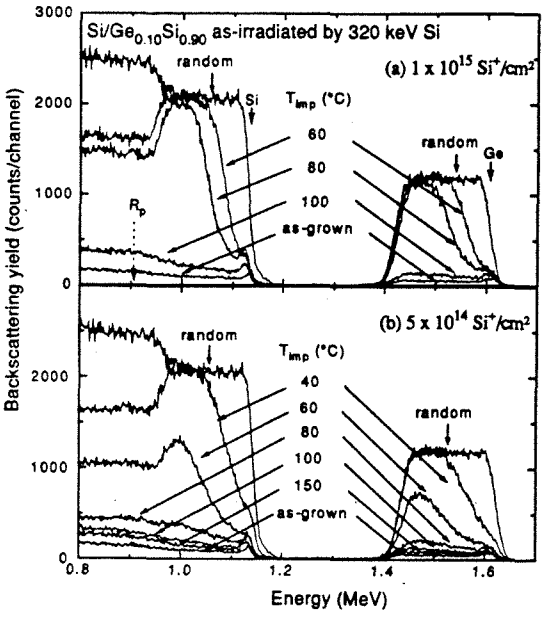

FIG. 1. 2 MeV ^{4}He channeling spectra for the ⟨100⟩ axial direction of Si/GeSi samples as irradiated at temperatures of 40–150 °C with 320 keV Si ions to doses of 5×10^{14} Si^+/cm^2 (bottom) and 1×10^{15} Si^+/cm^2 (top). The spectra for a ⟨100⟩ and randomly oriented beam incident on a virgin sample are also included for reference. The surface energies for Si and Ge signals are indicated with arrows. The energy corresponding to the projected range of 320 keV Si ions is labeled as R_p. The detector angle is 170° with respect to the direction of the incident ^{4}He beam.

dure is described in the Appendix. Figure 2 plots the extracted maximum relative damage against the irradiation temperature for all as-irradiated GeSi epilayers and for various doses. At a fixed dose, the induced maximum relative damage always decreases with increasing irradiation temperature. The striking feature of this figure is that at sufficiently high temperatures of irradiation, virtually all detectable damage disappears as measured by channeling spectrometry. The temperature at which this occurs increases with increasing dose. In terms of absolute temperature, the transition from full amorphization to a barely detectable amount of damage is very abrupt. For example, the maximum relative damage created with a dose of 1×10^{15} Si^+/cm^2 reaches 100% (amorphization) at 60 °C, but it plunges to only ~2% when the irradiation temperature is increased to 100 °C, i.e., in an interval of only 11% in absolute temperature.

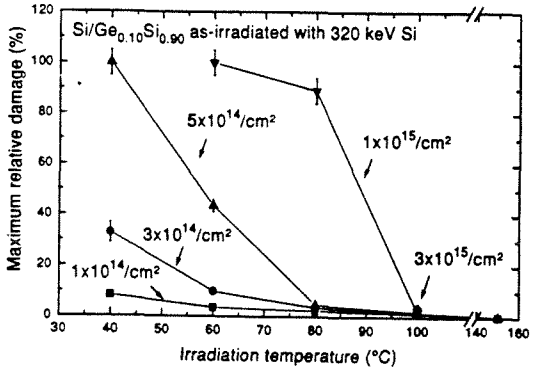

FIG. 2. The values of the maximum relative damage extracted from the channeling spectra plotted against the irradiation temperature for all as-irradiated GeSi epilayers with the dose of 320 keV Si ions as the parameter.

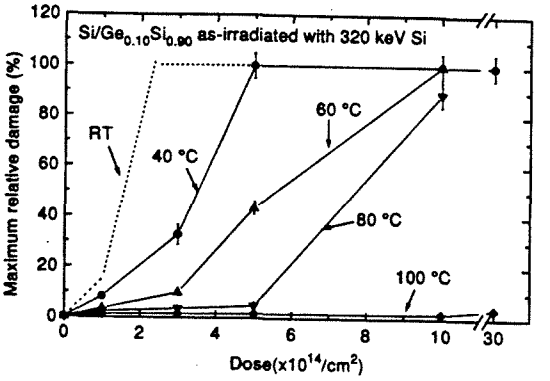

FIG. 3. The values of the irradiation-induced maximum relative damage in GeSi plotted against the dose of 320 keV Si ions for all samples as irradiated at various temperatures. The dotted line is from Ref. 9 for GeSi irradiated at room temperature with 100 keV Si ions.

Figure 3 plots the data of Fig. 2 using the dose as the variable and irradiation temperature as a parameter. Also included as a dotted line is the dose-damage relationship obtained by Lie *et al.*[9] for $Ge_{0.10}Si_{0.90}$ irradiated at room temperature, however, with an ion energy of 100 keV, which is different from the current study. It is evident that as the irradiation temperature decreases, the transition from little to 100% damage occurs over narrower dose intervals.

Figure 3 also reveals that the relationship between the maximum relative damage and the Si ion dose is nonlinear at all irradiation temperatures. This nonlinearity between the induced damage and the ion dose has been reported for bulk Si irradiated at liquid nitrogen and room temperatures with various ion species and energies.[6,9,40] It has also been observed in bulk Ge and epi-Ge_xSi_{1-x} (x=0.10–0.22),[9] irradiated with Si at room temperature. In those cases the maximum relative damage first increases slowly and linearly with dose until a threshold value of 15% is reached, and then rises rapidly until the sample is amorphized. The results presented in Fig. 3 are consistent with this dose dependence of the accumulated damage, but the number of data points is too limited to definitely establish such a dependence at every temperature.

Figure 4 shows two sets of 2 MeV ^{4}He channeling spectra obtained along the ⟨100⟩ axial direction for Si/GeSi irradiated at 60 °C with doses of 5×10^{14} (bottom) and 1×10^{15} Si^+/cm^2 (top), after annealing in additive succession at 200, 300, and 550 °C for 30 min each. The spectra for a ⟨100⟩ and

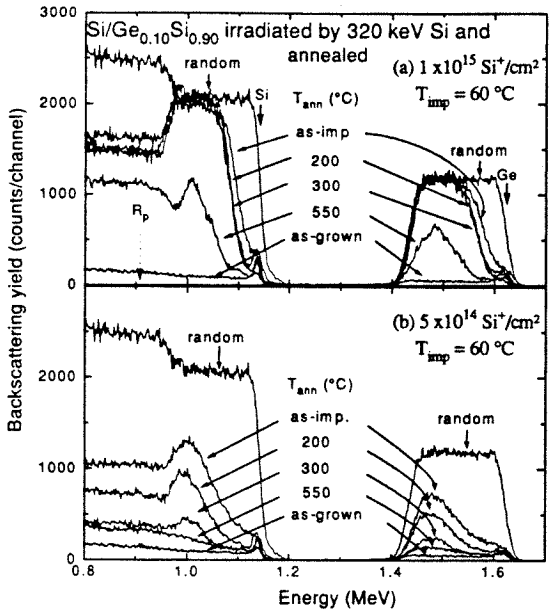

FIG. 4. 2 MeV ^{4}He channeling spectra for the ⟨100⟩ axial direction of $Si(100)/Ge_{0.10}Si_{0.90}$ samples irradiated at 60 °C with doses of 320 keV Si ions of 5 and 10×10^{14} Si^+/cm^2 before and after annealing in high vacuum ($\sim10^{-7}$ Torr) at 200–550 °C for 30 min each and additively. The spectra for a ⟨100⟩ and for a randomly oriented beam incident on a nonimplanted sample are also plotted for reference. The surface energies for Si and Ge signals and the energy for the projected range of the 320 keV Si ions induced by the implantation of 320 keV Si ions are labeled in the identical fashion as in Fig. 1.

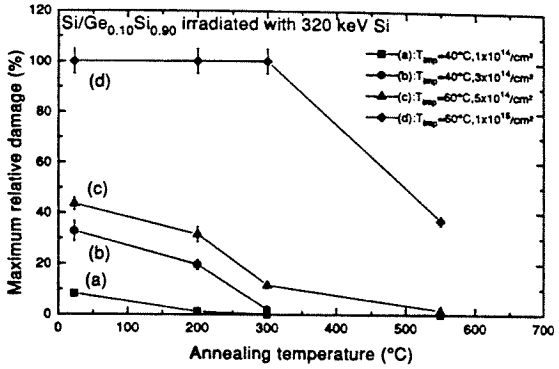

FIG. 5. Annealing of the maximum relative damage in four samples selected for their different values of damage. The temperature and doses of implantation are presented in the insert. Only sample (d) is amorphized after irradiation. The annealing was performed in high vacuum ($\sim10^{-7}$ Torr) for 30 min at each temperature in succession.

for a randomly oriented beam incidence on a nonimplanted sample are also plotted for reference. The sample as irradiated with a dose of 1×10^{15} Si^+/cm^2 has a buried amorphous layer which is ~295 nm thick, while the other sample irradiated with 5×10^{14} Si^+/cm^2 is not amorphized. We observe that the peak values in the backscattering yield decrease as the annealing temperature increases. After annealing at temperatures below 300 °C, the channeling spectra for the amorphous GeSi layer do not noticeably change, but those for the nonamorphized sample do, indicating the removal of irradiation-induced defects. Upon annealing at 550 °C, the buried amorphous layer evidently regrows from both sides, leaving a distinct peak in the backscattering yield at roughly halfway across the amorphous layer, presumably where the two regrowth fronts meet.

To highlight the annealing behavior of the implantation-induced damage, we selected four samples with different values of initial maximum relative damage and present the annealing results in Fig. 5. The irradiation temperature and doses of these samples are included in the insert within the figure; the values of maximum retained relative damage in the samples are plotted against the maximum annealing temperatures in the range of 200–550 °C. A continuous amorphous layer was formed only in sample (d) after irradiation. The retained damage generally decreases as the annealing temperature increases; the annealing characteristics of the amorphized and the nonamorphized samples are, however, quite different. The maximum relative damage of nonamorphized samples (a)–(c) decreases significantly for 200–300 °C anneals, and becomes very small after a 550 °C anneal. This dependence is similar to that of self-irradiated Si.[6] For the amorphized sample (d), however, the additive annealing at 200 and 300 °C for 30 min each has no detectable effect on the retained maximum relative damage. Upon further annealing at 550 °C, the retained maximum relative damage finally decreases but still remains at a significant ~37% level. This behavior is much different from that of self-irradiated amorphous Si films on Si(100) annealed at 550 °C for 30 min,[6,41,42] as is discussed later in this article. We therefore conclude that irradiation-induced amorphization is detrimental to the recovery of crystallinity in metastable strained GeSi on Si(100).

B. Irradiation-induced increase in strain

Figure 6 shows three sets of measured (solid circle) and simulated (solid line) x-ray rocking curves of (400) diffraction for: (a) an as-grown strained $Si(100)/Ge_{0.10}Si_{0.90}$ sample; (b) the same sample after irradiation at 40 °C with 320 keV Si ions to a dose of $3\times10^{14}/cm^2$; and (c) the sample as in (b) subsequently annealed at 200 °C first, and then at 300 °C for another 30 min. The origin of the abscissa in Fig. 6 is placed at the Bragg angle $\theta_B=34.575°$ of the Si substrate peak. Figures 7(a)–7(c) show three sets of depth profiles of the total perpendicular strain (solid line) and the static Debye–Waller factor (dotted line) assumed for the simulations in Figs. 6(a)–6(c). The initial strain assumed for the nonirradiated sample (a) is also shown as a dashed-dotted line in Figs. 7(b) and 7(c) for reference, and so is the position of the original Si-GeSi interface. The profiles for the static Debye–Waller factor in Figs. 7(b) and 7(c) are scaled approximately proportionally to the increased amounts of the perpendicular strain. In so doing, we follow the procedure previously adopted by Sperioso[43] and Tsai *et al.*[8]

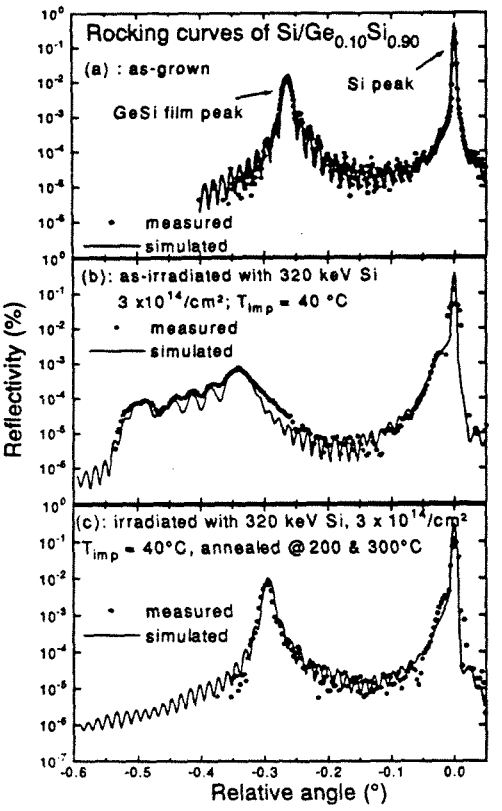

FIG. 6. Measured (solid circle) and simulated (solid line) x-ray rocking curves for (400) diffraction from (a) an as-grown (nonirradiated) strained $Si(100)/Ge_{0.10}Si_{0.90}$ sample, (b) the same sample after irradiation at 40 °C by 320 keV Si ions with a dose of 3×10^{14} Si^+/cm^2, and (c) the sample in (b) subsequently annealed at 200 °C for 30 min first, and then at 300 °C for another 30 min. The origin of the abscissa is placed at the Bragg angle $\theta_B = 34.575°$ of the Si substrate. The peaks for both Si and GeSi are labeled (a).

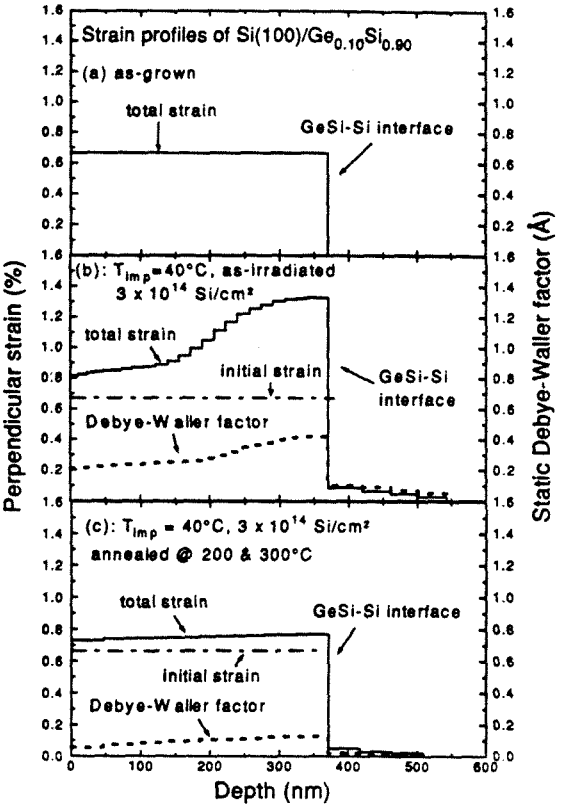

FIG. 7. (a)–(c) Depth profiles of the total perpendicular strain (solid line) and the static Debye–Waller factor (dotted line) assumed for the simulations in Figs. 6(a)–6(c). The initial strain of the nonirradiated sample (a) is indicated in (b) and (c) for reference. The position of the original GeSi-Si interface is also labeled.

The rocking curve of the virgin sample [Fig. 6(a)] exhibits small periodic oscillations and a sharp and strong film peak, characteristic of epitaxial films with very good crystalline quality. The fit between the measured and the simulated rocking curves is excellent. Figure 6(b) shows that irradiation creates additional positive perpendicular strain in the originally strained GeSi, as indicated by the wider separation between the peaks of the film and the substrate. The irradiation also induces strain in the Si substrate, as the sidelobe on the left-hand side of the Si peak reveals [$\sim -0.03°$ in Fig. 6(b); see also Fig. 7(b)]. The irradiation-induced damage in GeSi significantly reduces the GeSi peak intensity in Fig. 6(b). Figure 6(c) shows that annealing at 200 and 300 °C for 30 min removes nearly ~90% of the irradiation-induced perpendicular strain [cf. Figs. 6(a) and 6(b)]. The epi-GeSi diffraction peak in Fig. 6(c) is again sharp and strong with its associated small oscillations, which indicates that a great proportion of the induced strain and damage disappear after annealing. Figure 7(c) shows that a fairly uniform excess of strain of about 10% still remains in the layer. The discontinuity for the profiles of the Debye–Waller factor at the GeSi-Si interface is consistent with the ⟨100⟩ channeling spectrum (not shown here) where a discontinuity in the backscattering yield is also observed.[44] After annealing most of the damage has disappeared, as shown in Fig. 7(c). The corresponding backscattering yield in the channeling spectrum is also much reduced [see Fig. 5, sample (b), at 300 °C].

The extracted strain profiles as shown in Figs. 7(a)–7(c) establish that the maximum increase in the perpendicular strain occurs at the Si-GeSi interface for our irradiation experiments. The maximum in the increase of strain can be directly estimated within 10% accuracy from the angular position of the major peak furthest from that of the substrate in the rocking curves, without the need of carrying out the simulations. We have used this procedure to obtain the irradiation-induced increase in the maximum perpendicular strain of other samples and present the strain values in Figs. 8–10 below. Note, though, that due to the loss of the diffraction intensity as the irradiation-induced damage increases,

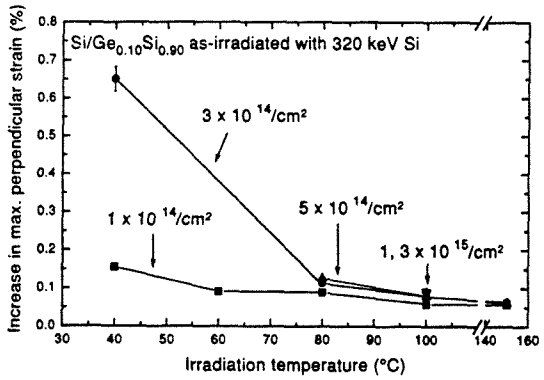

FIG. 8. The increase in the maximum perpendicular strain generated by 320 keV Si irradiation of Si(100)/GeSi samples plotted vs the irradiation temperatures for doses of $1-30\times10^{14}$ Si/cm^2. Due to a loss of diffraction intensity as the irradiation-induced damage increases, strain data for heavily damaged and for amorphous samples are not available.

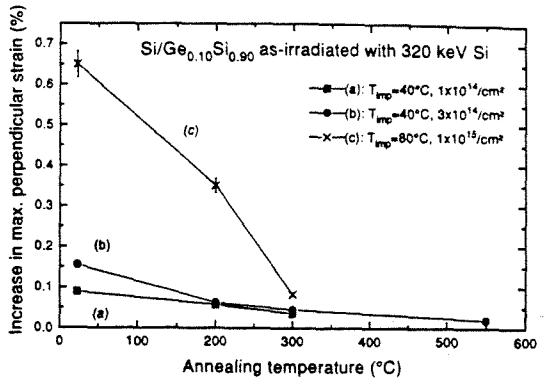

FIG. 9. Recovery of the maximum perpendicular strain for three strained Si(100)/GeSi samples selected for their different values of strain induced by the irradiation of 320 keV Si ions at temperatures and doses presented in the insert. The annealing was performed in high vacuum (10^{-7} Torr) for 30 min at each temperature in succession.

the strain data for heavily damaged and for amorphized samples are not available for presentation in Figs. 8–10. All of the samples discussed in Figs. 8–10 have a common small value of parallel strain that was not noticeably influenced by irradiation and annealing at temperatures up to 550 °C; this means that no significant strain relaxation took place in any of these samples.

Figure 8 plots the increase in maximum perpendicular strain versus irradiation temperatures for as-irradiated Si/GeSi samples at various doses. One notices that at a constant dose the increase in the maximum perpendicular strain falls off rapidly with increasing irradiation temperature. For sufficiently high substrate temperatures, little perpendicular strain is induced by irradiation. The perpendicular strain thus shows the same type of temperature dependence as the damage does in Fig. 2.

Figure 9 shows the recovery of the maximum perpendicular strain against the maximum annealing temperature for three strained Si(100)/GeSi structures possessing different strain values after irradiation. The irradiation temperature and the doses of Si ions are presented in the insert within the figure. The data indicate that if the sample is not amorphized, only a small amount of the added maximum perpendicular strain is retained after 550 °C annealing for all doses. The same observation was made for the damage in Fig. 5. The strain recovery thus parallels that of the damage. The total perpendicular strain also never falls below its initial value. These facts can be simply interpreted by assuming that it is the induced damage that causes the strain. This notion has been stated before.[6,9] Thus, as long as the irradiation does not amorphize Si/GeSi, induced damage and perpendicular strain are largely reversible.

C. Irradiation-induced increase in strain versus damage

We have shown in Fig. 8 that the relationship between the irradiation temperature and the increase in the perpendicular strain is quite similar to that of the induced damage in Fig. 2. The irradiation induced maxima in strain and damage have been reported to be roughly linearly related to each other with a proportionality factor of ~0.013 for as-irradiated bulk Si and Ge at room temperature.[9] The result in bulk Ge and Si was interpreted as meaning that it is the irradiation-induced damage that creates strain and that equal increments of damage roughly produce equal increment of strain. It is therefore interesting to further examine the relationship between induced damage and strain for as-irradiated GeSi.

Figure 10 plots the increase in the maximum perpendicular strain versus the maximum relative damage for as-

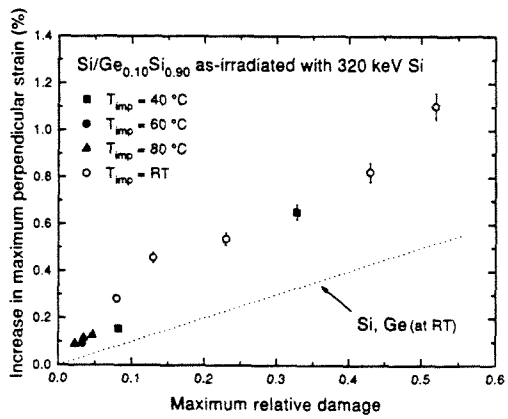

FIG. 10. The increase in the maximum perpendicular strain plotted against the maximum relative damage for strained Si(100)/GeSi irradiated at various temperatures. The dotted line is the strain-damage relationship taken from Ref. 9 for 100 keV Si-irradiated bulk Si and Ge. The data for room-temperature irradiation (open circles) are taken from Ref. 9 for a pseudomorphic $Ge_{0.10}Si_{0.90}$ film irradiated with 100 keV Si. The solid symbols are data from this work, where the irradiation temperature is above room temperature, and the Si ion energy is 320 keV.

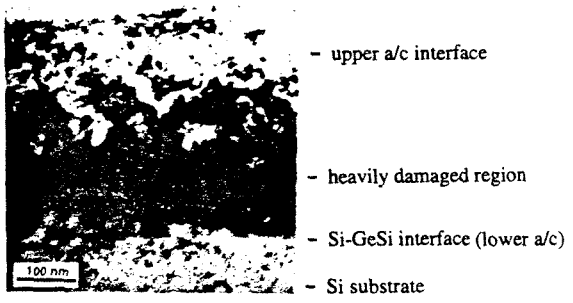

FIG. 11. Cross-section transmission electron micrograph obtained from a strained $Ge_{0.10}Si_{0.90}$ layer irradiated at 60 °C with 1×10^{15} Si^+/cm^2 and subsequently annealed successively at 200, 300, and 550 °C for 30 min each. The channeling spectrum for this sample plotted in Fig. 1. The amorphized GeSi layer regrew after annealing: extensive residual damage is present within the regrown GeSi layer. There is a thin layer ~20 nm thick located right above the Si-GeSi interface which appears to be of good crystallinity. The irradiation energy is 320 keV.

irradiated $Si(100)/Ge_{0.10}Si_{0.90}$ at several irradiation temperatures. The solid symbols are data from the present work for irradiation at temperatures above room temperature, utilizing an ion energy of 320 keV. The dotted line is the strain-damage relationship obtained from Ref. 9 for bulk Si and Ge irradiated at room temperature with 100 keV Si ions. The data plotted for room-temperature irradiation (open circles) are also taken from Ref. 9 and are for pseudomorphic $Ge_{0.10}Si_{0.90}$ irradiated at room temperature with 100 keV Si ions, where the ion range is less than the thickness of the epilayer.

For any given values of the maximum relative damage, the corresponding increases in the maximum perpendicular strain in Fig. 10 all lie significantly above the dotted line; this result shows that the relationship between irradiation-induced maximum damage and strain in strained GeSi differs from that in bulk Si and Ge and that the relationship may depend on the implantation temperature as well. Channeling analysis determines damage in a microscopically unspecific way, so that it is possible that a single value of damage plotted on the abscissa of Fig. 10 can correspond to different microstructures of the retained defects for different samples, and hence also to different amounts of added strain.[10] A deeper understanding of the strain-damage relationship of Fig. 10 must come from microscopic analysis of the defect structures responsible for the strain, and is likely to be complex.

D. Amorphization

Next, we demonstrate that if a continuous amorphous layer is formed in a metastable strained $Ge_{0.10}Si_{0.90}$ layer by irradiation, neither its initial crystallinity nor its initial strain state can be recovered by postirradiation steady-state annealing.

Figure 5 shows that the maximum relative damage of an amorphized sample recovers only poorly [sample (d) at 550 °C]. Figure 11 is a cross-section transmission electron micrograph of this sample after consecutive annealings at 200, 300, and 550 °C for 30 min each. The channeling spectrum for this sample has been plotted in Fig. 1; the amorphous region reaches down to the original Si/GeSi interface in the case of the as-implanted sample. The rate of solid-phase regrowth for Si-irradiated strained $Ge_{0.10}Si_{0.90}$ is close to 0.1 nm/s at 550 °C.[21,25] Annealing of an amorphous $Ge_{0.10}Si_{0.90}$ layer on crystalline Si at 550 °C for 30 min should thus yield a regrown crystalline layer around 180 nm in thickness. In the present case, the amorphous layer is buried and can regrow from both sides. Thus the entire 295 nm amorphous layer becomes crystalline again after 30 min annealing at 550 °C.

Various regions are labeled on the transmission electron micrograph as shown in Fig. 11. The surface of the Si/GeSi heterostructure is indicated. The position of the upper and the lower amorphous-to-crystalline interfaces for the irradiation-induced buried amorphous band are indicated by labels "upper a/c interface" and "Si-GeSi interface (lower a/c)." The positions of these a/c interfaces are calculated from the backscattering spectrum of an as-implanted sample and they are shown in Fig. 11 on an annealed sample merely for reference. The lower a/c interface in the as-implanted sample corresponds to the Si-GeSi interface. In Fig. 11, localized strain is observed due to the presence of a band of high-density residual defects, which is labeled as "heavily damaged region" in the micrograph. Above it is a band containing dislocation loops whose sizes decrease toward the surface of the wafer. The defects gradually change to a collection of point-defect clusters of decreasing size when approaching the surface. The GeSi at the top is almost free of defects.

Just above the Si-GeSi interface is a thin layer of GeSi of ~20 nm that is not significantly damaged. Similar results have been reported by Hong *et al.*[25] for a strained $Si(100)/Ge_{0.10}Si_{0.90}$ epilayer amorphized by room-temperature Si irradiation. They also found an approximately 30-nm-thick GeSi layer of good crystalline quality located between the original a/c interface and the beginning of dislocations after annealing at 550 °C. Below the GeSi/Si interface, occasional point-defect clusters are present in Fig. 11. It can be seen therefore that there is heavy residual damage within the regrown GeSi layer, but the residual damage in the Si substrate is small. This means that most of the irradiation-induced damage in Si is removed by annealing at 550 °C; regrowth of the GeSi, however, results in poor crystallinity.

X-ray rocking curves of (400) diffraction for a strained $Si(100)/Ge_{0.10}Si_{0.90}$ sample amorphized at 40 °C with 5×10^{14} Si^+/cm^2 are plotted in Fig. 12 before and after successive annealings at 550, 600, 700, and 800 °C for 30 min each. There is a continuous buried amorphous GeSi layer in this as-irradiated sample (Fig. 1). The rocking curve for a virgin sample is also included for reference. The origin of the abscissa is placed at the Bragg angle $\theta_B=34.575°$ of the Si substrate peak. Some data points of the spectra are omitted in this plot for the sake of clarity.

Because of irradiation-induced damage, the intensity of the GeSi peak is reduced by two orders of magnitude after irradiation. There is also significant induced strain in the Si substrate after the irradiation, as a peak at $\sim-0.03°$ near the Si substrate peak reveals. After annealing at 550 and 600 °C,

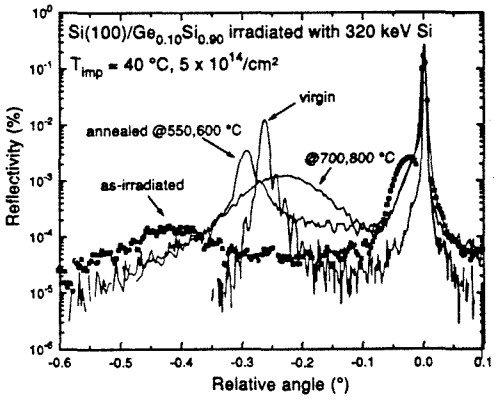

FIG. 12. X-ray rocking curves of (400) diffraction for a $Si(100)/Ge_{0.10}Si_{0.90}$ sample irradiated at 40 °C with 5×10^{14} Si^+/cm^2 before and after successive annealing at 550, 600, 700, and 800 °C for 30 min each. As irradiated, the sample has a continuous buried amorphous layer. The rocking curve for a virgin sample is also included for reference. The origin of the abscissa is placed at the Bragg angle $\theta_B=34.575°$ of the Si substrate peak. Some data points of the spectra are omitted for the sake of clarity.

the irradiated sample still shows significant broadening in the GeSi diffraction peak and also a reduced intensity. Both results indicate that the crystalline quality of the annealed GeSi is considerably inferior to that of a virgin sample. An increase in the maximum perpendicular strain still exists in GeSi after the annealing. After this sample is further annealed at 700 or 800 °C for 30 min, substantial strain relaxation takes place. The separation between the GeSi and Si peaks decreases to ~0.22° and the full width at half-maximum of the GeSi peak is broadened by more than a factor of 10; this broadening corresponds to an increase in the threading dislocation density by a factor of ~100. We conclude that once a metastable strained GeSi is amorphized, postirradiation steady-state annealing cannot recover the initial state of strain or crystallinity. We thus believe that irradiation-induced amorphization in strained metastable GeSi should be avoided for electronic device applications.

IV. DISCUSSION

For Si/GeSi irradiated at elevated temperatures, we have shown in Fig. 1 that damage enhancement in GeSi over Si still persists for irradiation temperatures of 40–80 °C. This observation is consistent with the results published by Haynes and Holland.[12,13] Figure 2 also shows that for as-irradiated samples, the transition from full amorphization to virtually no detectable damage is very abrupt with increasing irradiation temperature. Haynes and Holland have suggested that this abrupt reduction in the retained damage is a result of the increase in mobility of point defects at elevated irradiation temperatures so that defects can diffuse out of the collision cascades. Our data agree well with those of Haynes and Holland in showing that the retained damage becomes quite small for irradiation temperatures greater than ~100 °C.

We have also shown in Fig. 8 that the irradiation-induced perpendicular strain for prestrained $Ge_{0.10}Si_{0.90}$ decreases with increasing temperature of irradiation and also becomes rather small for irradiation at ~100 °C. A decrease in implantation-induced damage and/or strain with increasing irradiation temperature has been reported for Si, Ge, relaxed GeSi, GaAs, and InP.[32,45–47] Morehead and Crowder[37] have proposed a simple model to estimate the temperature dependence of irradiation-induced damage. That model implies that the maximum relative damage created by implantation is linearly proportional to the ion dose. The model has been used in the past in connection with irradiation-induced damage in Si, Ge, and unstrained Ge_xSi_{1-x};[12,13,45,48] however, as shown in Fig. 3 and in Refs. 6, 9, 10, and 49, the relationship between the maximum retained damage and the ion dose is clearly nonlinear in general. Thus, this particular model is not generally applicable to the present case.

The results reported here lead to the conclusion that ion implantation at temperatures of ~100 °C or above has a number of advantages over room-temperature implantation for strained metastable Si/Ge_xSi_{1-x} heterostructures. First, our data in Figs. 11 and 12 reveal that for the applications of metastable strained $Ge_{0.10}Si_{0.90}$ epilayers, implantation-induced amorphization must be avoided. Once amorphized, even 800 °C annealing for 30 min will not reestablish the initial perfection of the $Ge_{0.10}Si_{0.90}$ film, and furthermore the strain will relax. Moderate doses ($\geq2.5\times10^{14}/cm^2$) of Si into epitaxial $Ge_{0.10}Si_{0.90}$ at room temperature will amorphize the layer. This dose is about a third of that needed to amorphize Si.[6,9] Performing hot implantation at ~100 °C or above circumvents this problem of amorphization.

Second, even when the $Ge_{0.10}Si_{0.90}$ epilayer is not amorphized, our channeling measurements indicate that the annealing requirements increase with increasing defect concentrations. Strained Si/GeSi typically shows significant relaxation at furnace annealing temperatures roughly 100 °C higher than their growth temperatures, which are usually ~500–700 °C.[33] Since strain relaxation is accompanied by the generation of defects such as dislocations, and these defects are deleterious for electronic devices, the postimplantation annealing window for Si/GeSi becomes quite narrow. Hot implantations reduce the damage and strain introduced by irradiation, and therefore reduce the requirements for subsequent annealing as well.

These conclusions are based on damage and strain considerations only. Residual damage generally correlates with incomplete electrical activation of dopants.[19] To justify these conclusions for the doping of GeSi epilayers, experiments with implantations of electrically active ions are still required. So far, implantations of Sb (Refs. 25, 29, 31, and 50) and P (Ref. 20) have been described in the literature, both in strained Ge_xSi_{1-x} epilayers, but at room temperature only ($x=0.07–0.18$ and 0.12, respectively).

When the $Ge_{0.10}Si_{0.90}$ epilayer is amorphized with a thin surface region still remaining crystalline, the amorphous layer will regrow from both sides upon thermal annealing. A distinct layer of remaining defects forms where the two regrowth fronts eventually meet (Fig. 4). A similar effect exists for Si(100). Transmission electron micrographs show that the remaining defects are shear-type dislocations loops and have been attributed to local misorientation of the regrowth inter-

faces as they meet.[51] Regrowth of an amorphized layer from both the surface and the substrate can also occur in GaAs.[52] The residual defects in that case consist of a broad band of high residual damage that is not resolved into a single dominant type of defect. In that case the origin of the band is attributed to a maximum distance (~40 nm) that either interface can move before defects precipitate in the form of clusters. The results of the present transmission electron micrograph in Fig. 11 differ from both previous cases. There is a distinct region about 20–30 nm thick of good crystalline quality just next to the Si/GeSi interface. The critical thickness for pseudomorphic $Ge_{0.10}Si_{0.90}$ epilayers on Si(100) is ~22 nm, according to Paine *et al.*[21,22] In this case, a GeSi layer on Si initially regrows coherently to this critical thickness, then subsequently relaxes with defects. This, therefore, is a third possible interpretation for the existence of a defected regrown region in strained Si/GeSi. This fact has been generally recognized before in regrowth studies of amorphized strained GeSi.[24,27,28] Convincing evidence in support of this interpretation comes from a study of regrowth of an amorphized $Ge_{0.10}Si_{0.90}$ that was not strained before irradiation. The critical thickness in that case is infinite. After annealing the full 210 nm of the initially amorphized layer is of good crystalline quality.[25] A 20–30-nm-thick regrown layer of good crystalline quality is missing on the front side of the $Ge_{0.10}Si_{0.90}$ layer in Fig. 11. A plausible reason is that the surface layer of $Ge_{0.10}Si_{0.90}$ is of lesser crystalline quality than the Si substrate after irradiation. The residual damage in this front region after regrowth is clearly visible in the backscattering spectrum of 550 °C annealed sample at 1.1 and 1.6 MeV in Fig. 4.

V. CONCLUSIONS

A primary conclusion of this study is that high-temperature irradiations are required in order to minimize the residual damage and strain change observed in Si-irradiated metastable strained $Ge_{0.10}Si_{0.90}$ after steady-state thermal annealing. Although amorphized $Ge_{0.10}Si_{0.90}$ strained layers regrow by solid-phase epitaxy, their initial strain state cannot be recovered even after annealing at 800 °C. Therefore, we conclude that in order to preserve the strain state of irradiated and annealed metastable epitaxial $Ge_{0.10}Si_{0.90}$ layers on Si, the irradiations must be performed at a temperature that is high enough to avoid amorphization.

ACKNOWLEDGMENTS

This work was supported by the Semiconductor Research Corporation under Contract No. 94-SJ-100, a coordinated program between Caltech and UCLA. D.Y.C.L. is greatly indebted to Dr. T. Siu for his generous support. We would also like to thank Dr. C. J. Tsai for providing the x-ray simulation program; G. He for the control program of the rocking curve system; and R. Gorris and M. Easterbrook for technical assistance. A.V. is a Postdoctoral Researcher, NFWO (National Fund for Scientific Research, Belgium).

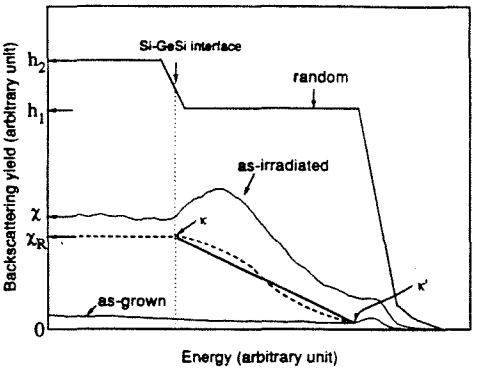

FIG. 13. A schematic drawing illustrating how to approximately extract the actual random fraction of the ^{4}He beam in irradiation-damaged Si/GeSi. An energy spectrum for channeled ^{4}He ions backscattering from ion-irradiated Si/GeSi is plotted, together with spectra for a ⟨100⟩ and randomly oriented beam incident on a virgin sample. The corrected level of the random fraction of the proton beam in Si, χ_R, can be estimated as $\chi_R=\chi(h_1/h_2)$, where χ, h_1, and h_2 are all labeled in the figure. We draw a straight line from a point κ' on the aligned spectrum of a virgin sample near the beginning of the damaged region, to the point κ at the Si-GeSi interface. The random fraction of the beam in damaged epitaxial GeSi on Si, given by the straight line $\kappa\kappa'$, is a good approximation of the actual random fraction of the beam (dashed line) in GeSi.

APPENDIX

Figure 13 shows a schematic drawing of backscattering spectra for a ⟨100⟩- and randomly oriented ^{4}He beam incident on a virgin and an ion-irradiated Si/GeSi sample. It has been reported that irradiation-induced damage in bulk Si and Ge can be estimated using a simple straight-line approximation, as described in Refs. 38 and 39. This method approximates the random fraction of the beam in the damaged region by drawing a straight line from a point on the aligned spectrum of a virgin sample near the beginning of the damaged region, to a point just behind the damaged region on the aligned spectrum of the damaged sample. Once the random fraction of the beam is known, the maximum of the induced damage can be easily calculated. This extraction procedure, however, has to be modified for Si/GeSi heterostructures. Due to the sudden increase in the concentration of Si atoms as the beam transverses from GeSi into Si, a steplike increase in the yield is expected at the interface, as indicated in Fig. 13, where the yields on either side of the step are labeled as h_1 and h_2. The measured backscattering yield χ for an aligned implanted sample thus does not properly represent the actual random fraction of the beam χ_R.[38] The actual random fraction of the beam after the interface χ_R can be estimated by setting $\chi_R=\chi(h_1/h_2)$. The spectrum in the top part of Fig. 4 for the sample annealed at 550 °C confirms the validity of this estimation. The first 20–30 nm of $Ge_{0.10}Si_{0.90}$ immediately adjacent to the Si substrate are of good crystalline quality, and therefore generate a backscattering yield of magnitude χ_R (at ~0.97 MeV). The spectrum yields χ_R~42%; the estimation gives ~45%. The extraction procedure for the straight line that gives a close approximation for the actual random fraction of the beam (dashed line) in the

damaged GeSi is illustrated in Fig. 13. Using the straight line $\kappa\kappa'$ and the measured channeling spectrum, the maximum relative damage can be calculated with Eq. (5.21) of Ref. 38.

The extraction procedure described above neglects the effect of the relatively small retained damage in the Si substrate as well as the effect of misfit dislocations at the Si-GeSi interface and the yield of the as-grown sample. These factors are not expected to alter significantly the extracted maximum of relative damage.

[1] R. People, IEEE J. Quantum Electron. **QE-22**, 1696 (1986).
[2] C. A. King, J. L. Hoyt, and J. F. Gibbons, IEEE Trans. Electron Devices **ED-36**, 2093 (1989).
[3] D. K. Nayak, J. C. S. Woo, J. S. Park, and K. L. Wang, IEEE Electron Device Lett. **EDL-12**, 154 (1991).
[4] Y. H. Lee, N. N. Gerasimenko, and J. W. Corbett, Phys. Rev. B **14**, 4506 (1976).
[5] J. F. Gibbons, Proc. IEEE **60**, 1062 (1972).
[6] G. Bai and M.-A. Nicolet, J. Appl. Phys. **70**, 649 (1991).
[7] D. Y. C. Lie, A. Vantomme, F. Eisen, M.-A. Nicolet, V. Arbet-Engels, and K. L. Wang, Mater. Res. Soc. Symp. Proc. **262**, 1079 (1993).
[8] C. J. Tsai, A. Dommann, M.-A. Nicolet, and T. Vreeland, Jr., J. Appl. Phys. **69**, 2076 (1991).
[9] D. Y. C. Lie, A. Vantomme, F. Eisen, T. Vreeland, Jr., M.-A. Nicolet, T. K. Carns, and K. L. Wang, J. Appl. Phys. **74**, 6039 (1993).
[10] D. Y. C. Lie, A. Vantomme, F. Eisen, T. Vreeland, Jr., M.-A. Nicolet, V. Arbet-Engels, and K. L. Wang, J. Electron. Mater. **23**, 369 (1994).
[11] T. P. Sorjeen, O. W. Holland, M. K. El-Ghor, and C. W. White, Mater. Res. Soc. Symp. Proc. **128**, 593 (1989).
[12] T. E. Haynes and O. W. Holland, Appl. Phys. Lett. **61**, 61 (1992).
[13] T. E. Haynes and O. W. Holland, Nucl. Instrum. Methods B **81**, 901 (1993).
[14] M. Vos, C. Wu, I. V. Mitchell, T. E. Jackman, J.-M. Baribeau, and J. P. McCaffrey, Nucl. Instrum. Methods B **66**, 361 (1992).
[15] M. Vos, C. Wu, I. V. Mitchell, T. E. Jackman, J.-M. Baribeau, and J. P. McCaffrey, Appl. Phys. Lett. **58**, 951 (1991).
[16] D. J. Eaglesham, J. M. Poate, D. C. Jacobson, M. Cerullo, L. N. Pfeiffer, and K. West, Appl. Phys. Lett. **58**, 523 (1991).
[17] B. T. Chilton, B. J. Robinson, D. A. Thompson, T. E. Jackman, and J.-M. Baribeau, Appl. Phys. Lett. **54**, 2 (1989).
[18] S. M. Sze, *VLSI Technology* (McGraw-Hill, Singapore, 1988), p. 356.
[19] J. Gyulai, in *Ion Implantation: Science and Technology*, edited by J. F. Ziegler (Academic, Orlando, FL, 1984), pp. 139–210.
[20] D. Y. C. Lie, T. K. Carns, N. D. Theodore, F. Eisen, M.-A. Nicolet, and K. L. Wang, Mater. Res. Soc. Symp. Proc. **321**, 485 (1994).
[21] D. C. Paine, D. J. Howard, N. G. Stoffel, and J. H. Horton, J. Mater. Res. **5**, 1023 (1990).
[22] D. C. Paine, N. D. Evans, and N. G. Stoffel, J. Appl. Phys. **70**, 4278 (1991).
[23] G. Bai and M.-A. Nicolet, J. Appl. Phys. **71**, 4227 (1992).
[24] R. G. Elliman, W.-C. Wong, and P. Kringhøj, Mater. Res. Soc. Proc. **321**, 375 (1994).
[25] Q. Z. Hong, J. G. Zhu, J. W. Mayer, W. Xia, and S. S. Lau, J. Appl. Phys. **71**, 1768 (1992).
[26] S. Mantl, B. Holländer, W. Jäger, B. Kabius, H. J. Jorke, and E. Kasper, Nucl. Instrum. Methods B **39**, 405 (1989).
[27] C. Lee, T. E. Haynes, and K. S. Jones, Appl. Phys. Lett. **62**, 501 (1993).
[28] P. Kringhøj, R. G. Elliman, and J. L. Hansen, Mater. Res. Soc. Proc. **321**, 461 (1994).
[29] Z. Atzmon, M. Eisenberg, P. Revesz, J. W. Mayer, S. Q. Hong, and F. Schaffer, Appl. Phys. Lett. **60**, 2243 (1992).
[30] S. Q. Hong, Q. Z. Hong, and J. W. Mayer, Appl. Phys. Lett. **63**, 2053 (1993).
[31] S. Q. Hong, Q. Z. Hong, and J. W. Mayer, J. Appl. Phys. **72**, 3821 (1993).
[32] F. F. Morehead, Jr. and B. L. Crowder, Radiat. Eff. **6**, 27 (1970).
[33] R. Hull and J. C. Bean, in *Strained-layer Superlattices: Materials Science and Technology*, edited by T. P. Pearsall (Academic, London, 1991), Chap. 1.
[34] D. Y. C. Lie (unpublished).
[35] J. M. Baribeau, T. E. Jackman, D. C. Houghton, P. Maigné, and M. W. Denhoff, J. Appl. Phys. **63**, 5738 (1988).
[36] C. R. Wie, T. A. Tombrello, and T. Vreeland, Jr., J. Appl. Phys. **59**, 3743 (1986).
[37] J. F. Ziegler, J. P. Biersack, and U. Littmark, *The Stopping and Range of Ions in Matter* (Pergamon, London, 1985).
[38] L. C. Feldman, J. W. Mayer, and S. T. Picraux, *Materials Analysis by Ion Channeling* (Academic, London, 1982), p. 125.
[39] F. Eisen, in *Channeling: Theory, Observation, and Applications*, edited by D. V. Morgan (Wiley, London, 1973), Chap. 14, p. 426.
[40] G. Bai, Ph.D. thesis, California Institute of Technology, 1991.
[41] J. W. Mayer, L. Eriksson, and J. A. Davis, *Ion Implantation in Semiconductors* (Academic, New York, 1970), p. 110.
[42] L. Csepregi, E. F. Kennedy, J. W. Mayer, and T. W. Sigmon, J. Appl. Phys. **49**, 3906 (1978).
[43] V. S. Sperioso, J. Appl. Phys. **52**, 6094 (1981).
[44] A. Vantomme, J. H. Song, D. Y. C. Lie, F. Eisen, M.-A. Nicolet, V. Arbet-Engels, and K. L. Wang, Mater. Res. Soc. Symp. Proc. **326**, 121 (1994).
[45] T. E. Haynes and O. W. Holland, Appl. Phys. Lett. **59**, 452 (1991).
[46] F. Eisen, J. S. Harris, B. Welch, R. D. Pashley, D. Sigurd, and J. W. Mayer, in *Ion Implantation in Semiconductors and Other Materials*, edited by B. L. Crowder (Plenum, New York, 1974), p. 631.
[47] U. G. Akano, I. V. Mitchell, F. R. Shepherd, and C. J. Miner, Can. J. Phys. **70**, 789 (1992).
[48] O. W. Holland and T. E. Haynes, Appl. Phys. Lett. **61**, 3148 (1992).
[49] O. W. Holland, S. J. Pennycook, and G. L. Albert, Appl. Phys. Lett. **55**, 2503 (1989).
[50] Z. Atzman, M. Eisenberg, Y. Shacham-Diamand, J. W. Mayer, and F. Schäffler, J. Appl. Phys. **75**, 377 (1994).
[51] K. S. Jones, S. Prussin, and E. R. Weber, Appl. Phys. A **45**, 1 (1988).
[52] M. G. Grimaldi, B. M. Paine, M.-A. Nicolet, and D. K. Sadana, J. Appl. Phys. **52**, 4038 (1981).

Appendix 3

Solid-phase epitaxial regrowth and dopant activation of P-implanted metastable pseudomorphic $Ge_{0.12}Si_{0.88}$ on Si(100)

D. Y. C. Lie[a)]
M/S 116-81, California Institute of Technology, Pasadena, California 91125

N. D. Theodore
Motorola Inc., MD-M360, 2200 West Broadway Road, Mesa, Arizona 85202

J. H. Song[b)] and M.-A. Nicolet
M/S 116-81, California Institute of Technology, Pasadena, California 91125

(Received 21 November 1994; accepted for publication 17 January 1995)

Several 265-nm-thick metastable pseudomorphic $Ge_{0.12}Si_{0.88}$ films grown on a Si(100) substrate by molecular-beam epitaxy were implanted at room temperature with 100 keV phosphorus ions to a dose of $1.5\times10^{15}/cm^2$. The implantation amorphizes the top portion (~190 nm) of the GeSi layer and leaves the rest of the film single crystalline. Implanted and nonimplanted samples were subsequently annealed simultaneously in vacuum for 30 min from 400 to 800 °C. The implanted samples undergo layer-by-layer solid-phase-epitaxial regrowth during annealing at or above 500 °C. The regrown GeSi layer is relaxed with a high density of threading dislocations ($\sim10^{10}$–$10^{11}/cm^2$). The nonamorphized portion of the layer remains fully strained when annealed between 400 and 600 °C. At or above 700 °C misfit dislocations are observed at the $Si/Ge_{0.12}Si_{0.88}$ interface. After 800 °C annealing the strain in the whole epilayer is fully relaxed. The strain relaxation is facilitated by the implantation. The presence of phosphorus in GeSi raises its regrowth velocity by about an order of magnitude over that of $Ge_{0.12}Si_{0.88}$ amorphized by irradiation of Si. The implanted phosphorus reaches ~100% activation after the completion of solid-phase-epitaxial regrowth. The room-temperature sheet electron mobility in GeSi is ~20% below that of a Si sample implanted and annealed under the same conditions. It is concluded that metastable $Ge_{0.12}Si_{0.88}$ on Si(100) amorphized at room temperature by P implantation and recrystallized by solid-phase epitaxy cannot recover its crystalline perfection and its pseudomorphic strain upon steady-state furnace annealing. © *1995 American Institute of Physics.*

I. INTRODUCTION

Si/Ge_xSi_{1-x} heterostructures offer adjustable band gaps, improved carrier mobilities over Si homostructures, and compatibility with the mature Si-based integrated-circuit (IC) technology. Ion implantation is currently the dominant technology to introduce precise amounts of dopants into semiconductors, and is very likely to remain so in the next decade.[1] Hull *et al.* reported that the high-point-defect densities introduced by implantation can significantly enhance the strain relaxation process in stacked Si/GeSi/Si heterostructures.[2] Dislocations that accompany strain relaxation can cause large leakage currents and also substantially reduce the speed and gain of devices made with Si/GeSi heterojunctions.[3–6] Kasper and Schaffler indicate that the successful fabrication of a proposed complementary Si/GeSi modulation-doped field-effect transistor (MODFET) requires the successful application of ion implantation and subsequent annealing.[7] When using ion implantation and annealing for Si/Ge_xSi_{1-x} heterostructures, one usually desires to minimize residual damage and avoid strain relaxation while maximizing the activation of dopants. Recent studies have revealed that implantation-induced damage in Ge_xSi_{1-x} and its subsequent annealing behavior are quite different from those of Si and Ge.[8–17] For example, Si is routinely amorphized to take advantage of solid-phase epitaxial regrowth during subsequent annealing to facilitate dopant activation, minimize channeling tails, and decrease residual extended-defect densities resulting from implantation. For metastable strained Ge_xSi_{1-x} layers, however, numerous reports indicate that implantation-induced amorphization and solid-phase regrowth can result in relaxed GeSi of poor crystalline quality.[18–25]

Solid-phase-epitaxial regrowth of amorphous Si and Ge thin films has been studied in detail for decades. The regrowth process has been shown to be thermally activated, with well-defined activation energies.[26] Paine and co-workers[21] recently reported that the growth velocity is decreased in strained GeSi when compared to that of Si, and that the activation energy for the regrowth of strained Ge_xSi_{1-x} layers is rather insensitive to the value of x. Elliman, Wong, and Kringhøj[27] have reported that a thermodynamically stable GeSi film remained fully strained after regrowth; a metastable GeSi that relaxes at high temperatures also relaxes during regrowth. Even though there have been several other reports of solid-phase-epitaxial regrowth of Ge_xSi_{1-x} layers, studies of dopant incorporation and activation which take advantage of the regrowth of strained Ge_xSi_{1-x} layers have only been reported by Atzmon *et al.*[28–30] and Hong, Hong, and Mayer[31,32] where Sb ions where used. In the present article we study the implantation

[a)]Electronic mail: donaldl@romeo.caltech.edu
[b)]On leave from Yonsei University, Seoul 120-749, Korea.

 0021-8979/95/77(10)/5160/7/$6.00 © 1995 American Institute of Physics

of the practically useful P ions.[22] The focus of this study is on the stability of the heterostructure after ion implantation and annealing, as well as on the material and electrical properties of P-implanted GeSi after solid-phase-epitaxial regrowth.

II. EXPERIMENTAL PROCEDURE

Pseudomorphic $Ge_{0.12}Si_{0.88}$ layers were grown at ~450 °C on Si(100) substrates by ultrahigh-vacuum molecular-beam epitaxy at the University of California at Los Angeles. The GeSi layers were not intentionally doped. The thickness of the GeSi film is ~265 nm, as determined by both MeV ^{4}He backscattering spectrometry and cross-sectional transmission electron microscopy. The samples are metastable, meaning that the thickness of the film exceeds the theoretical limit for pseudomorphic growth.[33] The layers are of excellent crystalline quality, with a minimum channeling yield of ~3% for both Si and Ge signals. Double-crystal x-ray rocking curves with Fe$K\alpha_1$ radiation (λ=0.1936 nm) confirm the pseudomorphic nature of the heterostructure, with zero parallel strain within the experimental sensitivity ($\sim 10^{-4}$), and a perpendicular strain value of 0.87%. This measured value is in excellent agreement with the value of 0.88% calculated from linear elasticity theory. The dislocation density in the virgin pseudomorphic film is below the detection limit ($\sim 10^6$/cm^2) of the x-ray double-crystal diffractometry and cross-sectional transmission electron microscopy. After chemically cleaning these Si/GeSi samples were implanted at room temperature in high vacuum ($\sim 10^{-7}$ Torr) with 100 keV ^{31}P ions to a dose of 1.5×10^{15}/cm^2. During implantation the sample normal was tilted by 7° with respect to the direction of the incident beam to minimize channeling. The ion doses reported here are within ±5% accuracy. The projected range and the straggling of the P ions, according to the TRIM-92 simulation code, are about 125 and 43 nm, respectively.[34] Both virgin and implanted samples were annealed in vacuum ($\sim 3\times10^{-7}$ Torr) at temperatures ranging from 400 to 800 °C. X-ray double-crystal rocking curves of both (400) symmetrical and (311) asymmetrical diffraction were obtained at room temperature in air as little as 1 h after implantation, as well as several months later; the spectra remain the same over this period. There is no detectable increase in the channeling yield as a result of the ^{4}He irradiation. The damage and strain present in the Si/GeSi were monitored using MeV ^{4}He ion channeling/backscattering spectrometry, double-crystal x-ray diffractometry, and/or cross-sectional transmission electron microscopy after each annealing step. We also measured dopant-activation percentages and values of sheet electron mobility in the regrown GeSi layers and compared them with those of a Si control sample. These electrical properties of the layers were characterized by Hall-effect and resistance measurements using the van der Pauw technique.

III. RESULTS AND DISCUSSION

Figure 1(a) presents a set of 2 MeV ^{4}He ⟨100⟩ channeling spectra for as-grown metastable pseudomorphic $Si/Ge_{0.12}Si_{0.88}$ samples before ("virgin") and after annealing

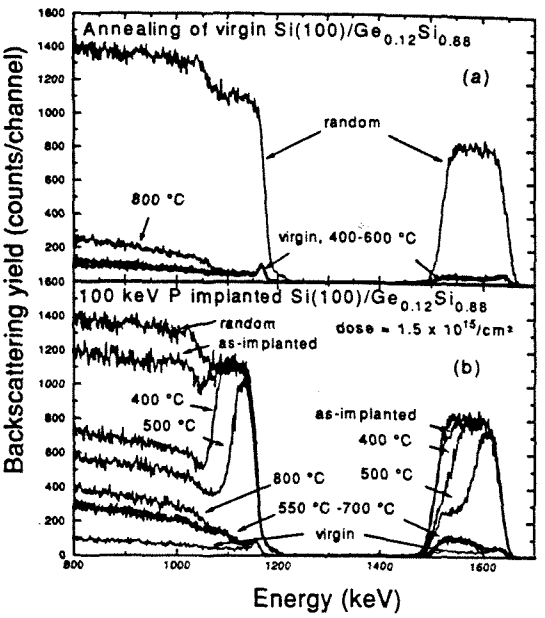

FIG. 1. 2 MeV ^{4}He ⟨100⟩ channeling spectra of pseudomorphic $Si(100)/Ge_{0.12}Si_{0.88}$ samples: (a) as grown (virgin) and annealed in vacuum from 400 to 800 °C for 30 min; (b) implanted with 1.5×10^{15}/cm^2 of 100 keV ^{31}P ions at room temperature and after 30 min vacuum annealing from 400 to 800 °C. The spectrum for the random beam incidence is also plotted in both (a) and (b) for reference.

in vacuum from 400 to 800 °C, as well as a spectrum for random beam incidence. The minimum yield for the as-grown sample is ~3%, which indicates its very good crystallinity.[35] The channeling spectra for this sample annealed between 400 and 700 °C are almost indistinguishable from those of an as-grown sample; however, after annealing at 800 °C we observe a steplike increase in the backscattering yield near 1060 keV. The steplike increase in the backscattering yield can be explained by the presence of numerous dislocations near the Si/GeSi interface, and can be attributed to strain relaxation of the epi-GeSi.[36] This interpretation is supported by data presented in later parts of this article.

Figure 1(b) shows a set of 2 MeV ^{4}He ⟨100⟩ channeling spectra from the implanted samples. The backscattering yield corresponding to the near-surface region of GeSi for an as-implanted sample reaches that of the random spectrum, indicating that the top portion of the film is amorphized down to a depth of ~195 nm. Upon annealing at 400 °C, the backscattering yield originating from near the amorphous/crystalline interface decreases significantly, which means that some of the implantation-induced defects near the amorphous/crystalline interface disappear at this low temperature. At 500 °C there is clear evidence of layer-by-layer solid-phase-epitaxial regrowth from the amorphous/crystalline interface, but not from the surface; the regrowth further decreases the GeSi backscattering yields. After annealing at 550, 600, or 700 °C the backscattering yields of the entire $Ge_{0.12}Si_{0.88}$ layer drop further, ending in a channel-

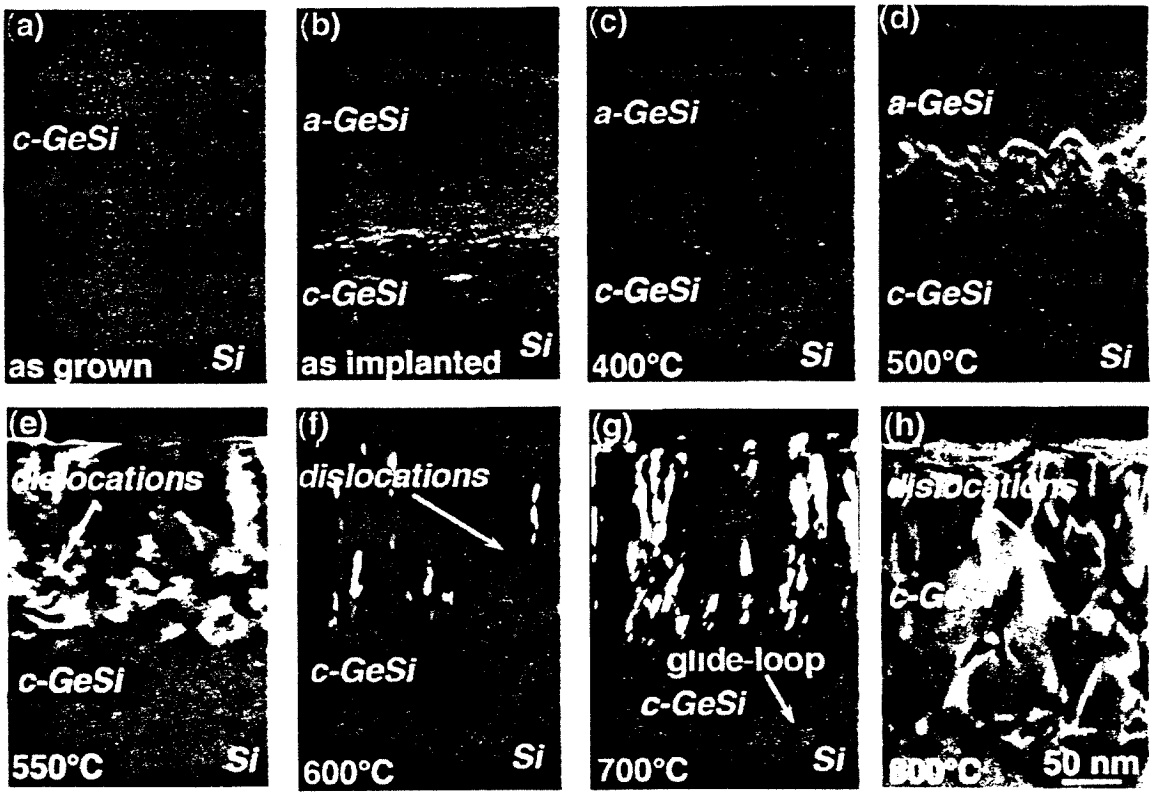

FIG. 2. Cross-sectional transmission electron micrographs of Si(100)/$Ge_{0.12}Si_{0.88}$ samples: (a) as grown; (b) as implanted with 100 keV 1.5×10^{15} P ions/cm^2 at room temperature; (c) implanted and annealed at 400 °C; (d) implanted and annealed at 500 °C; (e) implanted and annealed at 550 °C; (f) implanted and annealed at 600 °C; (g) implanted and annealed at 700 °C; and (h) implanted and annealed at 800 °C. All anneals were performed in vacuum for a common duration of 30 min. The micrographs are a combination of bright-field and dark-field images. Bright-field images have had their contrast inverted to enhance visibility of dislocations in the layers.

ing minimum yield of ~6% at 800 °C. Similar trends of decreasing backscattering yields have been reported for amorphized GeSi and proven to be a result of solid-phase epitaxy.[19,24] This value for the recrystallized sample is higher than that of the as-grown samples (~3%), which indicates that the regrown layers have inferior crystalline quality. After annealing at 800 °C the steplike increase in the backscattering yields near 1060 keV is again clearly visible.

Figure 2 consists of a set of cross-sectional transmission electron micrographs obtained from the Si/$Ge_{0.12}Si_{0.88}$ samples shown in Fig. 1, starting from the as-grown (virgin) sample (a) through to the implanted and 800 °C annealed sample (h). We did not observe any dislocations or other defects in the as-grown sample. One sees that the as-implanted GeSi film is amorphized only over the first 190±9 nm, which agrees well with the thickness of ~195 nm estimated from the backscattering data of Fig. 1(b). The amorphous-to-crystalline transition region is wavy and about 50 nm thick. Point-defect clusters are found within this transition region. The Si-GeSi interface appears unaffected by the ion bombardment. At 400 °C [Fig. 2(c)], the top portion of the GeSi film remains amorphous, with the thickness being the same as that of the as-implanted film. The unchanged thickness of amorphous GeSi observed in Figs. 2(b) and 2(c) indicates that solid-phase epitaxy of GeSi is negligible at 400 °C. This observation confirms the results reported by Paine and co-workers.[21] Some smoothing of the amorphous/crystalline interface has occurred after this low-temperature annealing. At 500 °C [Fig. 2(d)] the amorphous/crystalline interface has moved up toward the surface. The thickness of the amorphous GeSi layer has decreased to ~85±25 nm. There are dislocations and damage present near the original amorphous/crystalline interface. For Si treated similarly, a band of dislocation loops is commonly observed near the original amorphous/crystalline interface that are thought to be due to excess interstitials that coalesce near the end-of-range region of the implanted ions.[37] A similar mechanism is likely to be operative in GeSi.

The entire GeSi layer has recovered its single crystallinity at 550 °C. This confirms that solid-phase regrowth has proceeded to completion at 550 °C. The recrystallized layer contains a high density of threading dislocations (~10^{10}–10^{11} cm^{-2}), but none are observed in the bottom portion of the GeSi layer that was not amorphized by the implantation. There is no evidence of interfacial misfit dislocations at the Si-GeSi interface either, within the resolution

limit ($\sim 10^5$–10^6 cm^{-2}) of cross-sectional transmission electron microscopy. Unlike the sample annealed at 500 °C, the dislocation loops near the original amorphous/crystalline interface have disappeared. What may have occurred is that as the regrowth front moves upward, it generates threading dislocations that extend from the ends of the dislocation half-loops situated near the amorphous/crystalline interface. These threading dislocations then extend all the way through the regrown layer, while leaving the bottom portion of the GeSi film and the Si-GeSi interface unaffected. We do not observe any misfit dislocations at that interface, which indicates that within the resolution limit of cross-sectional transmission electron microscopy the bottom GeSi layer remains fully strained. Figure 2(f) is a micrograph of the implanted sample annealed at 600 °C. The micrograph indicates that the threading dislocations often occur in pairs, suggesting the formation of hairpin dislocations. Figure 2(g) is a similar image of a sample annealed at 700 °C. The micrograph shows the threading arm of a dislocation half-loop that extends through the implanted region down to the Si-GeSi interface. Based on this evidence, we hypothesize that at 700 °C dislocation half-loops first form at the bottom of the regrown GeSi layer during annealing, and then glide down upon {111} planes until parts of the loop intersect the Si-GeSi interface. Each dislocation loops can then open out, leaving a segment of misfit dislocation lying at the Si-GeSi interface. At 800 °C [Fig. 2(h)] a high density of threading dislocations exists throughout the entire GeSi layer. This observation supports the interpretation of the previously discussed steplike increase in the backscattering yield at 800 °C (see Fig. 1) as resulting from strain relaxation at the Si-GeSi interface.

Paine and co-workers[21] have reported that the regrowth velocity in nominally undoped $Ge_{0.12}Si_{0.88}$ is negligible at 400 °C (<0.01 nm/min), but reaches ~0.24 nm/min at 500 °C and ~4.2 nm/min at 550 °C. Figures 1(b) and 2(d) show that the thickness of the regrown GeSi is $\sim 105 \pm 25$ nm after 500 °C annealing, which corresponds to a regrowth velocity of $\sim 3.6 \pm 0.8$ nm/min. This regrowth velocity in heavily P-doped GeSi is thus about 10–20 times faster than that of undoped GeSi. Previous studies by Csepregi *et al.* have shown that implantation of P ions into Si(100) enhances the solid-phase regrowth velocity of amorphous Si by a factor of 6 at 500 °C.[38] In that case they suggested that the increase in the regrowth velocity is associated with local impurity concentrations in the proximity of the amorphous/crystalline interface. Suni *et al.*[39] have reported that electrically active impurities increase the regrowth velocity of both Si and Ge. Our work shows that the introduction of phosphorus atoms also enhances the regrowth velocity in strained $Ge_{0.12}Si_{0.88}$. The detailed mechanism of this enhancement of regrowth velocity is not well understood at this time.[24,26,40]

Figure 3(a) presents the x-ray rocking curves for (400) diffraction from nonimplanted samples before (virgin, dotted line) and after thermal annealing at 400–800 °C each. The origin of the abscissa in Fig. 3 is placed at the Bragg angle $\theta_B = 45.475°$ of the Si substrate peak. The spectrum for the as-grown sample (virgin, dotted line) has a sharp and symmetrical peak at $-0.48°$ that is generated by the GeSi layer. This value indicates that the GeSi is fully compressively

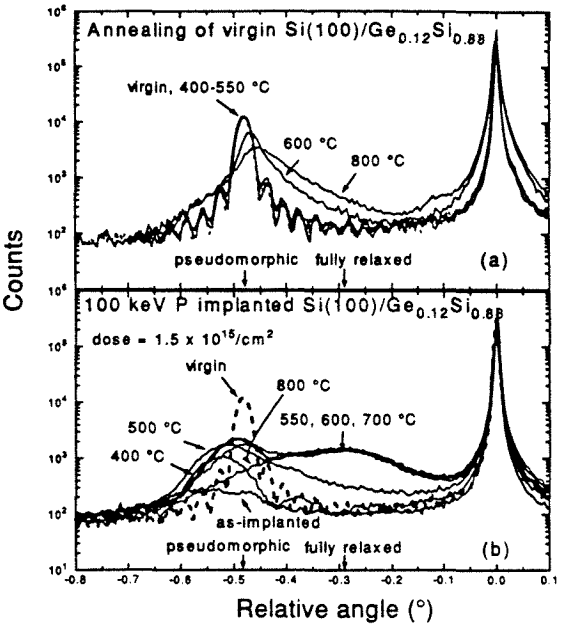

FIG. 3. Double-crystal x-ray rocking curves of (400) symmetrical diffraction for pseudomorphic $Si(100)/Ge_{0.12}Si_{0.88}$ samples (a) as grown (virgin, dotted line) and annealed in vacuum from 400 to 800 °C and (b) as implanted with $1.5 \times 10^{15}/cm^2$ ^{31}P ions of 100 keV at room temperature and after 30 min vacuum annealing from 400 to 800 °C.

strained. The small periodic oscillations in this rocking curve yield a thickness of about 260 nm for the GeSi layer, in good agreement with the values obtained from the backscattering spectrum and transmission electron micrograph of this sample. The spectrum is consistent with a constant strain throughout the epitaxial layer, as simulations indicate. The slight shift of the GeSi peak to lower values at 600 °C shows that the sample starts to relax at 600 °C, and that the strain is further relieved at 800 °C. According to Vegard's law, a fully relaxed $Ge_{0.12}Si_{0.88}$ layer should have an x-ray-diffraction peak positioned at $\sim -0.29°$, which indicates that this nonimplanted sample is far from fully relaxed after annealing at 800 °C. Dislocations accompanied with strain relaxation are known to broaden x-ray-diffraction peaks.[41] The significant broadening observed at 800 °C is thus due to the formation of dislocations after strain relaxation.

Figure 3(b) plots similar rocking curves for P-implanted samples. The spectrum for a virgin sample is also plotted (dotted line) for reference. We interpret the rocking curve results with the help of an x-ray dynamical simulation program,[42] and the corresponding cross-sectional transmission electron micrographs and channeling spectra presented in Figs. 1 and 2. If the as-implanted GeSi epilayer was entirely amorphous, there would be no diffraction peak other than that of the substrate; however, there is a weak and broad peak whose maximum is beyond $-0.48°$. We therefore deduce from this spectrum that the bottom portion of the GeSi film is still crystalline but additionally strained by defects.

Upon annealing at 400 °C the peak increases in intensity and sharpens, peaking roughly at $\sim -0.52°$. This behavior indicates that some implantation-induced defects in the layer have been removed, but that some damage and excess strain persist. A sample annealed at 500 °C displays an even stronger but nonsymmetrically broadened peak, located between $\sim -0.2°$ and $-0.7°$. Computer simulations attempting to match this profile show that additional damage is removed and that the strain profile becomes nonuniform with depth. The combined results of Figs. 1 and 2 establish that this GeSi film consists of three layers: a top amorphous layer of ~85 nm, an intermediate regrown crystalline layer of ~105 nm with dislocation loops and point-defect clusters, and a bottom crystalline strained layer of ~75 nm. The rocking curve is a combination of the diffracted signals emanating from the two crystalline layers. The damaged regrown layer is responsible for the diffraction intensity observed between $\sim -0.2°$ and $-0.4°$, which suggests that some of the regrown layer is at least partly relaxed.

Samples annealed between 550 and 700 °C exhibit two distinctly different peaks: The first peak is very broad and centered around $\sim -0.29°$, which corresponds to the Bragg angle of a fully relaxed $Ge_{0.12}Si_{0.88}$ film. Judging from the position and the intensity of this broad peak, we infer that the regrown layer is fully relaxed and has a crystalline quality inferior to that of the as-grown sample. The second peak is now located at $\sim -0.48°$, exactly where the Bragg angle of a pseudomorphic $Ge_{0.12}Si_{0.88}$ film would be. This indicates that defects in the lower crystalline portion of the GeSi film are further removed. The whole epilayer is relaxed at 800 °C, which agrees well with information obtained from channeling spectrometry and transmission electron microscopy ($\sim 10^{10}$–10^{11} dislocations/cm^2). If we compare the rocking curves of samples annealed at 800 °C with and without implantation [Figs. 3(a) and 3(b)], it is clear that the implanted sample relaxes much more extensively than the nonimplanted one. We propose that this enhanced strain relaxation observed in these P-implanted GeSi layers is caused by the dislocation loops that arise in the end-of-range region and glide toward the Si/GeSi interface [Fig. 2(g)]. Hull *et al.* have also reported an enhancement of strain relaxation for metastable Si/GeSi/Si implanted with B or As below the amorphization dose.[2] They attribute this enhancement to a high densities of point defects introduced by implantation, which can serve as nucleation sites for subsequent dislocation formation. In our case, for the regrowth of P-implanted GeSi, the point defects induced by implantation are expected to form prismatic dislocation loops at or near the end-of-range region during annealing.[43] The prismatic loops can transform into dislocation sources which produce glide dislocations, that then glide down to the Si-GeSi interface. Our results thus confirm and prove that implantation-induced damage can substantially enhance the strain relaxation of metastable Si/GeSi.

Solid-phase regrowth of phosphorus-implanted amorphous Si(100) is much cleaner than what is observed here for strained $Ge_{0.12}Si_{0.88}$(100).[44] Several groups have reported that if a strained GeSi layer is metastable, as in our case, the regrown layer will relax once it grows to a thickness greater

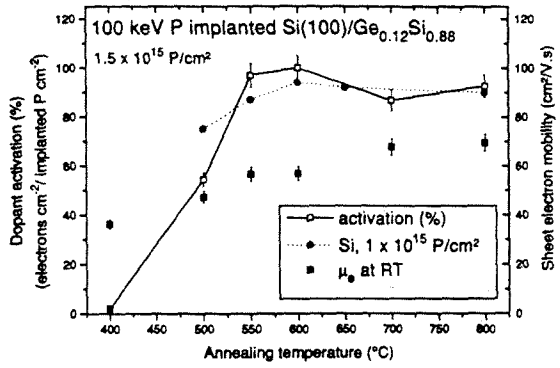

FIG. 4. The ratio in % (□) of electrons/cm^2 obtained from Hall measurements to the implanted P atoms/cm^2 for pseudomorphic Si(100)/$Ge_{0.12}Si_{0.88}$ implanted with 1.5×10^{15}/cm^2 ^{31}P ions of 100 keV as a function of the isochronal annealing temperature. The implantation was performed at room temperature and the duration of annealing at each temperature was 30 min. Corresponding data for Si implanted at room temperature with 280 keV ^{31}P are plotted for comparison (dotted lines, from Ref. 46). The values of the sheet electron mobility (■) are also plotted.

than its equilibrium critical thickness.[13,21,24,45] The critical thickness is defined as the pseudomorphic layer thickness at which the work done by the layer stresses during defect formation equals the work that is required to introduce the defects.[33] Paine and co-workers[21] and LeGoues and co-workers[25] have calculated the critical thickness of GeSi for the formation of specific extended defects. Above this critical thickness the formation of the specific extended defects is energetically feasible. These calculations yield a critical thickness for $Ge_{0.12}Si_{0.88}$ of only ~20 nm.[21] We therefore hypothesize that in the present study the $Ge_{0.12}Si_{0.88}$ regrows pseudomorphically up to this critical thickness of ~20 nm; as the layer regrows further, it relaxes and becomes defective.

These considerations lead to an interesting question: the growth temperatures for both molecular-beam epitaxy and solid-phase epitaxy are about the same in our case (~500 °C); why then can the samples grown by molecular-beam epitaxy exceed their equilibrium critical thickness by more than an order of magnitude, but the samples grown by solid-phase epitaxy cannot? One obvious explanation has been suggested by Kringhøj and co-workers[45] who argue that during molecular-beam epitaxy the GeSi alloy grows at an atomically sharp crystalline/vacuum interface, whereas the crystallization during solid-phase epitaxy occurs at a rugged amorphous/crystalline interface. The rugged amorphous/crystalline interface enhances the defect nucleation. However, the kinetic barriers for defect nucleation during solid-phase regrowth of GeSi and the possible effects of strain and impurities are not fully understood.[13,20,27] Our results presented so far show that a pseudomorphically strained metastable $Ge_{0.12}Si_{0.88}$ layer on Si(100) amorphized by P implantation does not recover its crystallinity and its pseudomorphic strain upon solid-phase regrowth induced by steady-state annealing.

Another important parameter for an implanted semiconductor is the percentage of dopants that is electrically active. We have measured this quantity and plot it in Fig. 4 versus the annealing temperature. The experimental points (open squares) are connected by solid straight lines to guide the eye. The solid circles present data for Si implanted with 280 keV P and subsequently annealed for 30 min in vacuum.[46] In the current study, about 50% of the phosphorus implanted into the $Ge_{0.12}Si_{0.88}$ is activated after 500 °C annealing, and almost all of it is activated at 550 °C. According to Fig. 2, roughly half of the amorphous GeSi recrystallized after annealing at 500 °C, and the solid-phase regrowth is completed at 550 °C. The data in Fig. 4 thus suggest that most phosphorus atoms become electrically active as a result of solid-phase epitaxial regrowth. If the dose of the P implantation is insufficient to amorphize the GeSi layer, the dopant activation after annealing at 550 °C is incomplete.[47] Layer-by-layer solid-phase-epitaxial regrowth of P-implanted GeSi thus enhances the dopant activation, as it does for Si and Ge.[44,48,49] The dopant activation curve for this pseudomorphic GeSi layer implanted with 1.5×10^{15} P ions/cm^2 is very similar to that of Si implanted with 5×10^{15} P ions/cm^2, probably due to the similar extent of amorphization introduced by the ions.[22,50]

The sheet electron mobility values for the GeSi layers are also plotted in Fig. 4 (solid squares). The sheet electron mobility gradually rises and levels off at about 70 cm^2/V s at 800 °C. This mobility value is about 20% less than that obtained from a Si sample (85 ± 9 cm^2/V s) implanted and annealed under the identical conditions. For heavily doped semiconductors it is known that ionized impurity scattering is the dominant scattering process for electron transport.[51–54] Alloy scattering at room temperature can also contribute to this reduction of mobility in GeSi over that in Si.[54] Furthermore, it has been reported that scattering by a high density of dislocations lowers the electron mobility considerably.[53] For $T_{ann}<550$ °C, the values of electron mobility decrease and the dopant activation is poor. Our maximum mobility values are about 10% higher than those reported by Atzmon *et al.*, where Sb ions were used.[28]

IV. CONCLUSIONS

We conclude that if a continuous amorphous layer is formed in a pseudomorphic GeSi layer as a result of P implantation, the dopants can be ~100% activated after furnace annealing at or above 550 °C. Strain relaxes completely at 800 °C while that of nonimplanted GeSi does not; the strain relaxation of the P-implanted Si/GeSi is thus substantially enhanced. The electron mobility in the regrown layer is not enhanced over that of Si, and the recrystallized layer is full of dislocations. A pseudomorphic GeSi layer implanted only slightly with P so that no amorphization occurs can be annealed without losing its pseudomorphic strain if the annealing is done by rapid thermal processing rather than steady-state furnace.[55] It would be interesting to determine if this can be achieved for amorphized samples as well.

ACKNOWLEDGMENTS

This work was supported by the Semiconductor Research Corporation under a coordinated research program at Caltech and at UCLA, Contract No. 94-SJ-100. The authors are greatly indebted to Dr. F. Eisen at Caltech for his valuable guidance and discussions. We would also like to thank Dr. C. J. Tsai at Harvard University for providing the x-ray simulation program.

[1] See, for example, A. F. Tasch, Nucl. Instrum. Methods B **74**, 3 (1993) or M. I. Current, I. Yamada, N. W. Cheung, P. L. F. Hemment, and K. J. Reeson, in *Handbook of Ion Implantation Technology*, edited by J. F. Ziegler (Elsevier, Amsterdam, 1992), pp. 363–433.
[2] R. Hull, J. C. Bean, J. M. Bonar, G. S. Higashi, K. T. Short, H. Temkin, and A. E. White, Appl. Phys. Lett. **56**, 2445 (1990).
[3] C. A. King, J. L. Hoyt, and J. F. Gibbons, IEEE Trans. Electron Devices **ED-36**, 2093 (1989).
[4] P. S. Peercy, B. W. Dodson, J. Y. Tsao, E. D. Jones, D. R. Myers, T. E. Zipperian, L. R. Dawson, R. M. Biefeld, J. F. Klem, and C. R. Hills, IEEE Electron Devices Lett. **EDL-9**, 621 (1988).
[5] D. K. Nayak, K. Kamjoo, J. S. Park, Jason C. S. Woo, and K. L. Wang, IEEE Trans. Electron Devices **ED-39**, 56 (1992).
[6] R. Hull and J. C. Bean, in *Strained-layer Superlattices: Materials Science and Technology*, edited by T. P. Pearsall (Academic, London, 1991), Chap. 1, pp. 1–72.
[7] E. Kasper and F. Schaffler, in *Strained-layer Superlattices: Materials Science and Technology*, "Semiconductors and Semimetals," Vol. 33, edited by T. P. Pearsall (Academic, London, 1991), Chap. 3, pp. 295–296.
[8] T. P. Sorjeen, O. W. Holland, M. K. El-Ghor, and C. W. White, Mater. Res. Soc. Symp. Proc. **128**, 593 (1989).
[9] T. E. Haynes and O. W. Holland, Appl. Phys. Lett. **61**, 61 (1992).
[10] T. E. Haynes and O. W. Holland, Nucl. Instrum. Methods B **81**, 901 (1993).
[11] M. Vos, C. Wu, I. V. Mitchell, T. E. Jackman, J.-M. Baribeau, and J. P. McCaffrey, Nucl. Instrum. Methods B **66**, 361 (1992).
[12] D. J. Eaglesham, J. M. Poate, D. C. Jacobson, M. Cerullo, L. N. Pfeiffer, and K. West, Appl. Phys. Lett. **58**, 523 (1991).
[13] Q. Z. Hong, J. G. Zhu, J. W. Mayer, W. Xia, and S. S. Lau, J. Appl. Phys. **71**, 1768 (1992).
[14] D. Y. C. Lie, A. Vantomme, F. Eisen, M.-A. Nicolet, T. K. Carns, and K. L. Wang, J. Appl. Phys. **74**, 6039 (1993).
[15] D. Y. C. Lie, A. Vantomme, F. Eisen, M.-A. Nicolet, T. K. Carns, and K. L. Wang, J. Electron. Mater. **23**, 369 (1994).
[16] D. Y. C. Lie, A. Vantomme, F. Eisen, M.-A. Nicolet, V. Arbet-Engels, and K. L. Wang, Mater. Res. Soc. Symp. Proc. **262**, 1079 (1993).
[17] G. Bai and M.-A. Nicolet, J. Appl. Phys. **71**, 4227 (1992).
[18] M. Vos, C. Wu, I. V. Mitchell, T. E. Jackman, J.-M. Baribeau, and J. P. McCaffrey, Appl. Phys. Lett. **58**, 951 (1991).
[19] B. T. Chilton, B. J. Robinson, D. A. Thompson, T. E. Jackman, and J.-M. Baribeau, Appl. Phys. Lett. **54**, 2 (1989).
[20] D. C. Paine, D. J. Howard, N. G. Stoffel, and J. H. Horton, J. Mater. Res. **5**, 1023 (1990).
[21] D. C. Paine, N. D. Evans, and N. G. Stoffel, J. Appl. Phys. **70**, 4278 (1991).
[22] D. Y. C. Lie, T. K. Carns, N. D. Theodore, F. Eisen, M.-A. Nicolet, and K. L. Wang, Mater. Res. Soc. Proc. **321**, 485 (1994).
[23] C. S. Pai, S. S. Lau, I. Suni, and L. Csepregi, Appl. Phys. Lett. **47**, 1214 (1985).
[24] C. Lee, T. E. Haynes, and K. S. Jones, Appl. Phys. Lett. **62**, 501 (1993).
[25] F. K. LeGoues, M. Copel, and R. M. Tromp, Phys. Rev. Lett. **63**, 1826 (1989).
[26] G. L. Olson and J. A. Roth, Mater. Sci. Rep. **3**, 1 (1988).
[27] R. G. Elliman, W.-C. Wong, and P. Kringhøj, Mater. Res. Soc. Proc. **321**, 375 (1994).
[28] Z. Atzmon, M. Eisenberg, P. Revesz, J. W. Mayer, S. Q. Hong, and F. Schaffer, Appl. Phys. Lett. **60**, 2243 (1992).
[29] Z. Atzmon, M. Eisenberg, Y. Shacham-Diamand, J. W. Mayer, and F. Schäffer, Appl. Phys. Lett. **61**, 2902 (1992).
[30] Z. Atzmon, M. Eisenberg, Y. Shacham-Diamand, J. W. Mayer, and F. Schäffer, J. Appl. Phys. **75**, 377 (1994).

[31] S. Q. Hong, Q. Z. Hong, and J. W. Mayer, Appl. Phys. Lett. **63**, 2053 (1993).
[32] S. Q. Hong, Q. Z. Hong, and J. W. Mayer, J. Appl. Phys. **72**, 3821 (1993).
[33] J. W. Matthews and A. E. Blakeslee, J. Cryst. Growth **27**, 118 (1974).
[34] J. F. Ziegler, J. P. Biersack, and U. Littmark, *The Stopping and Range of Ions in Matter* (Pergamon, London, 1985).
[35] See, for example, W. K. Chu, J. W. Mayer, and M.-A. Nicolet, *Backscattering Spectrometry* (Academic, New York, 1978), Chap. 8, pp. 223–275.
[36] S. T. Picraux, B. L. Doyle, and J. Y. Tsao, *Strained-layer Superlattices: Materials Science and Technology*, "Semiconductors and Semimetals," Vol. 33, edited by T. P. Pearsall (Academic, London, 1991), Chap. 3, pp. 139–222.
[37] K. S. Jones, S. Prussin, and E. R. Weber, Appl. Phys. A **45**, 1 (1988).
[38] L. Csepregi, E. F. Kennedy, T. J. Gallagher, J. W. Mayer, and T. W. Sigmon, J. Appl. Phys. **48**, 4234 (1977).
[39] I. Suni, G. Göltz, M.-A. Nicolet, and S. S. Lau, Thin Solid Films **93**, 171 (1982).
[40] J. Gyulai, in *Handbook of Ion Implantation Technology*, edited by J. F. Ziegler (Elsevier, Amsterdam, 1992), pp. 69–117.
[41] J.-M. Baribeau, T. E. Jackman, D. C. Houghton, P. Maigné, and M. W. Denhoff, J. Appl. Phys. **63**, 5738 (1988).
[42] C. J. Tsai, A. Dommann, M.-A. Nicolet, and T. Vreeland, Jr., J. Appl. Phys. **69**, 2076 (1991); C R. Wie, T. A. Tombrello, and T. Vreeland, Jr., *ibid.* **59**, 3743 (1986).
[43] J. P. Hirth and J. Lothe, *Theory of Dislocations*, 2nd ed. (Wiley, New York, 1982).
[44] See, for example, J. F. Gibbons, Proc. IEEE **60**, 1062 (1972) or T. Tokuyama, M. Miyao, and N. Yoshihiro, Jpn. J. Appl. Phys. **17**, 1301 (1978).
[45] P. Kringhøj, R. G. Elliman, and J. L. Hansen, Mater. Res. Soc. Proc. **321**, 461 (1994).
[46] B. L. Crowder and F. F. Morehead, Jr., Appl. Phys. Lett. **14**, 313 (1969).
[47] D. Y. C. Lie, N. D. Theodore, and J. H. Song, Appl. Surf. Sci. (in press).
[48] J. W. Mayer, L. Eriksson, and J. A. Davis, *Ion Implantation in Semiconductors* (Academic, New York, 1970).
[49] J. Gyulai, in *Ion Implantation: Science and Technology*, edited by J. F. Ziegler (Academic, Orlando, FL, 1984), pp. 139–210.
[50] W. P. Maszara and G. A. Rozgonyi, J. Appl. Phys. **60**, 2310 (1986).
[51] G. Masetti, M. Severi, and S. Solmi, IEEE Trans. Electron Devices **ED-30**, 764 (1983).
[52] T. Manku and A. Nathan, IEEE Trans. Electron Devices **ED-39**, 2082 (1992).
[53] X. Fisful, *Heavily Doped Semiconductors* (Plenum, New York, 1969), p. 133.
[54] V. Venkataraman, C. W. Liu, and J. C. Sturm, J. Electron. Mater. **24**, (1994).
[55] D. Y. C. Lie, J. H. Song, N. D. Theodore, F. Eisen, M.-A. Nicolet, T. K. Carns, K. L. Wang, H. Kinoshita, T.-H. Huang, and D. L. Kwong, Mater. Res. Soc. Proc. **342**, 51 (1994).

APPENDIX 4

STRAIN EVOLUTION AND DOPANT ACTIVATION IN P-IMPLANTED METASTABLE PSEUDOMORPHIC Si(100)/$Ge_{0.12}Si_{0.88}$

D.Y.C. Lie, J.H. Song[+], F. Eisen, and M-A. Nicolet

M/S 116-81, California Institute of Technology, Pasadena, CA 91125

N.D. Theodore

Motorola Inc., Mesa, Arizona, AZ 85202

[+]On leave from Yonsei University, Seoul 120-749, Korea

ABSTRACT

A metastable $Ge_{0.12}Si_{0.88}$ layer 265 nm thick was deposited pseudomorphically on a Si(100) substrate and then implanted with 100 keV phosphorus ions at room temperature for doses of $5x10^{13}/cm^2$ to $1.5x10^{15}/cm^2$. The ions stop within the epilayer (projected range ~ 125 nm). MeV ^4He backscattering/channeling spectrometry, transmission electron microscopy, and double-crystal x-ray diffractometry were used to characterize the damage and strain in the films. The samples were subsequently annealed in high vacuum from 400-800°C for 30 min at each temperature. For the non-amorphized samples (doses of 5 and 10 $x10^{13}/cm^2$), most of the implantation-induced damage and strain disappear after annealing at 400-550°C, but the implanted P ions activate poorly. After annealing at 700-800°C, near complete activation is achieved but the strain relaxes. For the amorphized samples (dose of $1.5x10^{15}/cm^2$), the amorphous GeSi regrows by solid-phase epitaxy and the dopants are ~100% activated after annealing at 550 °C, but the regrown GeSi relaxes with a high density of dislocations. The strain relaxes more extensively upon annealing in an implanted sample than in a non-implanted one, other conditions being equal. This effect is more pronounced at higher ion doses, probably due to the increased amount of damage introduced at high doses.

Key Words: Silicon-Germanium, strain relaxation, implantation, dopant activation, solid-phase epitaxy.

I. INTRODUCTION

Si/Ge_xSi_{1-x} heterostructures can provide adjustable bandgaps and better carrier mobilities than those of Si homostructures. Their compatibility with the mature Si-based IC technology makes them attractive for high performance electronic and optoelectronic applications. Ion implantation is currently the preferred doping method in semiconductor device technology. Ion implantation introduces damage and strain in single-crystalline Si, GeSi and Ge. Annealing is required after the implantation to remove the induced damage and strain [1-3]. Strain relaxation of Si/GeSi is known to cause large leakage currents as well as reduce the gain and speed of Si/GeSi devices [4-6]. When applying ion implantation and annealing to Si/Ge_xSi_{1-x} heterostructures, besides minimizing the residual damage and maximizing dopant activation, one also wishes to minimize the strain relaxation in the heterostructure. Hull *et al.* reported that the high densities of point defects generated by implantation can significantly enhance the strain relaxation in non-amorphized Si/GeSi/Si heterostructures [7]. For strained Ge_xSi_{1-x}, implantation-induced amorphization and solid-phase epitaxy can result in strain-relaxed layers with dislocations [8-10]. In this study, we present systematic results for metastable pseudomorphic $Si/Ge_{0.12}Si_{0.88}$ implanted with P ions for both non-amorphized ($5x10^{13}/cm^2$ and $1x10^{14}/cm^2$) and amorphized ($1.5x10^{15}/cm^2$) cases. The focus of this paper is on the evolution of strain and the electrical properties and crystallinity of the P-implanted epi-GeSi after steady-state annealing in vacuum.

II. EXPERIMENTAL PROCEDURE

Undoped pseudomorphic $Ge_{0.12}Si_{0.88}$ films were deposited on Si(100) substrates at ~450°C by ultra-high vacuum molecular beam epitaxy at the University of California at Los Angeles. Both MeV ^4He backscattering spectra and cross-sectional transmission electron micrographs show that the GeSi film is 265±10 nm thick, a value which exceeds its thermal equilibrium thickness [11]. This heterostructure is thus metastable. The layers are of exceptional quality, exhibiting minimum channeling yields of ~3% for both Si and Ge signals. Double-crystal x-ray diffractometry using Fekα_1 radiation (λ=0.1936 nm) indicates that the GeSi is pseudomorphically grown on Si(100), with a perpendicular strain value of 0.87%, and no in-plane strain within the experimental sensitivity (~0.01%). This measured strain value agrees very well with the value of 0.88% calculated from the linear elasticity theory. The dislocation density in the virgin pseudomorphic film is below the detection limit (~10^5-10^6/cm^2) of both x-ray double-crystal diffractometry and cross-sectional transmission electron microscopy. These as-deposited Si/GeSi samples were then degreased by chemical cleaning and subsequently implanted at room temperature in high vacuum (~10^{-7} Torr) with 100 keV ^{31}P ions to doses of 5x10^{13}, 1x10^{14}, or 1.5x10^{15}/cm^2. The sample normal was tilted by 7° with respect to the direction of the incident beam to minimize the channeling effect during implantation. The ion doses reported here are within ± 5% accuracy. According to the TRIM-92 simulation code, the projected range (R_p) and the straggling (ΔR_p) of the P ions are about 125 nm and 43 nm, respectively [12]. We chose R_p to be only about half of the GeSi film thickness so that the damage at the Si-GeSi interface generated by the implantation is expected to be negligible for all as-implanted samples. Within the instrumental sensitivity, we did not find any noticeable damage at the Si-GeSi interface for all samples after the implantation. Both non-implanted and implanted samples were annealed in high vacuum (~5x10^{-7} Torr) at temperatures ranging from 400°C to 800°C for 30 min at each temperature. The implantation-induced damage and strain in all Si/GeSi samples were monitored

with MeV ^{4}He ion channeling/backscattering spectrometry, double-crystal x-ray diffractometry, and selected samples were characterized by cross-sectional transmission electron microscopy before and after annealing. The electrically active fractions of P ions in GeSi after implantation and annealing were determined by Hall effect and resistance measurements using a van der Pauw pattern.

III. RESULTS AND DISCUSSION

Figures 1(a)-(d) contain four sets of 2 MeV ^{4}He <100> channeling spectra of Si/$Ge_{0.12}Si_{0.88}$ samples before and after implantation and annealing. The channeling spectra for an as-deposited sample before (labeled "virgin") and after annealing at temperatures in the range from 400-800°C are plotted in Fig. 1(a), together with a spectrum of an as-deposited sample taken with random beam incidence (labeled "random"). When virgin samples are annealed between 400-600°C, their channeling spectra remain indistinguishable from that of an as-deposited sample; however, a step-like increase in the backscattering yield at energies near ~1060 keV is observed after annealing at 800°C. Cross-sectional transmission electron micrographs of this sample (not shown) indicate that this step-like increase is due to the formation of numerous dislocations which relieve the strain of the epi-GeSi film [13], as x-ray rocking curves of this sample also suggest (Fig. 2(a)).

Figures 1(b) and 1(c) present two sets of channeling spectra for the non-amorphized samples implanted to doses of $5x10^{13}$ P/cm^2 and $1x10^{14}$ P/cm^2, respectively. The maxima of the backscattering yields for these as-implanted samples in Figs. 1(b) and 1(c) reach roughly one-fifth and one-half of that of the random spectrum, which shows that a significant amount of damage is introduced by the implantation. The induced damage increases with ion dose. The channeling spectra of these non-amorphized samples annealed at 400-550°C are almost identical to that of an as-deposited sample, which means that within the sensitivity of MeV ^{4}He channeling

spectrometry, the implantation-induced damage has been removed at these low annealing temperatures. At 700-800°C, a step-like increase in the backscattering yield near the Si-GeSi interface is again observed in Figs. 1(b)-(c), which we again attribute to the formation of a high density of dislocations accompanied by strain relaxation.

Figure 1(d) shows a set of channeling spectra for the amorphized Si/GeSi samples, implanted with 1.5×10^{15} P/cm^2, before and after annealing. The backscattering yields that correspond to the surface portion of the epi-GeSi reach the level of the random spectrum, which indicates that a surface layer in the epi-GeSi is amorphized, (a thickness of 190±15 nm for the amorphous region is obtained from the width of the peak in the spectrum), but the rest of the layer is not. Annealing at 400°C strongly reduces the yield from the portion of the film just below the amorphous/crystalline interface. This change indicates that some implantation-induced defects disappear at 400°C, but the thickness of the amorphous GeSi is not changed significantly. The amorphous epi-GeSi begins to crystallize by solid-phase epitaxial regrowth at 500°C starting from the amorphous/crystalline interface and resulting in a reduction of the thickness of the amorphous GeSi to about half of its initial value. The entire amorphous GeSi has recrystallized after annealing at 550-700°C, as indicated by a channeling minimum yield of ~6%. This minimum yield is considerably higher than that of an as-deposited sample (~3%), which indicates that there are more defects in the regrown GeSi that act as scattering centers than there are in a virgin film. When annealed at 800°C, the backscattering yield increases at energies near and below ~1060 keV. This increase again is associated with the strain relaxation of the epi-GeSi, as will be discussed in greater detail in conjunction with Figs. 2-3.

To understand how strain evolves during implantation and annealing of the Si/GeSi heterostructure, it was characterized by double-crystal x-ray diffractometry after each implantation and/or annealing step. We interpreted these x-ray rocking curves using a computer simulation program based on x-ray dynamical diffraction theory [14-16], and the corresponding channeling spectra and cross-sectional transmission electron micrographs. We plot in Figs. 2(a)-

(d) the (400) rocking curves that correspond to the identical set of samples whose channeling spectra are shown in Figs. 1(a)-(d). Figure 2(a) shows the curve for an as-deposited sample ("virgin", open circles) that has a sharp, intense, symmetrical GeSi peak located at -0.48°, characteristic of a pseudomorphic GeSi layer of very good crystallinity. The peak broadens and moves slowly to the right with a reduced intensity after annealing at 700-800°C. The movement of the film peak position towards 0° indicates a smaller perpendicular lattice spacing in the epi-GeSi after annealing at 700-800°C. It is known that dislocations accompanied by strain relaxation can broaden x-ray diffraction peaks [17]. These facts, together with the transmission electron micrographs (not shown) and the channeling spectra in Fig. 1(a), indicate that the strain in the GeSi relaxes after annealing at 700°C, and is further relieved at 800°C. According to Vegard's law, a fully relaxed $Ge_{0.12}Si_{0.88}$ should have an film peak located at -0.29°; this non-implanted sample is thus far from being fully relaxed after annealing at 800°C.

The rocking curves of the as-implanted samples in Figs. 2(b)-(c) (dotted lines) show that implantation shifts the peak away from the substrate signal (at 0°). Additional compressive strain is thus introduced in the films by implantation. The induced amount of perpendicular strain increases with the ion dose, as does the implantation-induced damage (cf. Figs. 1(b)-(c)). The strong reduction in the signals from the epi-GeSi film with the increasing P ion dose in Figs. 2(b)-(c) is caused by the implantation-induced damage. The intensities and the shapes of these peaks recover roughly to that of an as-deposited film after annealing at 400°C. The position of the film peak also moves back near its original location, which means that much of the implantation-induced strain and damage is removed after the sample is annealed at 400°C. The induced strain further decreases slightly after annealing at 500-600°C, but a small amount of it remains, possibly created by the residual defects that are non-detectable by channeling spectrometry (cf. Figs. 1(b)-(c)). After the samples are annealed at 700-800°C, the GeSi peak clearly broadens and moves towards 0°, which indicates the films to be relaxed and of inferior crystalline quality compared to the as-deposited samples.

Figure 2(d) presents the rocking curves of the amorphized Si/GeSi after annealing. We see a very weak and broad peak between ~ -0.4° and -0.7° for the as-implanted sample (dotted line). This weak signal comes from the non-amorphized crystalline GeSi underlying the amorphous GeSi (cf. Fig. 1(d)), and its low intensity is caused by the damage within the layer. The GeSi peak increases in intensity and sharpens at ~ -0.52° after annealing at 400°C. Some of the implantation-induced damage has evidently been removed, but significant amounts of induced strain and damage still remain (cf. Fig. 1(d)). A stronger, non-symmetrical peak appears between ~ -0.2° to -0.7° after annealing at 500°C, which indicates additional damage annealing and that the perpendicular strain in GeSi is non-uniform in depth. Cross-sectional transmission electron micrographs of this particular sample (not shown) show that the GeSi film after annealing at 500°C consists of three portions: a top amorphous GeSi, an regrown crystalline GeSi in the middle, and a strained crystalline GeSi at the bottom [10]. The GeSi film peak thus is a superposition of the signals diffracted from the two crystalline layers. After annealing at 550-700°C, two distinctly different peaks show up: the first is very broad and centered around ~ -0.29°, which is the Bragg angle of a fully relaxed $Ge_{0.12}Si_{0.88}$. Considering the location and shape of this peak, as well as the results from the electron micrographs, we conclude that the regrown GeSi is relaxed and contains a high dislocation density. The second film peak is located at ~-0.48°, close to the Bragg angle of a pseudomorphic $Ge_{0.12}Si_{0.88}$. This peak suggests that additional induced strain is removed from the underlying crystalline GeSi. After annealing at 800°C, the entire epilayer is fully relaxed, producing a single broad GeSi peak (solid crosses) in Fig. 3(d). We can roughly estimate the dislocation density of this epilayer using the equation $\rho_t = (W_d)^2/9b^2$, where W_d is the full-width half maximum of the GeSi film peak broadened by dislocations only, and b is the Burger's vector of the dislocations [17]. By this method, the fully relaxed epi-GeSi is predicted to have a dislocation density of ~ $10^{10}/cm^2$. The dislocation density measured using transmission electron microscopy on the same sample is ~ 10^{10}-$10^{11}/cm^2$ and is consistent with the x-ray results.

Figure 3(a) compares the rocking curves of the Si/GeSi samples annealed at 800°C (Figs. 2(a)-(d)) with and without implantation. It is evident that the strain relaxation is enhanced by the implantation, and that the effect increases with the ion dose. Figure 3(b) shows the corresponding channeling spectra of the samples whose rocking curves are plotted in Fig. 3(a). The amount of residual damage after annealing at 800°C increases with the implantation dose. Hull *et al.* have observed a similar enhancement of strain relaxation in a strained Si/GeSi/Si implanted with either B or As below their amorphization doses [7]. They postulate that the defects created by implantation can serve as nucleation sites for the formation of incipient dislocation loops, which then lead to the relaxation of strain in GeSi. Our results thus further demonstrate that implantation-induced damage, which is a monotonic function of the ion dose [18-19], can substantially enhance the strain relaxation of both amorphized and non-amorphized Si/GeSi.

When performing ion implantation to dope a semiconductor, the percentage of electrically active dopants after annealing is critical. The fractions of the activated dopants for the implanted Si/GeSi are plotted in Fig. 4 versus the annealing temperatures. The experimental values obtained from the current study are compared with the data taken from Ref. 20 for 280 keV P-implanted Si. Figure 4 shows that if the GeSi is not amorphized, the activation at 550°C is poor (solid circles and solid triangles). However, the activation for the amorphized GeSi reaches ~100% after annealing at 550°C (solid diamonds). The activation of P ions in GeSi therefore benefits from solid-phase epitaxy. The same effect is well-known for both Si and Ge [20-22]. The dopant activation curves of Crowder and Morehead for 280 keV P implantations are reproduced in Fig. 4 for Si amorphized with $5x10^{15}$ P/cm^2 (open diamonds) and non-amorphized with $1x10^{13}$ P/cm^2 (open squares) [20]. The curves for GeSi and Si are very similar.

In summary, figures 1-2 show that for non-amorphized Si/GeSi, strain relaxes only after annealing at 700°C; amorphized films relax after annealing at 550°C. The regrown epi-GeSi contains a high density of dislocations (~10^{10}/cm^2), which is very different from implanted Si after solid-phase epitaxial regrowth [1,2].For both amorphized and non-amorphized samples,

steady-state annealing cannot achieve full activation without introducing strain relaxation of the epitaxial film. Further studies are currently underway to circumvent this problem of strain relaxation after implantation and annealing [16,23].

IV. CONCLUSIONS

We conclude that when metastable pseudomorphic Si/GeSi is doped with P-implantation, steady-state furnace annealing cannot achieve complete dopant activation in the epi-GeSi without losing its pseudomorphic nature and its crystalline perfection. Significant enhancement of strain relaxation is also observed for implanted Si/GeSi after annealing. Since the enhancement of strain relaxation increases with the implantation-induced damage in this current study, special precaution should be taken to minimize the damage introduced to the heterostructure by ion implantation and/or other processing steps.

ACKNOWLEDGMENTS

This work was supported by the Semiconductor Research Corporation under a coordinated research program at Caltech and at UCLA, contract no. 95-SJ-100. The authors are very thankful to Professor K.L. Wang, T.K. Carns, M. O. Tanner and S. Thomas at UCLA for the deposition of Si/GeSi samples and many valuable discussions.

References:

1. M. D. Giles in *VLSI Technology*, edited by S.M. Sze, ch. 8 (McGraw-Hill, Singapore, 1988)

2. J. F. Gibbons, Proc. IEEE, **60**, 1062 (1972).

3. J. W. Mayer, L. Eriksson, and J. A Davis, *Ion Implantation in Semiconductors*, (Academic Press, New York, 1970).

4. P.S. Peercy, B.W. Dodson, J.Y. Tsao, E.D. Jones, D.R. Myers, T.E. Zipperian, L.R. Dawson, R.M. Biefeld, J.F. Klem, and C.R. Hills, IEEE Electron Devices Lett. 9, 621 (1988).

5. C.A. King, J.L. Hoyt, and J.F. Gibbons, IEEE Trans. Electron Devices **36**, 2093 (1989).

6. D. K. Nayak, K. Kamjoo, J. S. Park, Jason C. S. Woo and K. L. Wang, **39**, 56 (1992).

7. R. Hull, J.C. Bean, J.M. Bonar, G.S. Higashi, K.T. Short, H. Temkin, and A.E. White, Appl. Phys. Lett. **56**, 2445 (1990).

8. D. C. Paine, N. D. Evans and N. G. Stoffel, J. Appl. Phys. **70**, 4278 (1991).

9. P. KringhØj and R. G. Elliman, Phys. Rev. Lett. **73**, 858 (1994).

10. D. Y. C. Lie, N.D. Theodore, J.H. Song, and M.-A. Nicolet, J. of Appl. Phys. **77** (in press).

11. J. W. Matthews and A. E. Blakeslee, J. Cryst. Growth **27**, 118 (1974).

12. J. F. Ziegler, J. P. Biersack and U. Littmark, *The Stopping and Range of ions in Matter,* (Pergamon Press, London, 1985).

13. S.T. Picraux, B.L. Doyle, and J.Y. Tsao, *Strained-layer Superlattices : Materials Science and Technology*, Semiconductors and Semimetals, Vol. 33, edited by T. P. Pearsall, ch. 3, pp. 205-207 (Academic Press, London, 1991).

14. C. R. Wie, T. A. Tombrello, and T. Vreeland, Jr., J. Appl. Phys. **59**, 3743 (1986).

15. C. J. Tsai, A. Dommann, M.-A. Nicolet and T. Vreeland, Jr., J. Appl. Phys. **69**, 2076 (1991).

16. For an example of the extracted strain and damage (static Debye-Waller factor) profiles for ion-implanted Si/GeSi, please see: D.Y.C. Lie, J.H. Song, A. Vantomme, F. Eisen, M.-A. Nicolet, and N.D. Theodore, J. Appl. Phys. **77** (in press).

17. J. M. Baribeau, T. E. Jackman, D. C. Houghton, P. Maigné and M.W. Denhoff, J. Appl. Phys. **63**, 5738 (1988).

18. D. Y. C. Lie, A. Vantomme, F. Eisen, T. Vreeland, Jr., M.-A. Nicolet, T. K. Carns and K. L. Wang, J. of Appl. Phys. **74**, 6039 (1993).

19. D. Y. C. Lie, A. Vantomme, F. Eisen, M.-A. Nicolet, T. K. Carns and K. L. Wang, J. Electron. Mater. **23**, 369 (1994).

20. B. L. Crowder and F. F. Morehead, Jr. Appl. Phys. Lett, **14**, 313 (1969).

21. G. L. Olson and J. A. Roth, Mater. Sci. Rep. **3**, 1 (1988).

22. J. Gyulai in *Ion implantaion : Science and Technology*, edited by J. F. Ziegler (Academic Press, Orlando, 1984).

23. D. Y. C. Lie, J.H. Song, M-A. Nicolet, and N.D. Theodore, Appl. Phys. Lett. **66**, 592 (1995).

Figure captions :

Fig. 1. 2 MeV ^{4}He <100> channeling spectra of metastable pseudomorphic Si(100)/$Ge_{0.12}Si_{0.88}$ before and after annealing in vacuum at temperatures ranging from 400°C to 800°C for 30 minutes at each temperature for samples (a): as-deposited ("virgin"); (b): implanted with $5x10^{13}$ P/cm^2; (c): implanted with $1x10^{14}$ P/cm^2; and (d) implanted with $1.5x10^{15}$ P/cm^2. A spectrum taken with random beam incidence ("random") is also plotted for reference. All implantation performed at room temperature at 100 keV.

Fig. 2. Double-crystal x-ray rocking curves of (400) symmetrical diffraction for pseudomorphic Si(100)/$Ge_{0.12}Si_{0.88}$ before/after annealing in vacuum at temperatures ranging from 400°C to 800°C for 30 min at each temperature for samples (a): as-deposited ("virgin"); (b): implanted with $5x10^{13}$ P/cm^2; (c): implanted with $1x10^{14}$ P/cm^2; and (d): implanted with $1.5x10^{15}$ P/cm^2. These rocking curves are for the same set of samples whose channeling effect spectra are presented in Fig. 1.

Fig. 3 (a) : Double-crystal x-ray rocking curves of (400) symmetrical diffraction for pseudomorphic Si(100)/$Ge_{0.12}Si_{0.88}$ annealed in vacuum at 800°C for 30 min for both implanted and non-implanted samples; Fig. 3(b): 2 MeV ^{4}He <100> channeling spectra of pseudomorphic Si(100)/$Ge_{0.12}Si_{0.88}$ samples whose rocking curves are shown in Fig. 3(a).

Fig. 4. The ratio in % of electrons/cm^2 obtained from Hall measurements to the implanted P atoms/cm^2 for pseudomorphic Si(100)/$Ge_{0.12}Si_{0.88}$ implanted with $5x10^{13}$ P/cm^2 (solid circles), $1x10^{14}$ P/cm^2 (solid triangles) and $1.5x10^{15}$ P/cm^2 (solid diamonds) at 100 keV as a function of the annealing temperature. The implantation was performed at room temperature and the duration of annealing at each temperature was 30 minutes. Corresponding data for 280 keV P implanted Si

are plotted for comparison (open diamonds for $5x10^{15}$ P/cm² and open squares for $1x10^{13}$ P/cm², from Ref. 20).

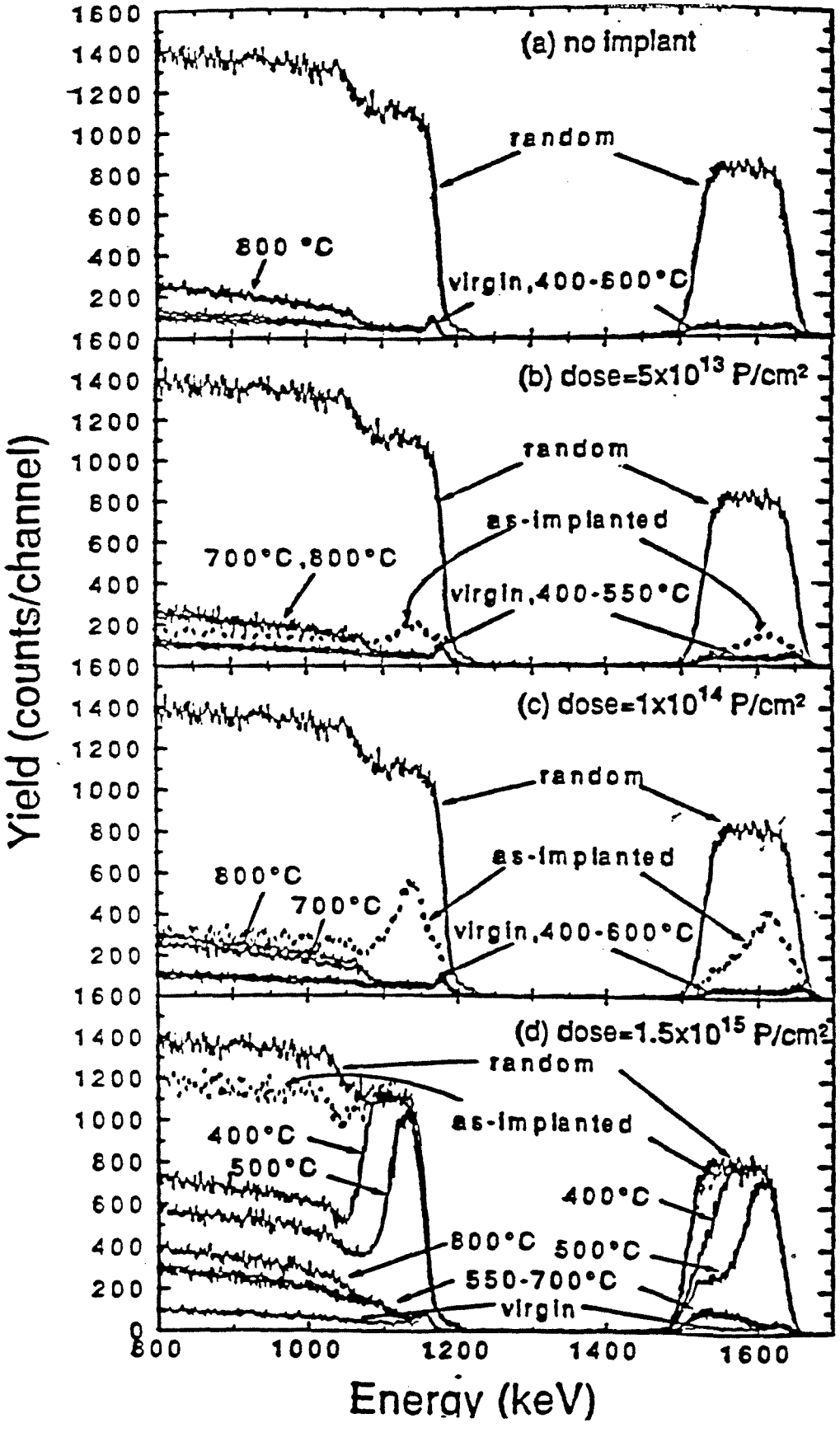
(a) no implant
random
800 °C
virgin,400-600°C
(b) dose=5x10^13 P/cm²
random
as-implanted
700°C,800°C
virgin,400-550°C
(c) dose=1x10^14 P/cm²
random
as-implanted
800°C
700°C
virgin,400-600°C
(d) dose=1.5x10^15 P/cm²
random
as-implanted
400°C
500°C
800°C
550-700°C
virgin
Yield (counts/channel)
Energy (keV)

Fig. 1

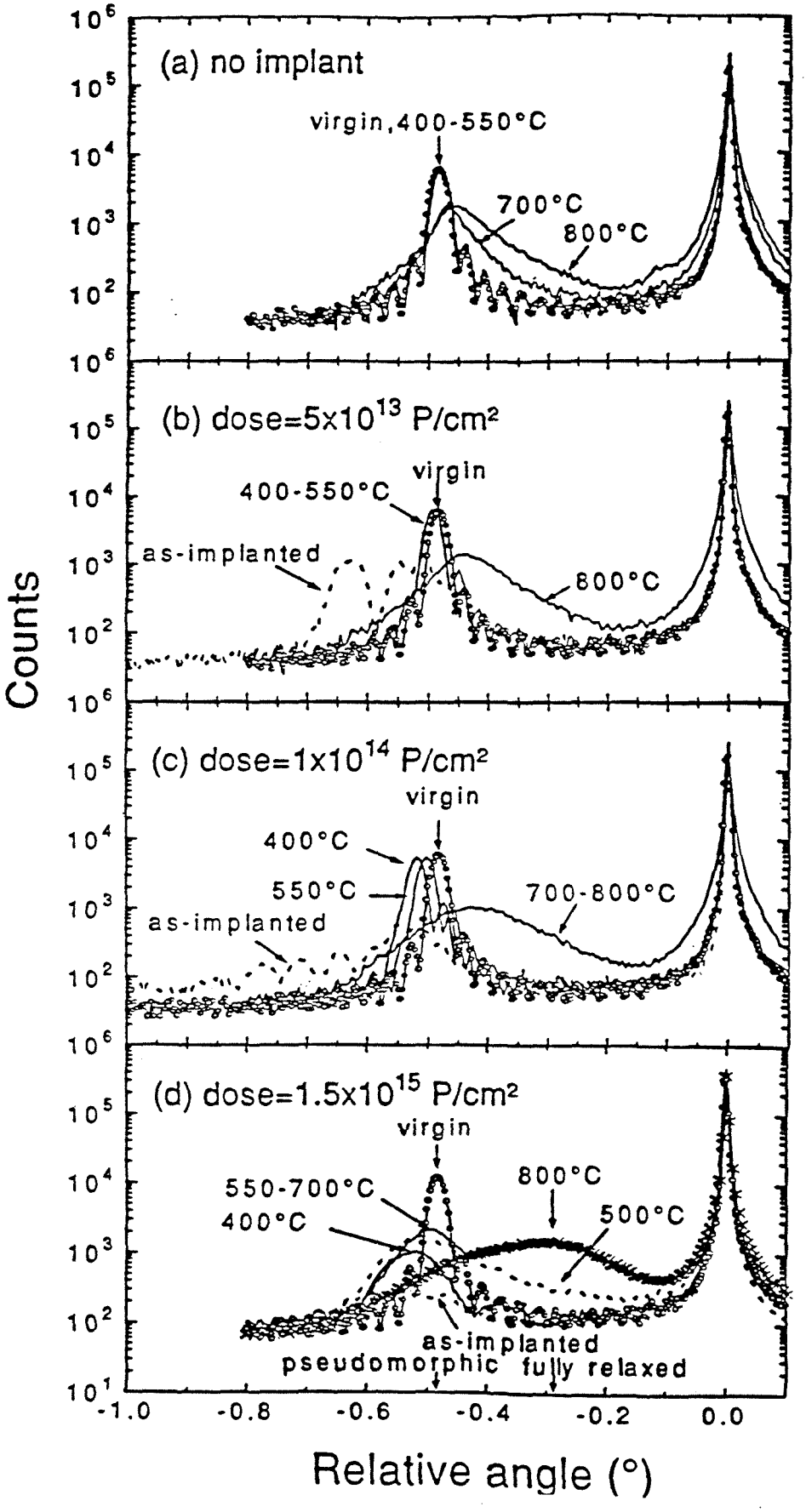
(a) no implant
virgin,400-550°C
700°C
800°C
(b) dose=5x10^13 P/cm²
virgin
400-550°C
as-implanted
800°C
(c) dose=1x10^14 P/cm²
virgin
400°C
550°C
700-800°C
as-implanted
(d) dose=1.5x10^15 P/cm²
virgin
550-700°C
400°C
800°C
500°C
as-implanted
pseudomorphic
fully relaxed
Counts
Relative angle (°)

Fig. 2

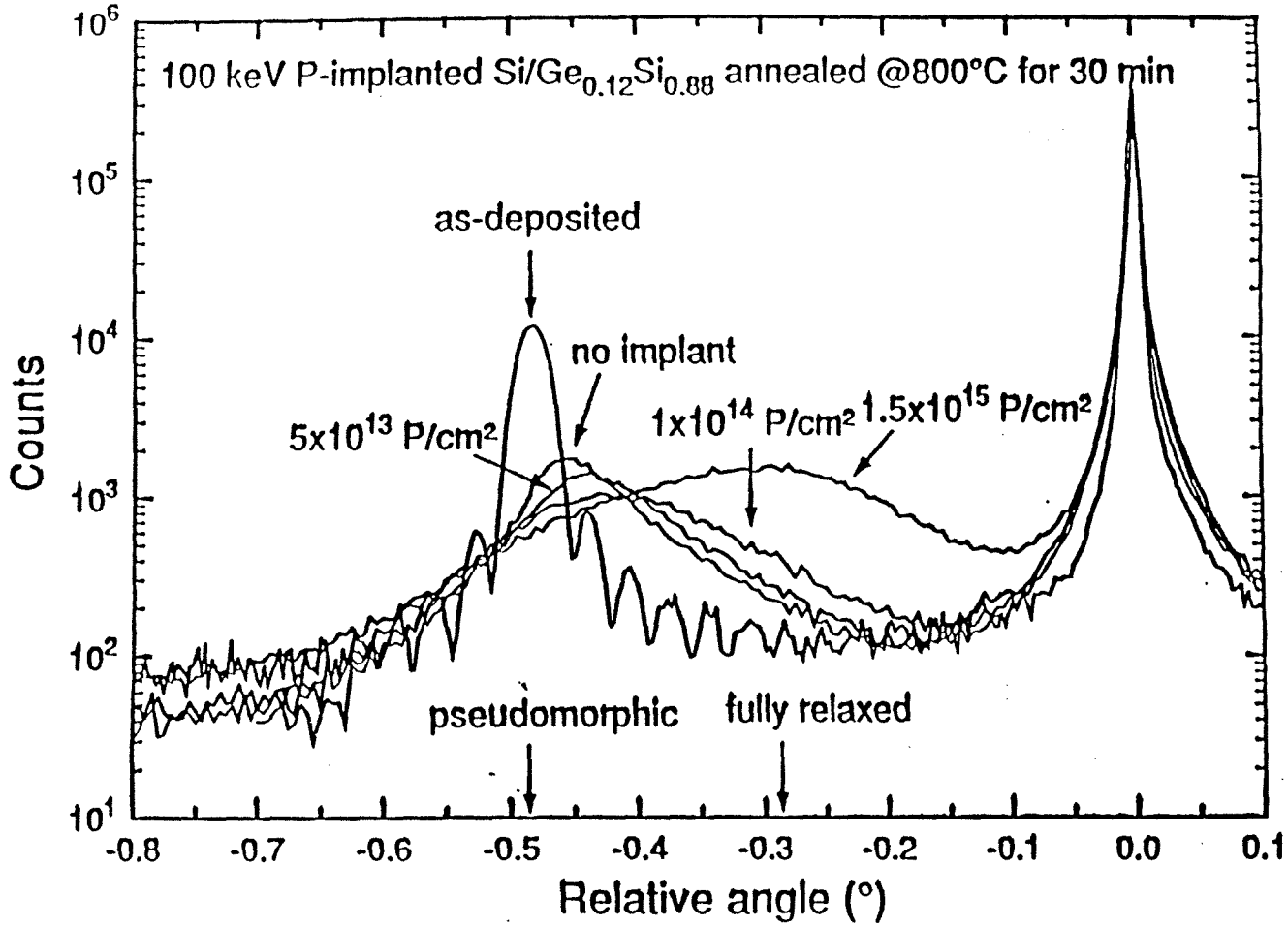
100 keV P-implanted Si/Ge0.12Si0.88 annealed @800°C for 30 min
as-deposited
no implant
5x10^13 P/cm²
1x10^14 P/cm²
1.5x10^15 P/cm²
pseudomorphic
fully relaxed
Counts
Relative angle (°)
10^6
10^5
10^4
10^3
10^2
10^1
-0.8
-0.7
-0.6
-0.5
-0.4
-0.3
-0.2
-0.1
0.0
0.1

Fig. 3(a)

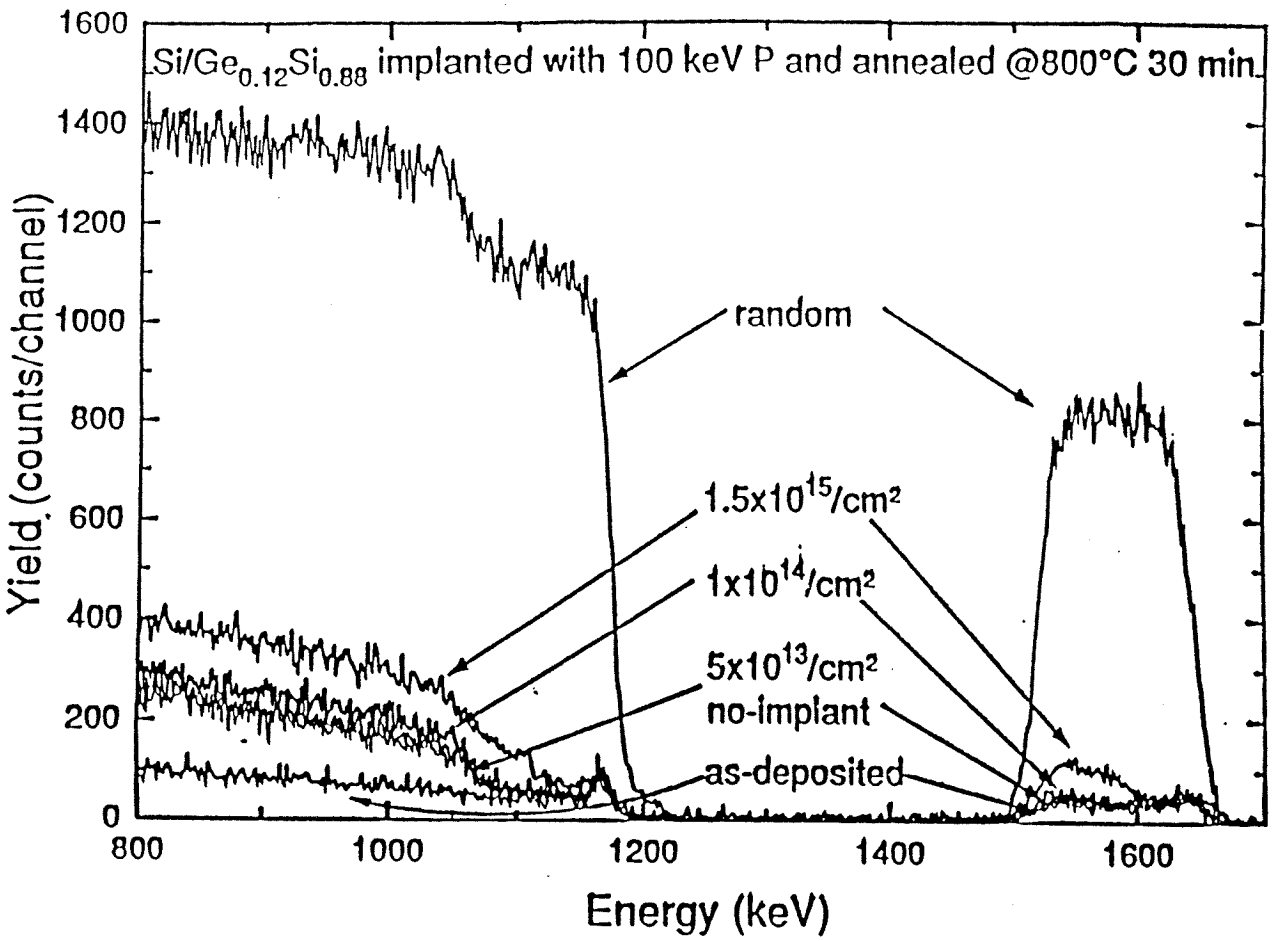
Si/Ge0.12Si0.88 implanted with 100 keV P and annealed @800°C 30 min.
random
1.5x10^15/cm²
1x10^14/cm²
5x10^13/cm²
no-implant
as-deposited
Yield (counts/channel)
Energy (keV)
0
200
400
600
800
1000
1200
1400
1600
800
1000
1200
1400
1600

Fig. 3(b)

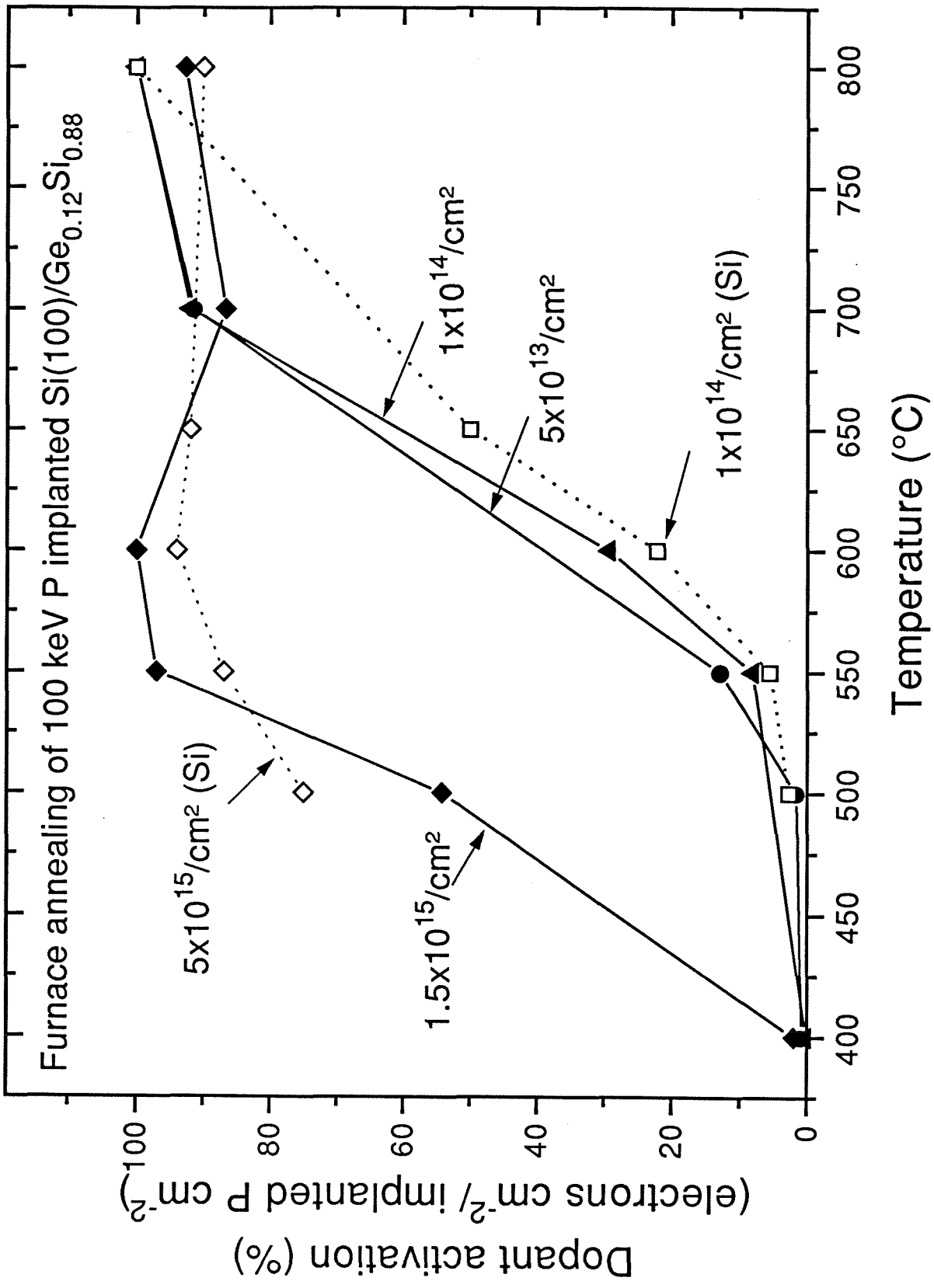
Furnace annealing of 100 keV P implanted Si(100)/Ge0.12Si0.88
Dopant activation (%)
(electrons cm-2/ implanted P cm-2)
Temperature (°C)
0
20
40
60
80
100
400
450
500
550
600
650
700
750
800
5x10^15/cm^2 (Si)
1.5x10^15/cm^2
1x10^14/cm^2
5x10^13/cm^2
1x10^14/cm^2 (Si)

Fig. 4

Appendix 5

Advantage of rapid thermal annealing over furnace annealing for P-implanted metastable Si/$Ge_{0.12}Si_{0.88}$

D. Y. C. Lie,[a] J. H. Song,[b] and M.-A. Nicolet
M/S 116-81, California Institute of Technology, Pasadena, California 91125

N. D. Theodore
Motorola Inc., Mesa, Arizona 85202

(Received 15 August 1994; accepted for publication 22 November 1994)

Metastable pseudomorphic $Ge_{0.12}Si_{0.88}$ films were grown by molecular beam epitaxy on Si(100) substrates and then implanted with 100 keV ^{31}P at room temperature for a dose of $5\times10^{13}/cm^2$. Samples were subsequently annealed by rapid thermal annealing (RTA) in nitrogen and by steady-state furnace annealing in vacuum. Both damage and strain introduced by implantation can be completely removed, within instrumental sensitivity, by RTA at 700 °C for 10–40 s. Vacuum annealing for 30 min at 500–550 °C removes most of the damage and strain induced by the implantation but the activation of the P is poor. At 700 °C, the activation is nearly 100%, but the crystallinity worsens and the pseudomorphic strain begins to relax. We conclude that for a lightly implanted metastable and pseudomorphic GeSi epilayer on Si, steady-state vacuum annealing cannot achieve good dopant activation without introducing significant strain relaxation to the heterostructure, while RTA can. © *1995 American Institute of Physics.*

In order to achieve continued improvement of electronic and optoelectronic devices, Si/Ge_xSi_{1-x} heterostructures are being studied extensively since they are silicon based and can provide adjustable band gaps and faster carrier mobilities. Ion implantation is currently the dominant technology for introducing controlled amounts of dopants into semiconductors. Hull *et al.* have reported that implantation-induced point defects can substantially enhance strain relaxation of metastable Si/GeSi/Si heterostructures.[1] Once GeSi relaxes, the accompanying dislocations are detrimental to electronic devices; the defects are responsible for large leakage currents and reduced carrier mobilities.[2–5] Strain relaxation also results in the reduction of $Si-Ge_xSi_{1-x}$ band gap differences. Kasper *et al.* believe that the implementation of a complementary Si/GeSi modulation doped field effect transistor (MODFET) will depend on the successful application of ion implantation and annealing techniques.[6] It is, therefore, important to investigate how to optimize the implantation and annealing conditions for Si/Ge_xSi_{1-x} in order to minimize residual damage and avoid strain relaxation, while maximizing the activation of dopants.[7–11]

We report in this letter a study of 100 keV ^{31}P implantation to dope a metastable pseudomorphic $Ge_{0.12}Si_{0.88}$ layer without amorphizing the layer or significantly damaging the Si–GeSi interface. After implantation, the samples were annealed in vacuum for 30 min from 400–800 °C, or by rapid thermal annealing (RTA) at 700 °C in nitrogen. We focus on the comparison of these two annealing techniques for the recovery of damage, strain, and dopant activation for P-implanted GeSi. The damage and strain in these layers were measured using 2 MeV ^4He ion channeling/backscattering spectrometry, double-crystal x-ray diffractometry (DCD), and cross-sectional transmission electron microscopy (XTEM). Hall effect and sheet resistivity measurements were obtained from the implanted and annealed samples to determine the percentage of activated dopants.

Undoped metastable[12] pseudomorphic $Ge_{0.12}Si_{0.88}$ layers 265 nm thick were deposited at ~450 °C on p^- Si(100) substrates by molecular beam epitaxy at the University of California at Los Angeles. Samples are of excellent crystalline quality, with a minimum channeling yield of ~3%. DCD shows that the film is fully strained, with a perpendicular strain value of 0.87% and zero parallel strain within experimental sensitivity ($\sim10^{-4}$). The calculated strain value from linear elasticity theory is 0.88%, which is in excellent agreement with the DCD results. We did not find any dislocations in the virgin sample by either DCD or transmission electron microscopy (TEM). The Si/GeSi heterostructure was then implanted in high vacuum ($\sim10^{-7}$ Torr) with 100 keV ^{31}P to a dose of $5\times10^{13}/cm^2$ at room temperature. During implantation, the sample was tilted by 7° to minimize channeling. According to the TRIM-92 simulation program, the projected range and straggling of 100 keV P ions are ~125 and 43 nm, respectively.[13]

Samples were annealed in either: (1) a high-vacuum tube furnace ($\sim3\times10^{-7}$ Torr) at 400, 500, 550, 700, and 800 °C for 30 min each; or (2) a nitrogen ambient at 695±7 °C by RTA for 10, 20, or 40 s using an AG Associate's HeatPulse 410 oven with a turn-on ramp rate of ~80°/s. The electrical properties of the implanted layers were characterized by Hall effect and sheet resistance measurements using a van der Pauw pattern.

We present in Fig. 1(a) a set of 2 MeV ^4He ⟨100⟩ axial channeling spectra for Si(100)/$Ge_{0.12}Si_{0.88}$ implanted with 5×10^{13} P/cm^2 at 100 keV and subsequently annealed in vacuum from 400–800 °C for 30 min each. Also shown in Fig. 1(a) are the channeling and the random spectra of a virgin sample. The backscattering yield of the channeling

[a]Electronic mail: donald@ iago.caltech.edu
[b]On leave from Yonsei University, Seoul 120-749, Korea.

 0003-6951/95/66(5)/592/3/$6.00 © 1995 American Institute of Physics

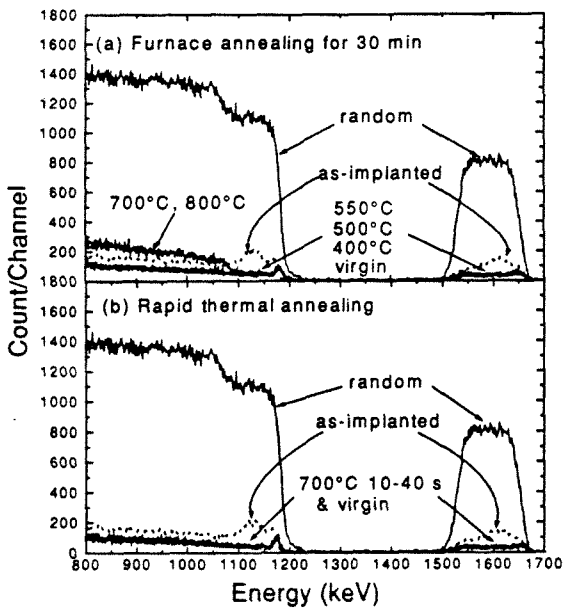

FIG. 1. 2 MeV ^{4}He ⟨100⟩ channeling spectra for metastable pseudomorphic Si(100)/$Ge_{0.12}Si_{0.88}$ implanted at room temperature with 5×10^{13}/cm^2 P ions at 100 keV: (a) after 30 min vacuum furnace annealing from 400–800 °C. and (b) after RTA in a nitrogen ambient at 700 °C for 10–40 s. The channeling and random spectra of a virgin sample are also plotted in both figures as references.

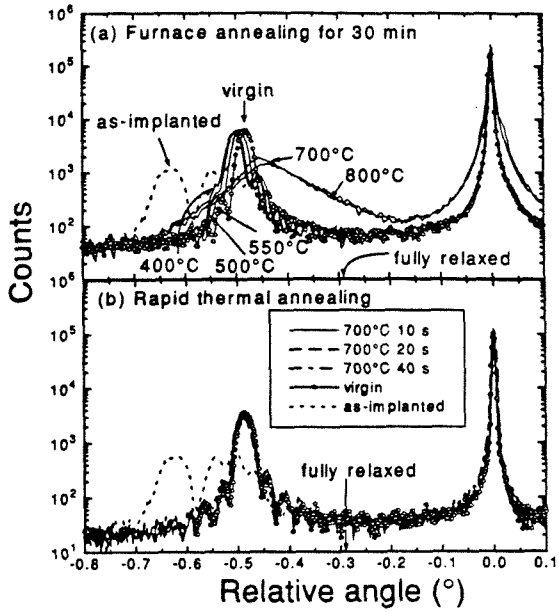

FIG. 2. Double-crystal x-ray rocking curves of (400) symmetrical diffraction for metastable pseudomorphic Si(100)/$Ge_{0.12}Si_{0.88}$ implanted at room temperature with 5×10^{13}/cm^2 P ions at 100 keV: (a) after 30 min vacuum annealing from 400–800 °C. and (b) after RTA in a nitrogen ambient at 700 °C for 10–40 s. The implantation conditions are the same as those used in Fig. 1.

spectrum for an as-implanted sample reaches about one-quarter of that of the random spectrum, indicating that the GeSi is damaged substantially by implantation. After the samples are annealed at 400–550 °C for 30 min, the channeling spectra are very similar to that of a virgin sample, suggesting that most of the implantation-induced defects were removed. After 700–800 °C annealing, the yield exhibits a steplike increase at and below the energy position of the Si–GeSi interface. A high density of dislocations can explain this increase.[14] Figure 1(b) shows a set of ⟨100⟩ channeling spectra for P-implanted Si/$Ge_{0.12}Si_{0.88}$ after RTA at 700 °C in a nitrogen ambient for 10–40 s. The spectra of samples after RTA are indistinguishable from that of a virgin sample, which means that no damage is detectable within the resolution of MeV ^{4}He channeling spectrometry.

We plot in Fig. 2(a) x-ray (400) rocking curves for the identical set of furnace annealed samples as shown in Fig. 1(a). The rocking curve of an as-implanted sample (dotted line) shows a negative angular shift of the epilayer signal with respect to that of the substrate (at 0°), indicating that additional compressive perpendicular strain is introduced to the film by implantation. Due to damage created by the ions, the intensity of the film peak decreases significantly. After the implanted sample is annealed at 400 °C, the intensity of the film peak recovers closely to that of a virgin film, and the position of the peak moves back near to that of a virgin sample. These changes suggest that many implantation-induced defects disappear after 400 °C annealing. For samples annealed at 500 and 550 °C, the induced strain decreases slightly further. A small amount of induced strain still remains at 550 °C, possibly caused by residual damage not detectable by channeling spectrometry.

For samples annealed at 700–800 °C, the film diffraction peak broadens and shifts towards to the substrate peak. The films are thus relaxed, with inferior crystalline quality to that of virgin samples. This observed strain relaxation is in agreement with the steplike increase in the dechanneling yield near the Si–GeSi interface [Fig. 1(a)]. The diffraction peaks from the Si substrates are also broadened after this relaxation. LeGoues *et al.*[15] have reported that in compositionally uniform Si/GeSi films, dislocations can penetrate deep into the substrates (~10 μm). It is well known that dislocations broaden x-ray diffraction peaks.[7,8] TEM micrographs of our relaxed GeSi films also show that dislocations penetrate into Si substrates.

We also plot in Fig. 2(b) (400) x-ray rocking curves for the identical set of samples as shown in Fig. 1(b) after RTA. DCD shows that the implantation-induced strain is completely removed after RTA for 10–40 s. This behavior is consistent with the absence of residual damage measured by ion channeling spectrometry [cf. Fig. 1(b)]. We also did not observe any defects in RTA-annealed samples by XTEM. High-resolution DCD is sensitive to threading dislocation densities $\geq10^6$ cm^2, comparable to values measurable by plan-view TEM,[16] while ⟨100⟩ channeling is only sensitive to dislocation densities $\geq10^8$/cm^2.[17]

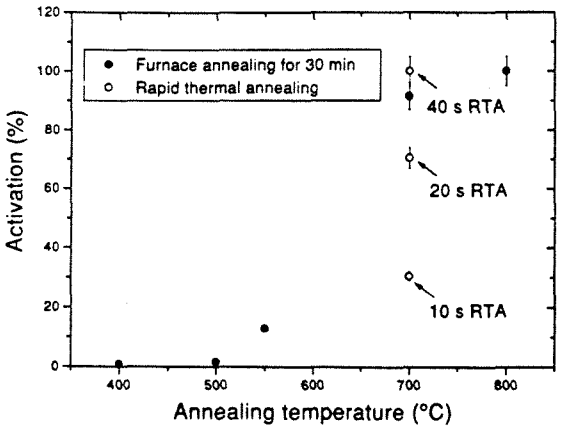

FIG. 3. The ratio of electrons/cm^2 (obtained from Hall measurements) to implanted atoms/cm^2 for P implantation into $Ge_{0.12}Si_{0.88}$ is plotted as a function of the annealing temperatures after the samples were annealed either in a vacuum furnace for 30 min each or by RTA at 700 °C in a nitrogen ambient for 10–40 s. All samples were implanted at room temperature with 5×10^{13} P/cm^2 at 100 keV.

The results presented so far in Figs. 1–2 show that RTA excels over steady-state annealing in removing both implantation-induced damage and strain for metastable $Si/Ge_{0.12}Si_{0.88}$. We now show that RTA outperforms furnace annealing in terms of dopant activation as well. Figure 3 plots the percentage of electrically activated phosphorous atoms in GeSi, obtained from Hall effect measurements for samples after both furnace annealing and RTA. For furnace-annealed GeSi, temperatures $\geq$700 °C are required to achieve usable activation. At these temperatures the GeSi layers relax considerably and have high resulting dislocation densities [$\sim10^9$–10^{10}/cm^2, cf. Figs. 1(a) and 2(a)]. In our study RTA was always performed at 700 °C, and the samples reached ~72% activation after only 20 s, and ~100% after 40 s.

Figure 3 shows that for postimplantation dopant activation, an annealing at 700 °C for only 40 s is sufficient; further annealing not only has no merit in enhancing activation or removing damage but further introduces unwanted strain relaxation. It can be argued that the advantage of performing RTA on implanted Si/GeSi is primarily because at 700 °C, very few dislocations can nucleate and propagate within only 40 s; i.e., strain relaxation in the implanted Si/GeSi requires annealing times longer than 40 s at 700 °C. Dopants, on the other hand, can activate well within this short time frame.

The similarity of the P activation between 700 °C-30 min furnace annealing and 700 °C-40 s RTA indicates that strain relaxation does not significantly affect activation in this case. Since no relaxation occurred in samples after RTA, we conclude that RTA is superior for processing P-implanted $Ge_{0.12}Si_{0.88}$, for a implant dose of 5×10^{13}/cm^2. This conclusion should also remain valid for lower implantation doses. Further investigations are currently underway.

This work was supported by the Semiconductor Research Corporation under a coordinated research program at Caltech and at UCLA, Contract No. 94-SJ-100. The authors would like to thank Dr. F. Eisen for his valuable guidance and suggestions. They thank Professor K. L. Wang, T. K. Carns, and M. Tanner for providing the Si/GeSi samples. The authors are also appreciative of Professor D. L. Kwong, H. Kinoshita, and T. H. Huang at UT-Austin for RTA experiments.

[1] R. Hull, J. C. Bean, J. M. Bonar, G. S. Higashi, K. T. Short, H. Temkin, and A. E. White, Appl. Phys. Lett. **56**, 2446 (1990).
[2] C. A. King, J. L. Hoyt, and J. F. Gibbons, IEEE Trans. Electron Devices **ED-36**, 2093 (1989).
[3] P. S. Peercy, B. W. Dodson, J. Y. Tsao, E. D. Jones, D. R. Myers, T. E. Zipperian, L. R. Dawson, R. M. Biefeld, J. F. Klem, and C. R. Hills, IEEE Electron Device Lett. **ED-9**, 621 (1988).
[4] D. Y. C. Lie, T. K. Carns, N. D. Theodore, F. Eisen, M.-A. Nicolet, and K. L. Wang, Mater. Res. Soc. Symp. Proc. **321**, 485 (1994).
[5] D. K. Nayak, K. Kamjoo, J. S. Park, Jason C. S. Woo, and K. L. Wang, IEEE Trans. Electron Devices **ED-39**, 56 (1992).
[6] E. Kasper and F. Schaffler, *Strained-Layer Superlattices: Materials Science and Technology*, Semiconductors and Semimetals, Vol. 33, edited by T. P. Pearsall (Academic, London, 1991), Chap. 4, pp. 295–296.
[7] D. Y. C. Lie, A. Vantomme, F. Eisen, M.-A. Nicolet, T. K. Carns, and K. L. Wang, J. Appl. Phys. **74**, 6039 (1993).
[8] D. Y. C. Lie, A. Vantomme, F. Eisen, M.-A. Nicolet, T. K. Carns, and K. L. Wang, J. Electron. Mater. **23**, 369 (1994).
[9] G. Bai and M.-A. Nicolet, J. Appl. Phys. **71**, 4227 (1992).
[10] D. Y. C. Lie, A. Vantomme, F. Eisen, M.-A. Nicolet, V. Arbet-Engels, and K. L. Wang, Mater. Res. Soc. Symp. Proc. **262**, 1079 (1993).
[11] A. Vantomme, J. H. Song, D. Y. C. Lie, F. Eisen, M.-A. Nicolet, T. K. Carns, and K. L. Wang, Mater. Res. Soc. Symp. Proc. **326**, 121 (1994).
[12] J. W. Matthews and A. E. Blakeslee, J. Cryst. Growth **27**, 118 (1974).
[13] J. F. Zielger, J. P. Biersack, and U. Littmark, *The Stopping and Range of Ions in Matter* (Pergamon, London, 1985).
[14] S. T. Picraux, B. L. Doyle, and J. Y. Tsao, in Ref. 6, pp. 139–222.
[15] F. K. Le Goues, K. Eberland, and S. S. Iyer, Appl. Phys. Lett. **60**, 2962 (1992).
[16] E. A. Fitzgerald, Mater. Sci. Rep. **7**, 87 (1991).
[17] J. M. Baribeau, T. E. Jackman, D. C. Houghton, P. Maigné, and M. W. Denhoff, J. Appl. Phys. **63**, 5738 (1988).